Spring 2019

Cooperative Lewis Pairs Based on High-Valent Early Transition Metal Halides and Synthesis of Their Nitride Complexes

Md. Mamdudur Rahman

Cooperative Lewis Pairs Based on High-Valent Early Transition Metal Halides and Synthesis of Their Nitride Complexes

by

Md. Mamdudur Rahman

Bachelor of Science
University of Dhaka, 2009

Master of Science
University of Dhaka, 2011

Submitted in Partial Fulfillment of the Requirements

For the Degree of Doctor of Philosophy in

Chemistry

College of Arts and Sciences

University of South Carolina

2018

Accepted by:

Dmitry V. Peryshkov, Major Professor

Richard D. Adams, Committee Member

Ken D. Shimizu, Committee Member

Erdem Sasmaz, Committee Member

Cheryl L. Addy, Vice Provost and Dean of the Graduate School

Dedication

To my parents.

Acknowledgements

First and foremost, I would like to thank my advisor Dr. Dmitry V. Peryshkov, who always had faith in me and always looked at the sunny side. I can never fully express my gratitude that how thankful I am to you. For always being patient, everything you have taught, by constantly guiding and inspiring me.

In addition to my advisor I would like to thank my doctoral committee members for finding time within their busy schedule for my defense exams, pointing out short comings in research, by guiding me in the right direction, and taught me to always ask for the fundamental aspects of my work.

To every one of the Peryshkov group and Shustova group. We have been a family. Specially, to Bennett Eleazer and Derek Williams for being more than friends, being compassionate in time of research or personal difficult moments. Precious Breedland, thank you for letting me teach you and learn as well.

To Mark D. Smith, for always finding time to look at my crystals and solving the mysteries, which has been key to my research. Dr. Perry J. Pellechia, for helping me with simple to difficult NMR problems. You have always explained and taught me more than I could ask for. Jose Amaya, Dr. Thomas Makris, for help with the EPR experiments and Madushanka Dissanayake and Dr. Aron Vannucci for help with electrochemistry experiments.

All those friends around the department who always encouraged me, kept me smiling by smiling back to me. To everyone in the office of department of Chemistry and Biochemistry, for they made my graduate studies possible and my friendly work environment. To everyone from the office of International Student Services, who did more than just their job and made my stay in this strange land easier for all these years and transforming it as my second home.

To My family that they have taught me, how to overcome inner conflicts, uphold moral values and for their love and constant support.

Acknowledgement is made to ASPIRE-I funding granted through the University of South Carolina, Office of the Vice President for Research, and the National Science Foundation under Award CHE-1654301 for partial support of this work.

Abstract

Herein, we report the activation of relatively strong C–H and C–O bonds under mild conditions by a cooperative interaction of $TaCl_5$ and PPh_3. An unprecedented activation of nitrile adducts of high-valent transition metals with the formation of novel zwitterionic imido complexes was observed. The scope of the reaction includes a range of substituted unactivated nitriles including the C–H bond activation of both aliphatic and aromatic nitriles.

The cooperative action of a Lewis acidic high-valent transition metal halide ($TaCl_5$ or $NbCl_5$) and a weakly nucleophilic base (NEt_3 or PPh_3) leads to the deprotonation of a coordinated nitrile and subsequent rearrangement to an azaallene/carbocation intermediate. The nucleophilic attack of the base on the intermediate results in the formation of the cationic vinyl imido group. The presence of sterically hindered nitriles and weakly nucleophilic bulky organic base resulted in dimerization of the imido complexes through C–C bond coupling. The C–O bond activation was observed when unactivated ethers (anisole and diethyl ether), ketone (acetophenone) and aldehyde (4-phenylbenzaldehyde) were employed as substrates. For example, the reaction of the $TaCl_5$–PPh_3 pair and anisole at room temperature led to the selective cleavage of the sp^3-C–O bond.

Remarkably, all the reported activation processes proceed through cooperative Lewis acid-Lewis base interactions and do not involve redox events at the metal center. These transformations highlight the special role of the high-valent transition metal halide in the activation process and distinguish the reactivity of the $TaCl_5$–PPh_3 system from both

non-metal-based frustrated Lewis pairs and late transition metal-based FLP-like systems. Further study will demonstrate that this conceptually novel cooperative Lewis pair has a potential to activate a variety of strong bonds in small molecules. Furthermore, during the exploration of chemistry of high-valent early metal halides, a series of novel molecular multimetallic nitride complexes of Ta(V) and Ti(IV) were synthesized.

Table of Contents

Dedication iii

Acknowledgements iv

Abstract vi

List of Tables ix

List of Schemes x

List of Figures xii

List of Abbreviations xvi

Chapter 1: Introduction to Cooperative Lewis Pairs Based on High-Valent Early Transition Metal Halides for Small Molecule Activation and Metal Nitrides 1

Chapter 2: Activation of C–O and C–H Bonds by the $TaCl_5$–PPh_3 Cooperative Lewis Pair 25

Chapter 3: Formation of a cationic vinyl imido group upon C-H activation of nitriles by trialkylamines in presence of $TaCl_5$ 62

Chapter 4: Activation of C–H bonds of alkyl- and arylnitriles by the $TaCl_5$–PPh_3 Lewis pairs 86

Chapter 5: Imido Group Interchange in Reactions of Zwitterionic Tantalum(V) Vinylimido Complexes and Nitriles. 117

Chapter 6: Synthesis of Early Transition Metal Nitride Clusters 146

Appendix A: Permissions to Reprint 165

List of Tables

Table 1.1 The basicity scale for selected organic bases.....10

Table 2.1 Chemical shifts in ppm from NMR results of different early metals Lewis acids and Et_3PO as Lewis base.....28

Table 2.2 Selected bond distances and bond angles of compounds **2E, 2F, 2G, 2H** 39

Table 2.3 Crystallographic table for single crystal X-ray data for $M(Et_3PO)_x$ (M = Ta, Nb, Zr; x = 1 or 2), and $TaCl_5$-PPh_3 adduct. 54

Table 2.4 Crystallographic table for single crystal X-ray data for compounds **2E, 2F, 2G, 2H, 2I.**.....56

Table 3.1 Crystallographic table for single crystal X-ray data for compounds **1, 2, 3,** and **4.** 82

Table 4.1 Crystallographic table for single crystal X-ray data for compounds **1, 2, 3, and 4.**.....111

Table 5.1 Crystallographic table for single crystal X-ray data for compound $[Ta(NCCMe_2\{DMAP\})Cl_4](DMAP)$ (3-^{i}Pr) 143

Table 6.1 Crystallographic table for single crystal X-ray data for compound Ta Star (**1**), **(1a**), Ti_4 Ladder (**2**), and Ti_9 Cluster (**3**). 161

List of Schemes

Scheme 1.1 $B(C_6F_5)_3$ catalyzed hydrosilylation of aromatic aldehydes, ketones, and esters. 4

Scheme 1.2 Activation of CO_2 in $B(C_6F_5)_3$-$P(^tBu)_3$ FLP system....4

Scheme 1.3 Examples of precatalysts for Noyori (A) (Ar = 4-$CH_3C_6H_4$), and Morris (B) systems.....5

Scheme 1.4 Dihydrogen activation by zirconocene complex.....6

Scheme 1.5 Formation of tantalacycle via coupling of Ta alkyne ligand with additional functionalities....7

Scheme 1.6 Late metal promoted activation of acetonitrile. 8

Scheme 1.7 Reaction of organosilane with dinitrile. 9

Scheme 1.8 $[Cp^*TaN(Cl)]_3$, ($Cp^* = C_5H_5(CH_3)_5$).....13

Scheme 1.9 $[(tBuCH_2)_2TaN]_5$ and R = $tBuCH_2$ (Bond distances are in the unit of Å) 14

Scheme 1.10 The cooperative reactivity of Group 5-Group 15 representative Lewis pair ($TaCl_5$・PPh_3) with a range of substrates.....15

Scheme 2.1 comparative examples for main group based FLP, Metal Based FLP and CLP system reported in this dissertation.....27

Scheme 2.2 General synthesis of complexes with acetophenone and bisphenyl aldehyde with $TaCl_5/PPh_3$ 33

Scheme 2.3 General synthesis of complexes with acetophenone and bisphenyl aldehyde with $TaCl_5/PPh_3$. 35

Scheme 2.4 Reaction of phenyl acetylene with $TaCl_5/PPh_3$ Lewis pair 38

Scheme 3.1 The synthesis of zwitterionic vinylimido complexes of Ta(V) upon deprotonation of coordinated nitriles (MeCN, EtCN, *i*-PrCN).....63

Scheme 3.2 Possible mechanisms of formation of zwitterionic vinyl imido complexes of Ta(V). 66

Scheme 3.3 The synthesis of $[HN(i\text{-}Pr)_2Et][Ta\{NC(CMe_2)CMe_2CN\}Cl_4]$ vinyl imido coordination polymer (**4**) 69

Scheme 4.1 The possible mechanism of the formation of $[TaCl_4\{NC(H)(PPh_3)C_6H_4(PPh_3)\}(NCC_6H_5)]^+$ (**1**$^+$) in the reaction of PhCN with the $TaCl_5$-PPh_3 Lewis pair. 90

Scheme 5.1 Examples of reactivity of imido complexes of early transition metals with nitriles ere..... 118

Scheme 5.2 Imido group interchange in zwitterionic Ta(V) vinylimido complexes..... 120

Scheme 5.3 Proposed mechanism of imido group interchange on the example of the 1-^{i}Pr to 1-Me conversion 121

Scheme 5.4 Evidence of a proton transfer from a nitrile to an imido group on the example of the 1-Me' to 1-Me'-d^2 conversion 122

Scheme 5.5Replacement of the ammonio group by triphenylphosphine (left, 2-Me) or DMAP (right, 3-^{i}Pr) in the zwitterionic vinylimido complex 1-^{i}Pr 122

Scheme 5.6 The prevalent decomposition pathway for the vinylimido complex 1-^{i}Pr upon prolonged heating without an added nitrile 126

List of Figures

Figure 2.1 Displacement ellipsoid plots of $[Ta_2OCl_8(OP(CH_2CH_3)_3)_2]$ $[TaCl_5OP(CH_2CH_3)_3]$ (**2A**) drawn at 50% probability of complexes Ta1/Ta2 and Ta5. Only the major disorder component of the Ta5 complex is shown. 29

Figure 2.2 Displacement ellipsoid plots of $[NbCl_4(OP(CH_2CH_3)_3)_2]_2[Nb_4O_2Cl_{18}]$ C_6H_6 (**2B**) drawn at 50% probability level. Superscripts denote symmetry-equivalent atoms...29

Figure 2.3 Displacement ellipsoids plot of (25% probability level) $ZrCl_4(OP(CH_2CH_3)_3)_2$. **(2C)** Superscripts denote symmetry-equivalent atoms 30

Figure 2.4 The displacement ellipsoid plot (50% probability) of the $TaCl_5 \cdot PPh_3$ adduct (**2D**) Hydrogen atoms are not shown. Selected distances (Å): Ta1–P1 = 2.792(1), Ta1–Cl1 = 2.303(1), Ta1–Cl2 = 1.316(1) 31

Figure 2.5 The $^{31}P\{^1H\}$ NMR spectrum of $TaCl_5 \cdot PPh_3$ in C_6D_6 32

Figure 2.6 Displacement ellipsoids of $[P(CH_2CH_3)(C_6H_5)_3][TaCl_6]$ (**2E**) drawn at the 60% probability level. Both $TaCl_6^-$ anions are located on crystallographic inversion centers and therefore only half of each is present per cation. 34

Figure 2.7 The displacement ellipsoid plot of $[PCH_3(C_6H_5)_3][TaCl_5(OC_6H_5)] \cdot (C_7H_8)_{0.25}$ (**2F**) (drawn at 50% probability level). Anion Ta1 and cation P1. Co-crystallized toluene disordered over a crystallographic inversion center are not shown 35

Figure 2.8 Displacement ellipsoid plots of the molecular structure of $TaCl_5(C_{26}H_{23}OP)$ (**2G**) 36

Figure 2.9 The displacement ellipsoid plot (50% probability) of $TaCl_5(OCH(C_{12}H_9)(P(C_6H_5)_3)) \cdot (C_6H_5Cl)_{0.5}$ (**2H**) Co-crystallized disordered C_6H_5Cl solvent molecules are not shown here. Hydrogens in PPh_3 moiety are omitted for clarity. 37

Figure 2.10 Displacement ellipsoid plot of the molecular structure of $Ta_2Cl_8(\eta^2\text{-}C_6H_5CCP(C_6H_5)_3)_2$ (**2I**) Displacement ellipsoids drawn at the 60% probability level. 38

Figure 3.1 Displacement ellipsoid plot of $[HNEt_3][Ta\{NC(CH_2)NEt_3\}Cl_5]$ (**1**) (50% probability. Hydrogen atoms, except for the vinyl group, have been omitted for clarity. The $[HNEt_3]^+$ cation is not shown.) 64

Figure 3.2 Displacement ellipsoid plot of Ta{NC(CHCH$_3$)NEt$_3$}Cl$_4$(NCCH$_3$) (**2**) (50% probability. Hydrogen atoms, except for the vinyl group, have been omitted for clarity) 67

Figure 3.3 Displacement ellipsoid plot of Ta{NC(CMe$_2$)NEt$_3$}Cl$_4$(NCHMe$_2$) (3) (50% probability. Hydrogen atoms have been omitted for clarity.) 68

Figure 3.4 Displacement ellipsoid plot of [HN(*i*-Pr)$_2$Et][Ta{NC(CMe$_2$)CMe$_2$CN}Cl$_4$]·CH$_3$CN (4) (50% probability. Hydrogen atoms have been omitted for clarity. The [HN(*i*-Pr)$_2$Et]$^+$ cation and CH$_3$CN solvent molecules are not shown). 70

Figure 3.5 Optimized structure of deprotonated intermediate TaCl$_4$(CH$_3$CN)(CH$_2$CN) ..76

Figure 4.1 (a) Scheme of Reaction of TaCl$_5$/PPh$_3$ pair with benzonitrile with the formation of the Ta(V) imido complex [TaCl$_4${NC(H)(PPh$_3$)C$_6$H$_4$(PPh$_3$)}(NCC$_6$H$_5$)][TaCl$_6$] (**1**). (b) A fragment of the ^{31}P{^{1}H} NMR spectrum of **1** in CD$_2$Cl$_2$. (c) The displacement ellipsoid plot (50% probability) of **1**. The majority of hydrogen atoms and carbon atoms of triphenylphosphonium groups and the benzonitrile ligand are omitted for clarity. The [TaCl$_6$]$^-$ counterion and co-crystallized chlorobenzene solvent molecules are not shown. 89

Figure 4.2 The DFT-optimized structure of the poposed substituted intermediate in the formation of **1.** Interatomic distances correspond to the formulation of the complex as a Ta(V) azaallenylidene. 91

Figure 4.3 The EPR spectrum of the reaction mixture during the synthesis of **1** in CH$_2$Cl$_2$.....95

Figure 4.4 (a) Reaction of the Ta(V) imido complex **1** and Hunig's base with formation of the bimetallic Ta(V) enediimido complex [TaCl$_4${NC(C$_6$H$_4$PPh$_3$)CC(PPh$_3$C$_6$H$_4$)CN}TaCl$_4$](NCC$_6$H$_5$)$_2$ (**2**). (b) The displacement ellipsoid plot (50% probability) of **2**. Co-crystallized CH$_2$Cl$_2$ solvent molecules are not shown. 96

Figure 4.5 (a) Reaction of TaCl$_5$/PPh$_3$ pair with acetonitrile with the formation of the vinylimido Ta(V) complex Ta{NC(PPh$_3$)CH$_2$}Cl$_4$(CH$_3$CN) (**3**). (b) A fragment of the ^{1}H NMR spectrum of **3** in CD$_2$Cl$_2$. (c) The displacement ellipsoid plot (50% probability) of **3**. The majority of hydrogen and carbon atoms of the triphenylphosphonium group and the acetonitrile ligand are omitted for clarity. The [TaCl$_6$]$^-$ counterion is not shown. 98

Figure 4.6 (a) Synthesis of the vinylimido Ta(V) complex Ta{NC(PPh$_3$)CH$_2$}Cl$_4$(CH$_3$CN) (**3**). (b) Synthesis of (TaCl$_4$){NC(PPh$_3$)CHCH(PPh$_3$)CN}TaCl$_4$)(NCC$_2$H$_4$CN)$_2$, the bimetallic Ta(V) *anti*-1,4-diimido-*s-trans*-1,3-butadiene complex (**4**). (c) The displacement ellipsoid plot (50%

probability) of **4**. (The majority of hydrogen atoms and carbon atoms of the succinonitrile ligand are omitted for clarity. Co-crystallized dichloromethane solvent molecules are not shown. 100

Figure 5.1 Displacement ellipsoid plot (50% probability) of **3-^{i}Pr**. Hydrogen atoms have been omitted for clarity. 124

Figure 5.2 ^{1}H NMR spectra of a mixture of **1-^{i}Pr** and excess MeCN. Notice the disappearance of the signals from **1-^{i}Pr** and the emergence of the signals from **1-Me** during the conversion. 130

Figure 5.3 ^{1}H NMR spectra of a mixture of **1-^{i}Pr** and excess EtCN. Notice the disappearance of the signals from **1-^{i}Pr** and the emergence of the signals from **1-Et** during the conversion 131

Figure 5.4. ^{1}H NMR spectra of a mixture of **1-Me** and excess EtCN. Notice the disappearance of the signals from **1-Me** and the emergence of the signals from **1-Et** during the conversion. The presence of $HNEt_3Cl$ is due to an equilibrium between $[Ta(NCCH_2\{NEt_3\})Cl_4](MeCN)]$ and $[Ta(NCCH_2\{NEt_3\})Cl_5](HNEt_3)]$ in CH_3CN. 132

Figure 5.5 The ^{1}H NMR spectrum of a mixture of **1-Et** and excess MeCN after heating for 2 weeks at 50 ºC 133

Figure 5.6 The ^{1}H NMR spectrum of a mixture of **1-Me** and 5 equiv. CD_3CN after heating at 40 ºC (partial conversion). Notice the appearance of a signal from C**D**$_2$HCN. Asterisks denote signals from the vinylimido group in Ta{NC=C**H**(**D**)NEt_3}$Cl_4(CD_3CN)$ and the remaining Ta{NC=C**H**$_2NEt_3$}$Cl_4(CD_3CN)$. 134

Figure 5.7 Fragments of ^{1}H NMR spectra of a mixture of **1-Me** and 5 equiv. CD_3CN after heating at 40 ºC. Notice the gradual appearance of a signal from C**D**$_2$HCN. 135

Figure 5.8 ^{1}H NMR spectra of a mixture of **1-Me** and excess PPh_3. Notice the disappearance of the signals from **1-Me** and the emergence of the signals from **2-Me** during the conversion. The presence of $HNEt_3Cl$ is due to an equilibrium between $[Ta(NCCH_2\{NEt_3\})Cl_4](MeCN)]$ and $[Ta(NCCH_2\{NEt_3\})Cl_5](HNEt_3)]$ in CH_3CN. 136

Figure 5.9 The ^{1}H NMR spectrum of **3-^{i}Pr** in CD_2Cl_2 137

Figure 5.10 The ^{13}C NMR spectrum of **3-^{i}Pr** in CD_2Cl_2 138

Figure 5.11 Kinetic data for the reaction of **1-^{i}Pr** with EtCN in CD_2Cl_2 at 40 ºC 139

Figure 5.12. Kinetic data for the reaction of **1-^{i}Pr** with CH_3CN (or CD_3CN) in CD_2Cl_2 at 40 ºC 140

Figure 5.13. The ^{1}H NMR spectrum of a reaction mixture after heating **1-^{i}Pr** at 45 ^{o}C in CD_2Cl_2 without an added nitrile (the spectrum has been recorded in the CD_2Cl_2/CD_3CN solvent mixture due to insolubility of products in CD_2Cl_2). Notice the disappearance of the signals from the starting imido complex and the emergence of the signals from the vinylimidocyanoalkyl group (labeled with asterisks) in 1:1:2 ratio. A similar complex has been synthesized in the reaction of $TaCl_5$ and ^{i}PrCN in the presence of Hunig's base...141

Figure 6.1 The X-ray crystallographic structure of $Ta_6N_5Cl_{15}(CH_3CN)_7$ (**1**)The top view showing pentagonal star shaped cluster and the side view at the bottom showing a planer geometry of the structure. The structure is simplified for clarity by removing methyl groups for the top view and only protons were omitted for the side view structure.....149

Figure 6.2 The X-ray crystallographic structure of {$Ta_6(N)_5Cl_{13}(C_2H_5N_2)_2(CH_3CN)_5$ (1a) The structure is simplified for clarity by removing all the chlorides and acetonitrile ligands.....150

Figure 6.3 Cyclic voltammogram of $Ta_6N_5Cl_{15}(CH_3CN)_7$ cluster.....151

Figure 6.4 X-ray crystallographic structure of the $Ti_4(\mu_3\text{-}N)_2Cl_{10}(CH_3CN)_6\cdot C_7H_8$. (**2**) Displacement ellipsoids drawn at the 60% probability level. For clarity, the methyl groups from acetonitrile ligands were omitted. 152

Figure 6.5 X-ray crystallographic structure of the $[H_3NSi(CH_3)_3]_3[Ti_9(\mu_3\text{-}N)_3Cl_{24}(NSi(CH_3)_3)_3]\cdot(C_7H_8)_3$(3).....153

List of Abbreviations

AN.....Acceptor Number

CLP .....Cooperative Lewis Pair

DCM ..... Methylene chloride

EtCN ..... Propionitrile

FLP.....Frustrated Lewis Pair

HMDS .....Hexamethyl disilazane

MeCN..... Acetonitrile

NMR ..... Nuclear Magnetic Resonance

PEt_3 ..... Triethylphosphine

PPh_3..... Triphenylphosphine

THF ..... Tetrahydrofuran

TMS .....Trimethylsilane

Chapter 1

Introduction to Cooperative Lewis Pairs Based on High-Valent Early Transition Metal Halides for Small Molecule Activation and Metal Nitrides.

1. Rahman, M. M.; Smith, M. D.; Peryshkov, D. V. *Organometallics*, **2018**, *37*, 2945-2949.
2. Rahman, M. M.; Smith, M. D.; Amaya, J. A.; Makris, T. M.; Peryshkov, D. V. *Inorg. Chem.*, **2017**, *56*, 11798–11803.
3. Rahman, M. M.; Smith, M. D.; Peryshkov, D. V. *Inorg. Chem.*, **2016**, *55*, 5101–51

1.1 Introduction:

Small molecule activation is an ever-increasingly attractive area of research in the field of organometallic chemistry; due in part to both fundamental challenges, such as cleavage of strong bonds, and vast opportunities that emerge for chemical synthesis, for instance the ability to selectively use small molecules as dinitrogen, dioxygen, or carbon dioxide as building blocks for the formation of C–N, C–O, or C–C bonds. After the second world war there has been a rapid rise in the consumption of chemically processed products and thus the development of chemical industries everywhere across the world largely backed by the petrochemical industry providing its much-needed feedstocks, which was possible for the continuous research in these areas. By the end of last century, the global environmental issues like the rising carbon dioxide concentration in the atmosphere, or depletion of fossil fuels in near future, played a significant role in burgeoning research interests to store renewable yet extractable energy in chemical bonds, as in artificial photosynthesis or fuel cells. At the same time the limited carbohydrate resources available can be used in more efficient ways (e.g., transforming nonconventional resources into viable products). Once we learn about our goals like solving common problems the choice of the right tool is always as important as the purpose it is going to serve. In this sense, if we target any substrate to work with, the inherent chemistry might leave us with few options. Catalytic chemistry has always given us the power of the "magic wand" to address these problems. As always it has been a favorite story to quote that how the Haber-Bosch process of synthetic nitrogen fixation has impacted the world. This apparently simple chemical fixation of nitrogen has been dominated by highly energy demanding heterogeneous catalysis. So, more energy efficient, mild, homogeneous catalytic systems

have become one of the most sought-after challenges of the "alchemy" of this era.[1] Homogeneous catalysis has always been a tool of choice because of its selectivity and efficiency in performing specific chemical reactions. Along with the selection of reaction specific catalytic metal center, the ligand manipulation gives us the power to develop a very potent and flexible catalyst. Conventionally, a reaction might take place at a metal center or often in the presence of a non-innocent ligand. Throughout the history of catalytic chemistry, we can largely see the influence of metal based catalysis where transition metals play a significant role. In a competitive manner, the sector for non-metal based catalysis has been sought-after for its own advantages over transition metal dependent catalytic chemistry. Main group based frustrated Lewis pair (FLP) chemistry, thus comes as a dynamic area to explore.

1.2 Frustrated Lewis-pairs:

Since the discovery of the frustrated Lewis pairs (FLPs), they have attracted enormous interest due to their potential usage in metal-free activation of small molecules.[2,3] The idea was generated when Piers and co-workers attempted to find an alternative option to resolve the problem associated with the Lewis acid system, BF_3-Et_2O. It was the exploitation of the synergistic effect of a nucleophile and electrophile to activate a substrate such as carbonyl functional group in presence of a Lewis acid system, BF_3-Et_2O instead of $ZnCl_2$.[4] In presence of organosilanes, the silyl group can attack the B-F bond and form fluorosilane by reducing the substrate, aldehyde or ketone, and transferring a hydride to the oxygen of carbonyl group.[5] With the use of perfluorinated $B(C_6F_5)_3$ as a Lewis acid, the siloxane group acted as a nucleophile to the carbocationic center of the

organoketone (**Scheme 1.1**).[6] Thus, instead of the stoichiometric reaction of Lewis acid with a substrate, a catalytic conversion can take place.

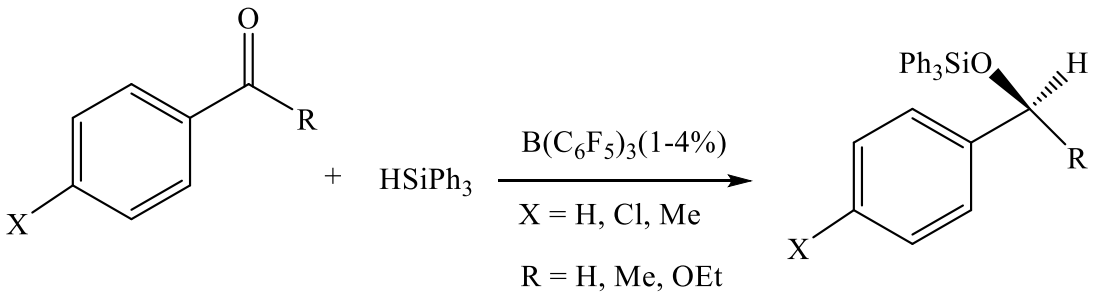

Scheme 1.1 $B(C_6F_5)_3$ catalyzed hydrosilylation of aromatic aldehydes, ketones, and esters.[4]

The combination of a sterically encumbered borane and a phosphine resulting in the unquenched Lewis acid-Lewis base pair led to a number of discoveries in the activation of dihydrogen[14], alkynes, carbon dioxide (**Scheme 1.2**), ketones, isonitriles, lactones, and other substrates.[7-13] These main-group based Lewis pair systems constitute a promising direction in the organometallic chemistry and catalysis; thus, generating an increased interest in the studies of cooperative action of Lewis bases and Lewis acids beyond non-metal centers.

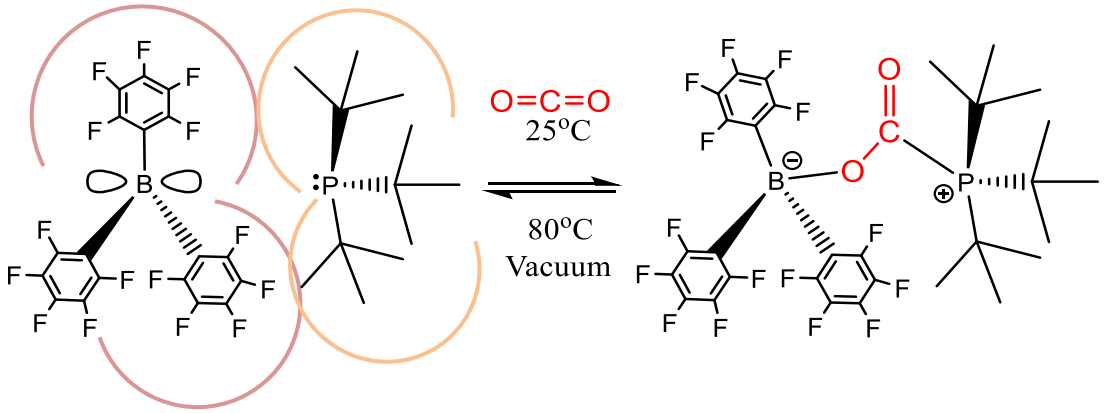

Scheme 1.2 Activation of CO_2 in $B(C_6F_5)_3$-$P(^tBu)_3$ FLP system.[13]

1.3 Cooperative Lewis-pairs:

In more recent times, Cooperative Lewis Pair (CLP) systems have emerged as the subclass of FLP systems as a collaborative effort of transitioning from main group based FLP chemistry to transition metal based organometallic chemistry.[15-21] To be noted here, in a CLP system, the Lewis acid and Lewis base may no longer be frustrated because of the absence of their steric hindrance but the cooperative effect of both entities may still be effective. For example, in our studied CLP systems, a bond between the Lewis acid and Lewis base pairs may form and can be isolated as a stable adduct (e.g., $TaCl_5$-PPh_3), while an FLP system cannot (**Scheme 1.2**).The cooperative effects between a Lewis acidic metal center and an intra- or intermolecular Lewis base functionality has been long recognized and utilized in a variety of bond activation processes where Noyori−Morris system (**Scheme 1.3**) act as only one of numerous prominent examples.[22-24]

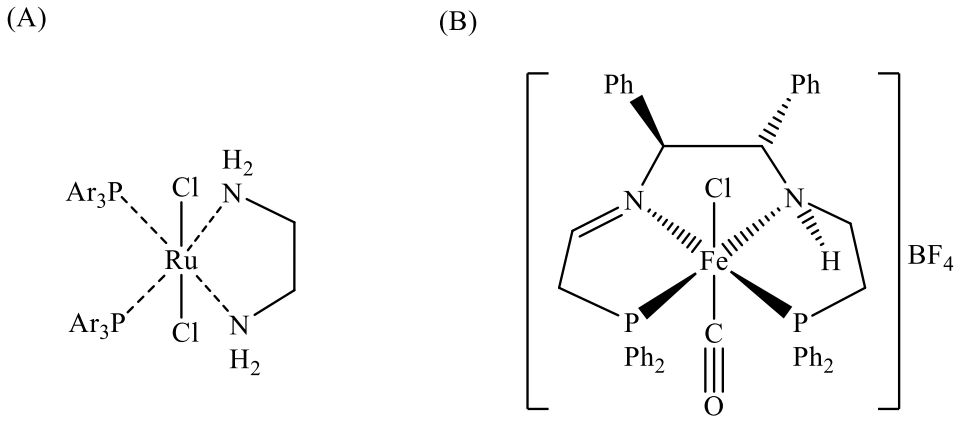

Scheme 1.3 Examples of precatalysts for Noyori (A) (Ar = 4-$CH_3C_6H_4$), and Morris (B) systems. [22-24]

In a rather uncommon example an ancillary metal center (e.g., cationic Ru) can transform an inactive system to an FLP system.[25] The mid and late transition metal-based

CLP systems (Pt, Re and $B(C_6F_5)_3$) are more preferred over early transition metal-based systems.[15,26] The fundamental disadvantage with early transition metal halides is their high oxophilicity, making the system inappropriate for many catalytic systems. Despite this fact, the study of early transition metal chemistry is still abundant. At the same time, an FLP-type behavior of cationic d^0 zirconocene species is a promising extension of the FLP concept to transition-metal-based Lewis acids. Specifically, these electron-deficient cationic zirconocene complexes bearing pendent phosphines have been shown to activate dihydrogen, which is an example of reactivity foreseen for main-group-based FLPs (**Scheme 1.4**).[16]

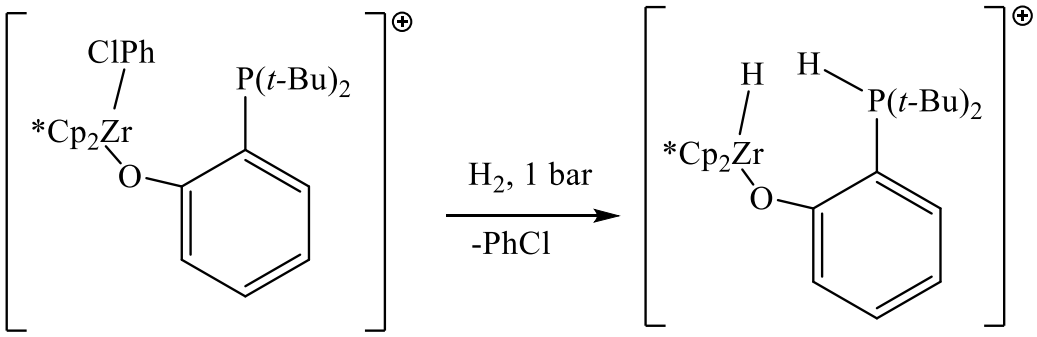

Scheme 1.4 Dihydrogen activation by zirconocene complex.[16]

FLPs are also known to activate many other organic small molecules. For example, the activation of organoethers involved with the main group based FLP chemistry has been reported on numerous occasions and so is with metal-based Lewis pair systems.[3,27] Organoalkynes, both the terminal and internal, are reported to be activated with low oxidation state early transition metal complexes. Templeton and co-workers have first reported about formation of Ta (I) η^2-RCCR complex.[28] Calderazzo and co-workers later have reported $[Nb(I)XCO)_2(RCCR')]_2$ (X = Br, I; R, R'= H, Ph) complexes. When PEt_3 was used in this system they simply replaced the halides and no interaction with

coordinated alkyne groups was reported. On numerous occasions Wigley, Yamamoto, Fryzuk, and Etienne have reported the formation of Ta (III), and Nb (III) alkyne cyclotrimer complexes by a two-electron reduction process.[28,30,31,33,34] These complexes can go through oligomerization with additional alkynes or substrates of other functionalities.

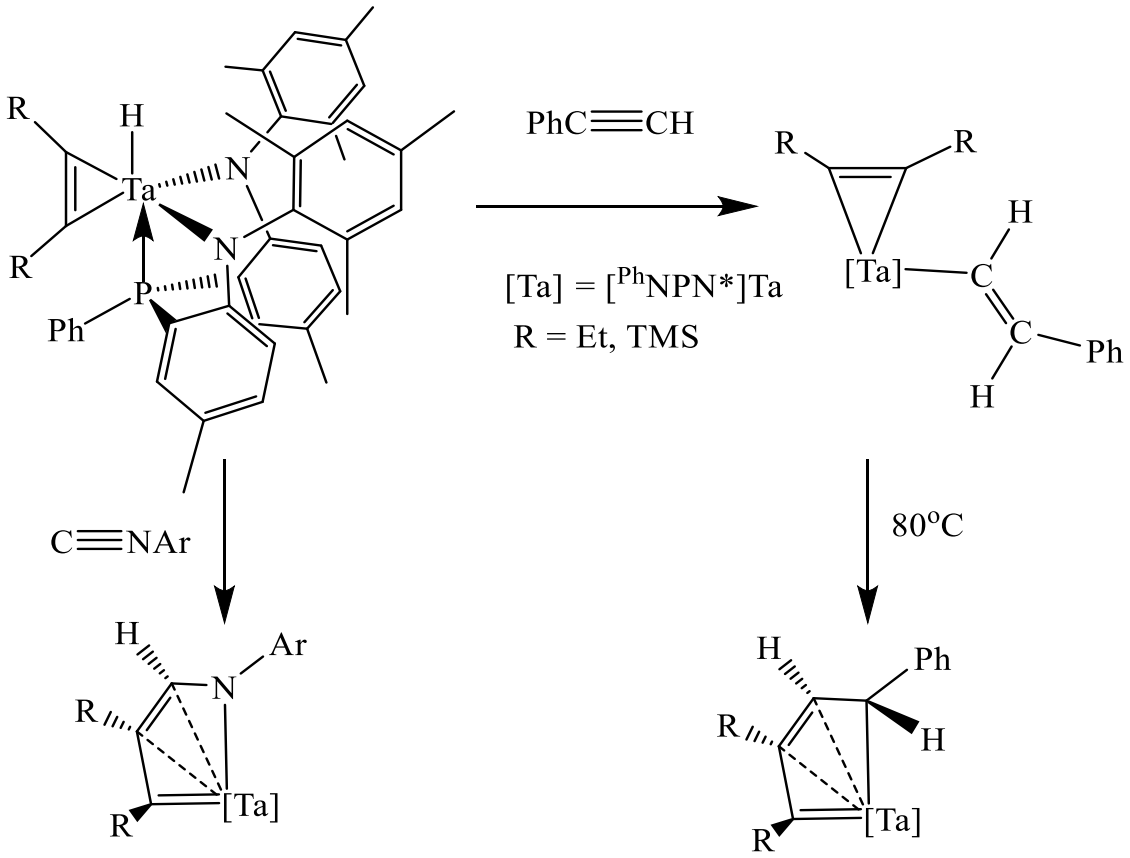

Scheme 1.5 Formation of tantalacycle via coupling of Ta alkyne ligand with additional functionalities.[31]

The number of substrates may vary with the steric bulkiness of the associated R groups.[30]. The reactions of these bridging alkynes and other unsaturated organic substrates generally occur by metallacyclization process (**Scheme 1.5**).[35,30,33] It was noted in the work by Fryzuk and coworkers that the phosphine ligand present in the system did not participate in any of the activation processes.[32]

Organonitriles enjoy popularity as versatile building blocks in organic synthesis. Acidic nitriles, such as malononitrile, can be deprotonated with strong bases with formation of nucleophilic carbanions, which have been employed in the synthesis of cyanoalcohols.[36-38] In contrast, C–H bonds of acetonitrile are generally stable towards deprotonation (pK_a = 31 in DMSO).[39] The stability of acetonitrile is a factor to its frequent use as a solvent in coordination chemistry; in fact, numerous basicity scales have been determined in acetonitrile.[40] Recently, activation of C–H bonds of nitriles coordinated to late transition metals (e.g., Ru (II), Cu (II), and Ni (II)) has been reported.[41-45] Once coordinated, acetonitrile has been shown to undergo deprotonation with strong bases such as DBU (1,8-Diazabicyclo[5.4.0]undec-7-ene), alkali- and transition metal alkoxides. Deprotonation of N-bound acetonitrile results in the formation of a carbanion[41,42] that, in some cases, has been shown to rearrange into C-bound cyanomethyl complexes (**Scheme 1.6**).[44,45]

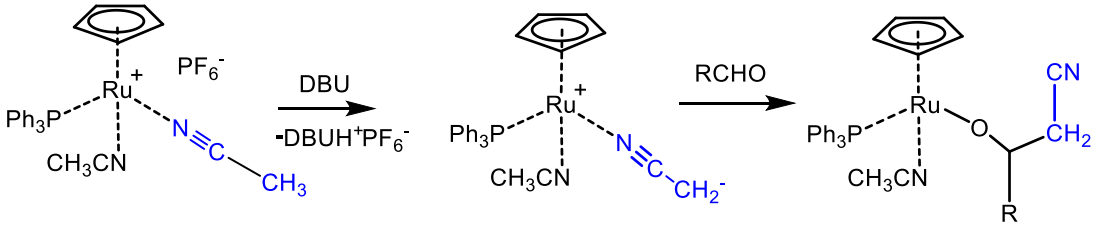

Scheme 1.6 Late metal promoted activation of acetonitrile.[41]

Furthermore, numerous nucleophilic and electrophilic addition reactions to the C≡N triple bond of metal-coordinated nitriles have been reported.[46-49] Calas R. has reported the activation of dinitriles as well as mononitriles with organosilanes and Lewis acidic $ZnCl_2$.[6] In the case of the dinitrile a cyclization reaction can take place accompanied by dehydrogenation (**Scheme 1.7**)

It is known that terminal imido groups have been used as ligands for high-valent early transition metal centers for several decades. In addition to being robust supporting ligands, these imido groups have been shown to participate in a wide range of stoichiometric reactions with unsaturated organic compounds, such as isocyanates, alkynes, alkenes, nitroso compounds, azides, and ketones.[50-57] Furthermore, there are a growing number of metathesis-type exchange reactions of high-valent imido complexes with carbodiimides, imines, amines, and, recently, isonitriles, in which the metal-containing product is also an imido complex, which often renders these transformations promising for catalysis.[58-63]

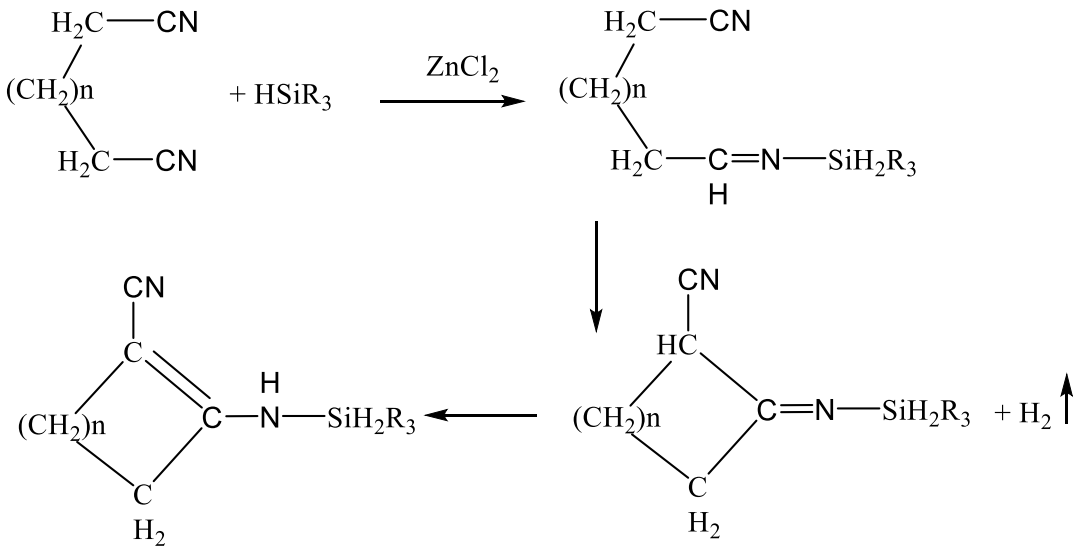

Scheme 1.7 Reaction of organosilane with dinitrile. [6]

1.4 The Gutmann-Beckett Scale:

The Gutmann-Beckett scale was developed for early transition metal halides and their derivatives to develop a comparative realization of their Lewis acidity in terms of an acceptor number (AN). In this scale, two reference points relating to the ^{31}P NMR chemical shifts of the phosphorus entity in triethylphosphine oxide (Et_3PO) were considered. As Et_3PO is coordinated to different acceptors via donor oxygen atom in a standard solvent of

least Lewis acidity (hexane) the chemical shifts changes with the studied compounds of variable Lewis acidity strengths.[64] This dissertation focuses to the study of early transition metal-based CLP chemistry for activation of different small molecules. A number of early transition metal halides and other derivatives were preliminarily selected and prepared. Based on their Lewis acidity preferred candidates were selected. The Gutmann-Beckett method has been used to construct a Lewis acidity scale for a number of species, including boranes, aluminum halides, and some transition metal halides.[65,66] Unfortunately, no data is available for $TaCl_5$, $NbCl_5$, or related derivatives. Therefore, a set of measurements were conducted to estimate Lewis acidity of the group 4 and 5 compounds that have been used in this work, and the results were compared with Lewis acids that are typical for metal-free FLP chemistry, such as $B(C_6F_5)_3$.

1.5 The Selection of Base:

Table 1.1 The basicity scale for selected organic bases.[98]

Base	pKa (ACN)
DBU	24.34
NEt_3	18.82
Proton sponge	18.62
pyridine	12.53
PEt_3	--
PPh_3	7.61
Ph_2NH	5.97
$(^iPr)_2NEt$	--
$(^iPr)_2NH$	--
Ph_2PCl	--
Ph_2NMe	--
$Ph_2PN((^iPr)_2$	--

One intriguing interest was to explore "the lower boundary" of the basicity of the Lewis base component that will still result in the cooperative reactivity. On this purpose of study of different Lewis bases in different Lewis pair systems, a series of organic bases were selected according to their basicity scale.[67] **Table 1.1** includes some of the selected and studied bases. These organic bases have shown to exhibit dual functions in some activation process, where a base itself can act as a nucleophile. These findings are elaborately discussed in **chapter 3** and **4**. Among the listed bases, $Ph_2PN^iPr_2$ was prepared by a literature synthetic procedure.[97]

1.6 Selection of Solvents

The solubility parameters of studied compounds have been observed to vary widely. Depending on the interaction with the compounds, the solvents may show variable coordination spheres around metal centers resulting in variable colored solution, formation of an adduct or involve in chemical reactions. For example, $TiCl_4$, as a liquid is readily soluble in toluene and gives a bright yellow-orange solution; whereas, with acetonitrile, it forms a yellow adduct and appears to be sparingly soluble. $ZrCl_4$ as a white powder has a hexa-coordinated polymeric system with bridging chlorides making it insoluble in many common organic solvents.[68] A preferred solvent (e.g., THF), can break down the polymeric formation and dissolve the metal halide by coordinating to the Zr metal center. $NbCl_5$ gives a deep orange solution in toluene. Although $TaCl_5$ should show better solubility in solvents with the increasing polarity it follows the trend as below,

Hexane << Tolune < Benzene < DCM < $CHCl_3$ < Et_2O < MeCN < THF.

Most of the studied compounds mentioned in **chapter 2**, are insoluble or sparingly soluble in moderately polar solvents such as toluene, or chloroform. A polar coordinating solvent

such as acetonitrile is often preferred over others. The compounds discussed in **chapter 3, 4,** and **5,** selection of a solvent is often difficult because of formation of either ionic, polymeric species, in fact, most of them are isolated as a hydrochloride salt. The synthesis of the imido complexes can often face the challenge in suitable solvent selection because of unavoidable reactivities with the cooperative system. For example, THF is known to polymerize in presence of $TaCl_5$.[99] The C-Cl bond in methylene chloride can be activated in presence of triethylamine. Most of the synthesized imido complexes can show nitrile exchange reactivities in presence of other organonitriles (**Chapter 5**) if used as a polar solvent. As these findings are discussed throughout the chapters of this dissertation selection of a suitable solvent can be challenging and limit the numbers of options. For example, a coordinating polar solvent lacking an alpha proton such as pivalonitrile can be one option to avoid relevant unwanted reactivities and still show sufficient solubility for some Lewis acidic metal halides and their imido complexes.

1.7 Early Transition Metal Nitrides:

There has been a growing interest in the study of early transition metal halide cluster compounds. These cluster compounds may often show a direct M-M bond between similar or different metal centers or a bridging atom may often accompany the compounds. For cluster compounds of V, Nb, Ta; the number of metal centers per cluster can vary from 2 to 6.[69] Among many early transition metal chalcogenide clusters reported, Smith *et al.* has synthesized the trinuclear tantalum cluster Ta_3QI_7 (Q = Se, Te) by a solid-state synthetic method.[70]

Among early transition metal nitrides, tantalum nitrides take on a special role in terms of their utility in the electronics industry. They can be used as a diffusion barrier for

copper by atomic layer deposition (ALD) method of a suitable tantalum precursor with ammonia (NH_3) or hydrazine (N_2H_4).[71,72] Among many synthetic methods for early transition metal nitrides tantalum nitrides can be grown from direct reaction between a precursor, $TaCl_5$ and with N_2 and H_2, NH_3, $LiNH_2$ and Li_3N via physical vapor deposition (PVD), chemical vapor deposition (CVD), or solvothermal synthesis.[73-76] There has been several methods known to synthesize tantalum nitrides from smaller clusters. For example, Plenio and co-workers have synthesized the benzene analogue of tantalum trimer $[Cp^*TaN(Cl)]_3$ (**Scheme 1.8**).[77,78] In these structures a repeated metal nitrogen double bond exists, where the pi bonds can provide additional stability to the structure.[79]

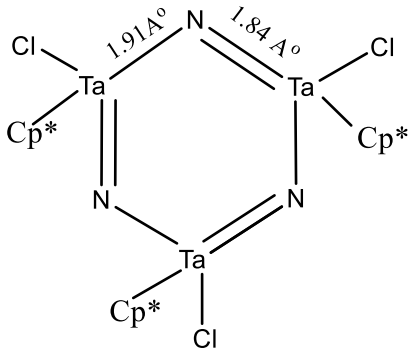

Scheme 1.8 $[Cp^*TaN(Cl)]_3$, ($Cp^* = C_5H_5(CH_3)_5$).

Wolczanski and co-workers later synthesized a similar trimer by substituting halide with methyl group $[Cp^*MeTaN]_3$[80] and ladder-like structures of Ta_5N_5 pentamer (**Scheme 1.9**). By variation of heating temperature and time, this precursor may yield amorphous to crystalline tantalum nitrides with variable crystal lattice structures.[81,82] Tantalum nitrides can show a significantly different physical and electrochemical properties based on their crystal lattice structures and tantalum to nitrogen ratios.[83,84] So far Terao N. has reported

a total of seven tantalum nitride phases which can inter-convert with applied heat under vacuum.[85]

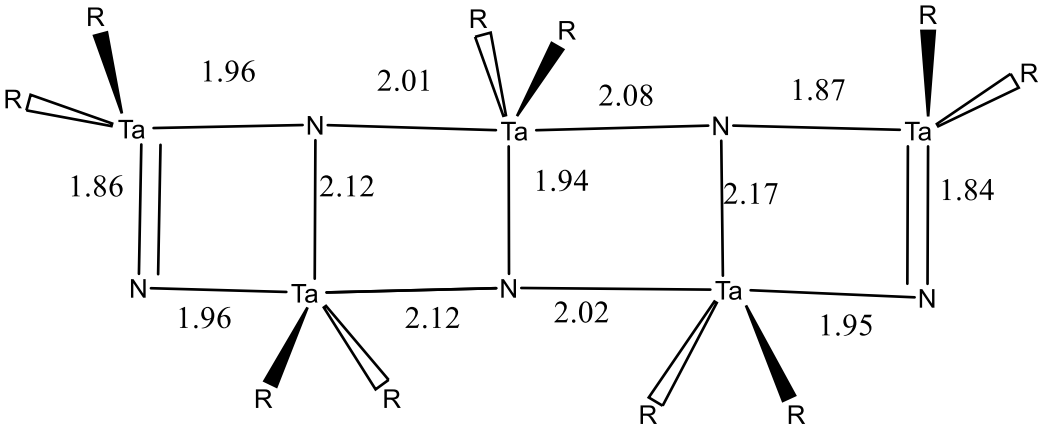

Scheme 1.9 $[(tBuCH_2)_2TaN]_5$ and R = $tBuCH_2$[80]. (Bond distances are in the unit of Å)

Tantalum nitrides alongside their oxides[86] are also studied for their photocatalytic activities under visible light as nanoparticles[87] and mesoporous Ta_3N_5 microsphere.[88] For photo-electrochemical water splitting, in photoanodes as thin film,[89,90] nanocrystals,[91] and nanotubes.[92,93] Mohandas and co-workers studied silica supported Ta_xN_y/TaO_xN_y nanoparticles as epoxidation catalysts with 99% selectivity.[94] There has been many reported works and patents of more suitable and volatile Tantalum imides and nitrogen containing precursors to be used for Ta_3N_5 preparation.[95,96] In our previous work, we have synthesized tantalum imido complexes by activation of alkyl and aryl nitriles in a facile synthetic pathway. These imido complexes may be used as a precursor to tantalum nitride synthesis.

1.8 The General Outline

In terms of reactivity of the early transition metal halides, $TaCl_5$/$NbCl_5$ have shown similar types of reactions. Similarly, deprotonation with $TiCl_4$ and $ZrCl_4$ have also been observed but they were not pursued at length. The scope of the further studies with other early transition metal halides remains open. However, $TaCl_5$ and their cooperative Lewis pair systems with various bases has been core concept of this dissertation. **chapter 2**, will entail the study about cooperative Lewis pairs, selection of reactive Lewis acids and their interaction with some diverse substrates as organic ethers, carbonyl compounds, and terminal alkynes. The **scheme 1.10** represents the major outlines of this dissertation.

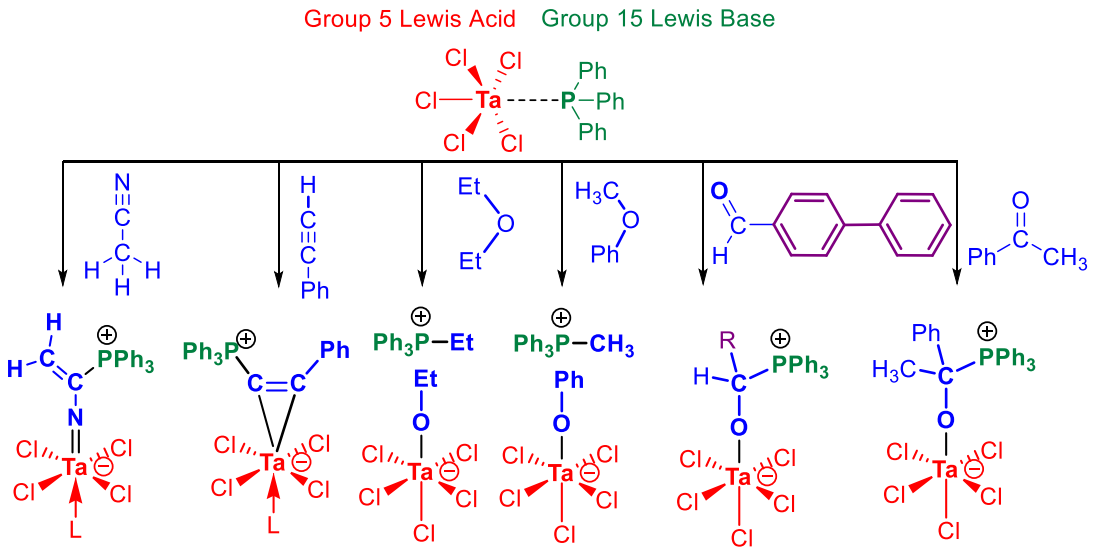

Scheme 1.10 The cooperative reactivity of Group 5-Group 15 representative Lewis pair ($TaCl_5$ · PPh_3) with a range of substrates.

Chapter 3 has concentrated on studies related to synthesis and reactivities with the CLP system of $TaCl_5$-NEt_3 as a major concept, but it also discusses about some complementary studies that have been pursued. **Chapter 4** entails the phosphine-based CLP system with $TaCl_5$ as the Lewis acid for organonitrile activation. Moreover, the chapter goes over the detailed studied of the novel reactivities with aromatic nitriles and

some alkyl dinitriles. **Chapter 5** has the area of studies about the reactivities of synthesized metal imido complexes. It will give a detailed narrative over the unforeseen exchange reactions of metal imido complexes with organonitriles and some preliminary studies about the reactivities with various organic substrates. In **Chapter 6**, a brief description of the study on early transition metal nitrides has been discussed. In summary, this dissertation can extend the area of early transition metal based cooperative Lewis pair systems. As our findings can abundantly support the idea of CLP chemistry, that a Lewis acidic metal center and Lewis base can act cooperatively despite neither being frustrated nor being active species independently but as a pair.

References

1. Chen, J., Crooks, R., Seefeldt, L., Bren, K., Bullock, R., Darensbourg, M., Holland, P., Hoffman, B., Janik, M., Jones, A., Kanatzidis, M., King, P., Lancaster, K., Lymar, S., Pfromm, P., Schneider, W. and Schrock, R. *Science*, **2008,** *360*(6391), eaar6611 (1-7).
2. D. W. Stephan, *Acc. Chem. Res.* **2015**, *48*, 306–316.
3. D. W. Stephan, G. Erker, *Angew. Chem. Int. Ed.* **2015**, *54*, 6400–6441.
4. Parks, D. and Piers, W. *J. Am. Chem. Soc.* **1996**, *118*(39), 9440-9441.
5. Doyle, M., West, C., Donnelly, S. and McOsker, C. *J. Org. Chem.*, **1976,** *112*(2), 129-140.
6. Calas, R. *Pure and Applied Chemistry*, **1966,** *13*(1-2), 61-80.
7. D. W. Stephan, *Org. Biomol. Chem.* **2008**, *6*, 1535–1539.
8. D. W. Stephan, *Dalton Trans* **2009**, 3129–3136.
9. M. Sajid, A. Stute, A. J. P. Cardenas, B. J. Culotta, J. A. M. Hepperle, T. H. Warren, B. Schirmer, S. Grimme, A. Studer, C. G. Daniliuc, R. Fröhlich, J. L. Petersen, G. Kehr, G. Erker, *J. Am. Chem. Soc.* **2012**, *134*, 10156–10168.
10. M. Sajid, G. Kehr, C. G. Daniliuc, G. Erker, *Angew. Chem. Int. Ed.* **2014**, *53*, 1118–1121.
11. Y. Zhang, G. M. Miyake, E. Y.-X. Chen, *Angew. Chem. Int. Ed.* **2010**, *49*, 10158–10162.
12. M. G. M. Knaus, M. M. Giuman, A. Pöthig, B. Rieger, *J. Am. Chem. Soc.* **2016**, *138*, 7776–7781.
13. D. W. Stephan, G. Erker, *Chem. Sci.* **2014**, *5*, 2625–2641.

14. G. C. Welch, J. D. Masuda, D. W. Stephan, *Inorg. Chem.* **2006**, *45*, 478–480.

15. S. J. K. Forrest, J. Clifton, N. Fey, P. G. Pringle, H. A. Sparkes, D. F. Wass, *Angew. Chem. Int. Ed.* **2015**, *54*, 2223–2227.

16. A. M. Chapman, M. F. Haddow, D. F. Wass, *J. Am. Chem. Soc.* **2011**, *133*, 18463–18478.

17. G. Erker, *Dalton Trans* **2011**, *40*, 7475–7483.

18. S. R. Flynn, D. F. Wass, *ACS Catal.* **2013**, *3*, 2574–2581.

19. N. S. Lambic, R. D. Sommer, E. A. Ison, *J. Am. Chem. Soc.* **2016**, *138*, 4832–4842.

20. O. J. Metters, S. J. K. Forrest, H. A. Sparkes, I. Manners, D. F. Wass, *J. Am. Chem. Soc.* **2016**, *138*, 1994–2003.

21. M. J. Sgro, D. W. Stephan, *Chem. Commun.* **2013**, *49*, 2610–2612.

22. Y. Shvo, D. Czarkie, Y. Rahamim, D. F. Chodosh, *J. Am. Chem. Soc.* **1986**, *108*, 7400–7402.

23. R. Noyori, T. Ohkuma, *Angew. Chem. Int. Ed.* **2001**, *40*, 40–73.

24. W. Zuo, A. J. Lough, Y. F. Li, R. H. Morris, *Science* **2013**, *342*, 1080–1083.

25. Boone, M. and Stephan, D. *J. Am. Chem. Soc.* **2013**, *135*(23), 8508-8511.

26. Bullock, R. *Science*, **2013,** *342*, 1054-1055.

27. Marchetti, F., Pampaloni, G. and Biancalana, L. *Inorg. Chim. Acta*, **2012,** *385*, 135-139.

28. Yasuda, H., Yamamoto, H., Arai, T., Nakamura, A., Chen, J., Kai, Y. and Kasai, N. Organometallics, **1991,** *10*(12), 4058-4066.

29. Oshiki, T., Tanaka, K., Yamada, J., Ishiyama, T., Kataoka, Y., Mashima, K., Tani, K. and Takai, K. *Organometallics,* **2003**, *22*(3), 464-472.

30. Strickler, J., Wexler, P. and Wigley, D. *Organometallics*, **1988,** *7*(9), 2067-2069.

31. Parker, K. and Fryzuk, M. *Organometallics*, **2014,** *34*(11), 2037-2047.

32. Parker, K. and Fryzuk, M. *Organometallics*, **2014,** *33*(21), 6122-6131.

33. Lorente, P., Carfagna, C., Etienne, M. and Donnadieu, B. *Organometallics*, **1996,** *15*(4), 1090-1092.

34. Oulié,, P., Bréfuel, N., Vendier, L., Duhayon, C. and Etienne, M. *Organometallics*, **2005,** *24*(17), 4306-4314.

35. Etienne, M., Carfagna, C., Lorente, P., Mathieu, R. and de Montauzon, D. *Organometallics,* **1999**, *18*(16), 3075-3086.

36. Kamila, S.; Zhu, D.; Biehl, E. R.; Hua, L. Org. Lett. 2006

37. Fukuda, Y.; Okamoto, Y. Tetrahedron 2002, 58, 2513−2521

38. Ankati, H.; Zhu, D.; Yang, Y.; Biehl, E. R.; Hua, L. *J. Org. Chem.* **2009,** *74*, 1658−1662.

39. Bordwell, F.G. Acc. Chem. Res. 1988, 21, 456–463.

40. Kaljurand, I.; Kütt, A.; Sooväli, L.; Rodima, T.; Mäemets, V.; Leito, I.; Koppel, I. A. *J. Org. Chem*. **2005**, *70*, 1019–1028.

41. Kumagai, N.; Matsunaga, S.; Shibasaki, M. *J. Am. Chem. Soc.* **2004**, *126*, 13632–13633

42. Fan, L.; Ozerov, O. V. *Chem. Commun*. **2005**, 4450–4453

43. Suto, Y.; Kumagai, N.; Matsunaga, S.; Kanai, M.; Shibasaki, M. *Org. Lett*. **2003**, *5*, 3147–3150

44. Chakraborty, S.; Patel, Y. J.; Krause, J. A.; Guan, H. *Angew. Chem. Int. Ed.* **2013**, *52*, 7523–7526

45. Oertel, A. M.; Ritleng, V.; Chetcuti, M. J.; Veiros, L. F. *J. Am. Chem. Soc.* **2010**, *132*, 13588–13589.

46. Kukushkin, V. Y.; Pombeiro, A. J. L. *Chem. Rev*. **2002**, *102*, 1771–1802

47. Kukushkin, V. Y.; Pakhomova, T. B.; Kukushkin, Y. N.; Herrmann, R.; Wagner, G.; Pombeiro, A. J. L. *Inorg. Chem*. **1998**, *37*, 6511–6517

48. Makarycheva-Mikhailova, A. V.; Bokach, N. A.; Kukushkin, V. Y.; Kelly, P. F.; Gilby, L. M.; Kuznetsov, M. L.; Holmes, K. E.; Haukka, M.; Parr, J.; Stonehouse, J. M.; Elsegood, M. R. J.; Pombeiro, A. J. L. *Inorg. Chem*. **2003**, *42*, 301–311

49. Lis, E. C.; Delafuente, D. A.; Lin, Y.; Mocella, C. J.; Todd, M. A.; Liu, W.; Sabat, M.; Myers, W. H.; Harman, W. D. *Organometallics*, **2006**, *25*, 5051–5058.

50. Hazari, N.; Mountford, P. *Acc. Chem. Res.*, **2005**, *38* (11), 839–849.

51. Schrock, R. R. *Chem. Rev*., **2009**, *109* (8), 3211–3226.

52. Chao, Y. W.; Wexler, P. A.; Wigley, D. E. *Inorg. Chem*. **1989**, *28* (20), 3860–3868.

53. Cundari, T. R. *J. Am. Chem. Soc*. **1992,** *114* (20), 7879–7888.

54. Polse, J. L.; Andersen, R. A.; Bergman, R. G. *J. Am. Chem. Soc.* **1998**, *120* (51), 13405–13414.

55. Tomson, N. C.; Arnold, J.; Bergman, R. G. Halo, *Organometallics* **2010**, *29* (13), 2926–2942.

56. Helgert, T. R.; Zhang, X.; Box, H. K.; Denny, J. A.; Valle, H. U.; Oliver, A. G.; Akurathi, G.; Webster, C. E.; Hollis, T. K. *Organometallics*, **2016,** *35* (20), 3452–3460.

57. Obenhuber, A. H.; Gianetti, T. L.; Berrebi, X.; Bergman, R. G.; Arnold, J. *J. Am. Chem. Soc.* **2014**, *136* (8), 2994–2997.

58. Zuckerman, R. L.; Krska, S. W.; Bergman, R. G. *J. Am. Chem. Soc.* **2000,** *122* (5), 751–761.

59. Cantrell, G. K.; Meyer, T. Y. *J. Am. Chem. Soc*. **1998**, *120* (32), 8035–8042.

60. Ong, T.-G.; Yap, G. P. A.; Richeson, D. S. *Chem. Commun.* **2003**, *20*, 2612–2613.

61. Guiducci, A. E.; Boyd, C. L.; Mountford, P. *Organometallics* **2006**, *25* (5), 1167–1187.

62. Gianetti Thomas L.; La Pierre Henry S.; Arnold John. *Eur. J. Inorg. Chem*. **2013**, *22-23*, 3771–3783.

63. Kriegel, B. M.; Bergman, R. G.; Arnold, J. *J. Am. Chem. Soc*. **2016,** *138* (1), 52–55.

64. M.A. Beckett, G.C. Strickland, J.R. Holland, and K.S. Varma, *Polymer*, **1996**, 37, 4629–4631

65. Beckett, M. A.; Brassington, D. S.; Coles, S. J.; Hursthouse, M. B. *Inorg. Chem. Commun*., **2000**, *3*, 530.

66. Konu, J. and Chivers, T. *Dalton Transactions*, **2006,** *32*, p.3941.

67. Kaljurand, I., Rodima, T., Pihl, A., Mäemets, V., Leito, I., Koppel, I. and Mishima, M. *Gas-Phase Journal of Organic Chemistry*, **2003**, *68*(26), 9988-9993.

68. Photiadis, G. and Papatheodorou, G. *Dalton Transactions,***1998**, *6*, 981-990.

69. Sokolov, M. and Fedin, V. *Coordination Chemistry Reviews*, **2004**, *248*(11-12), 925-944.

70. Smith, M. and Miller, G. *J. Am. Chem. Soc*., **1996,** *118*(48), 12238-12239.

71. Han, J., Kim, H., Lee, S., Kim, D., Park, B., Park, J., Jeon, D., Chung, T. and Kim, C. *Applied Surface Science*, **2016**, *362*, pp.176-181.

72. Burton, B., Lavoie, A. and George, S. *Journal of The Electrochemical Society*, **2008**, *155(7*), D508-516.

73. Bleau, J., Carmalt, C., O'Neill, S., Parkin, I., P. White, A. and Williams, D. *Polyhedron*, **2005,** *24*(3), pp.463-468.

74. Fitzmaurice, J., Hector, A. and Parkin, I. *Dalton Transactions*, **1993,** *16*, 2435.

75. Fix, R., Gordon, R. and Hoffman, D. *Chemistry of Materials*, **1993,** *5*(5), 614-619.

76. Mazumder, B., Chirico, P. and Hector, A. *Inorganic Chemistry*, **2008,** *47*(20), 9684-9690.

77. Dehnicke, K. and Strähle, J. *Angewandte Chemie Int. Edition in English*,**1992,** 31(8), pp.955-978.

78. Plenio, H., Roesky, H., Noltemeyer, M. and Sheldrick, G. *Angewandte Chemie International Edition in English*, **1988,** *27*(10), pp.1330-1331.

79. Wheeler, R., Hoffmann, R. and Straehle, J. *J. Am. Chem. Soc.*, **1986,** *108*, .5381-5387.

80. Holl, M., Kersting, M., Pendley, B. and Wolczanski, P. *Inorganic Chemistry*, **1990,** *29(8)*, 1518-1526.

81. Holl, M., Wolczanski, P. and Van Duyne, G. *Journal of the American Chemical Society*, **1990,** *112*, 7989-7994.

82. Banaszak Holl, M., Wolczanski, P., Proserpio, D., Bielecki, A. and Zax, D. *Chemistry of Materials*, **1996,** *8(10)*, pp.2468-2480.

83. Li, D., Tian, F., Duan, D., Bao, K., Chu, B., Sha, X., Liu, B. and Cui, T. *RSC Advances*, **2014**, *4(20)*, 10133-10139.

84. Hieber, K. *Thin Solid Films*, **1974,** *24(1)*, 157-164.

85. Terao, N. *Japanese Journal of Applied Physics*, **1971**, *10(2)*, 248-259.

86. Ambreen, S., Pandey, N., Mayer, P. and Pandey, A. *Beilstein Journal of Nanotechnology*, **2014,** *5*,.1082-1090.

87. Zhang, Q. and Gao, L. *Langmuir*, **2004,** *20(22)*, pp.9821-9827.

88. Cao, J., Ren, L., Li, N., Hu, C. and Cao, M. *Chemistry - A European Journal*, **2013,** *19(38)*, 12619-12623.

89. Abdel Haleem, A., Majumder, S., Perumandla, N., Zahran, Z. and Naruta, Y. *The Journal of Physical Chemistry C*, **2017,** *121(37)*, 20093-20100.

90. Hajibabaei, H., Zandi, O. and Hamann, T. *Chemical Science*, **2016,** *7(11)*, 6760-6767.

91. Kim, Y., Cha, S., Kwak, I., Kwon, I., Park, K., Jung, C., Cha, E. and Park, J. *ACS Applied Materials & Interfaces*, **2017,** *9(42)*, 36715-36722.

92. Cong, Y., Park, H., Wang, S., Dang, H., Fan, F., Mullins, C. and Bard, A. *The Journal of Physical Chemistry C*, **2012,** *116(27)*, 14541-14550.

93. Wang, L., Mazare, A., Hwang, I. and Schmuki, P. *Electrochemistry Communications*, **2016**, *72*, 27-31.

94. Mohandas, J., Abou-Hamad, E., Callens, E., Samantaray, M., Gajan, D., Gurinov, A., Ma, T., Ould-Chikh, S., Hoffman, A., Gates, B. and Basset, J. *Chemical Science*, **2017,** *8*(8), 5650-5661.

95. Hunter, S., Chen, S., Steren, C., Richmond, M. and Xue, Z. Organometallics, **2015**, *34*(24), 5687-5696.

96. Chen, T.; Xu, C.; Baum, T. Tantalum amide complexes for depositing tantalum-containing films, and method of making same, US 20060013943 A1, Jan 19, 2006.

97. Levason, W.; Light, M. E.; Reid, G.; Zhang, W. *Dalt. Trans.* **2014**, *43* (25), 9557–9566.

98. Kaljurand, I.; Kütt, A.; Sooväli, L.; Rodima, T.; Mäemets, V.; Leito, I.; Koppel, I. A. *J. Org. Chem.* **2005**, *70* (3), 1019–1028.

99. F. Marchetti, G. Pampaloni, T. Repo, *Eur. J. Inorg. Chem.* **2008**, *2008*, 2107–2112.

Chapter: 2

Activation of C–O and C–H Bonds by the $TaCl_5$–PPh_3 Cooperative Lewis Pair.

Rahman, M. M.; Smith, M. D.; Amaya, J. A.; Makris, T. M.; Peryshkov, D. V. *Inorg. Chem.*, **2017**, *56*, 11798–11803.

2.1 Introduction

The chemistry of Frustrated Lewis pair (FLP) is an ever expanding and active field. The great diversity of transition metal chemistry also led to the development of Lewis pairs composed of an electron-rich basic metal center and a main-group Lewis acid, thus reversing the roles of metal and non-metal components.[4] In general, the activation of a substrate upon coordination to a metal center for a subsequent attack by a reagent, such as a nucleophilic base, is an important reaction pathway for many metal-promoted transformations, for example, hydration or hydroamination of alkynes and alkenes.[2-6] High Lewis acidity of the metal center is often found to facilitate both coordination and activation steps.

Early transition metal complexes with low electron counts are strong Lewis acids and they have been demonstrated to participate in a multitude of ligand activation reactions. For instance, the chemistry of Nb and Ta complexes has been recently greatly expanded leading to discoveries of numerous transformations of small molecules.[10,11,20,12–19] Perhaps the simplest example of d^0 Group 5 compounds, their (Nb, Ta) chlorides, and bromides, are dimeric molecular species. In solution, these MX_5 halides form stable adducts with donor molecules; however, due to high Lewis acidity, the metal center tends to facilitate activation of a coordinated substrate. Ring-opening of THF, deoxygenation of phosphine oxides and sulfoxides by $NbCl_5$ and $TaCl_5$ have been recently reported.[17-20]

In this chapter, the facile activation of strong C–O and C–H bonds by a cooperative interaction of $TaCl_5$ and PPh_3 at room temperature have been narrated. Another illustration of the unusual reactivity of the $TaCl_5$–PPh_3 pair is the selective cleavage of $C(H_3)$–O bonds of anisole and the formation of the $[PPh_3Me][TaCl_5(OPh)]$ complex.

Main group based FLP:

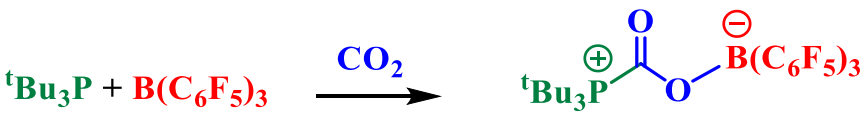

Metal based FLP:

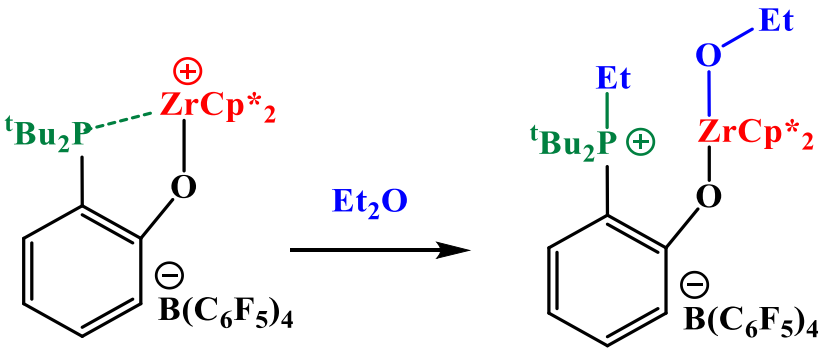

This work:

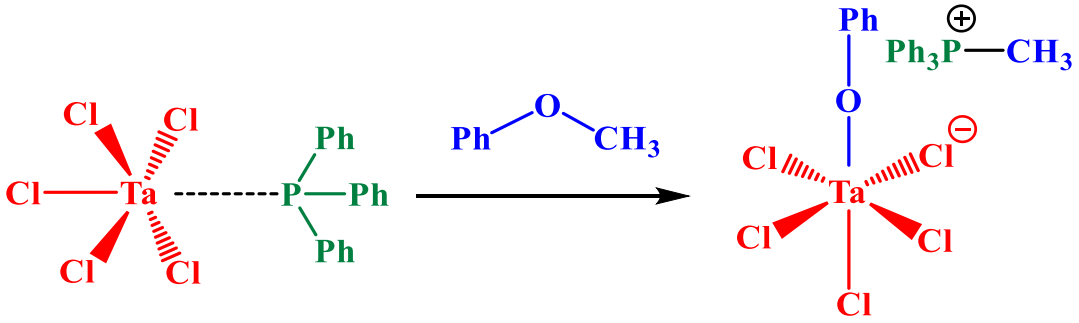

Scheme 2.1 comparative examples for main group based FLP [21], Metal Based FLP [22] and CLP system reported in this dissertation

2.2 Results and Discussion

A number of early transition metal halides and their derivatives were primarily selected as potential Lewis acids. The Lewis acidity of the following compounds in **table 2.1** have been studied by the Gutmann-Beckett method, which relies on the measuring the changes in the ^{31}P NMR chemical shifts of the Et_3PO upon coordination to a Lewis acid

center. By comparing the resulting acceptor numbers (AN), we were able to identify and understand the candidate Lewis acids and their unusual reactivities those have been the subject of study of this dissertation work.

Table 2.1 ^{31}P Chemical shifts in ppm from NMR results of different early metals Lewis acids and Et_3PO as Lewis base.

Lewis acids	Chemical Shifts (δ, ppm) of ^{31}P.		P-O bond distance(Å)		Acceptor Number [23] (AN = 2.21 x (δ_{sample} − 45.789)
	Singly coordinated	Doubly coordinated	Singly coordinated	Doubly coordinated	
Et_3PO*	45.789	--	1.46(1)	--	0
$(PhF_5)_3BOPEt_3$	37	--	1.4973(17)	--	82[24]
$TiCl_4$	92.153	89.353	--	--	102.46
$ZrCl_4$	96.493	93.715	--	1.521(3)	112.06
$ZrCpCl_3$	78.322	75.787	--	--	71.10
$NbCl_5$	102.766	95.296	--	1.5469(11)	**125.92**
$TaCl_5$	100.792	93.677	1.544(9)	1.528(5)	**121.56**
$TaCp^*Cl_4$	74.370	--	--	--	63.16
$Ta(^iPr)_2PhOCl_3$	82.688	--	--	--	81.55

Et_3PO* is a Lewis base that has been used for determining the chemical shifts upon forming coordination complexes with subject compounds.

Among all the selected early transition metal halides and their derivative compounds $TaCl_5$ and $NbCl_5$ possess the highest value for acceptor numbers, 121.56 and 125.92 consecutively. The acceptor numbers were determined by considering the value of Et_3PO in a solution of benzene, where benzene is accepted as the weakest Lewis acid. Thus, the value of ^{31}P chemical shift of Et_3PO in benzene was considered for the equation to calculate acceptor numbers (AN = 2.21 x ($\delta_{sample} - \delta_{weakest\ Lewis\ acid}$). **Figure 2.1** represents two crystallographically independent complexes $TaCl_5$-$OPEt_3$ and oxo-bridging $(TaCl_5$-$OPEt_3)_2O$ the co-crystallized and they both form adducts with a single coordination of PEt_3O. As our experimental results support the concept of the strong oxophilicity of $TaCl_5$

that was responsible for complete deoxygenation of Et_3PO. As a result, the oxo-bridged $(TaCl_5\text{-}OPEt_3)_2O$ formation was observed. As these early transition metal halides often prefer to stay as a hexacoordinated system, only one site to the metal center should be accessible to the phosphine oxide group. Interestingly we have found that the trans chloride is often flexible to be removed by a substituent as the bridging oxo group.

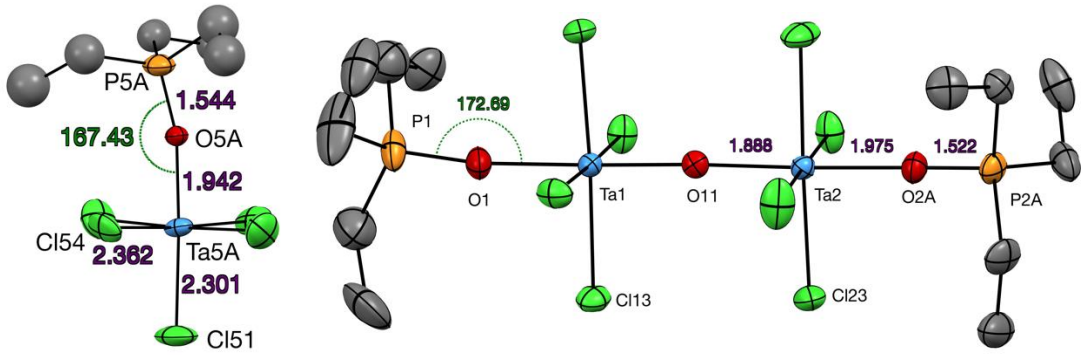

Figure 2.1. Displacement ellipsoid plots of $[Ta_2OCl_8(OP(CH_2CH_3)_3)_2]$ $[TaCl_5OP(CH_2CH_3)_3]$ (**2A**) drawn at 50% probability of complexes Ta1/Ta2 and Ta5. Only the major disorder component of the Ta5 complex is shown.

The adducts of $NbCl_5$ with Et_3PO can have both single or double coordination of Et_3PO. The **Figure 2.2** shows the molecular structure of isolated crystal for the

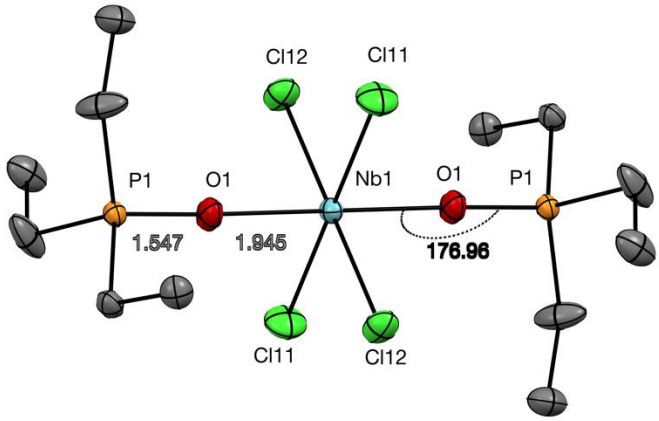

Figure 2.2. Displacement ellipsoid plots of $[NbCl_4(OP(CH_2CH_3)_3)_2]_2[Nb_4O_2Cl_{18}]$ C_6H_6 (**2B**) drawn at 50% probability level. Superscripts denote symmetry-equivalent atoms.

hexacoordinated system with two equivalents of Et_3PO in trans position, where one of the chloride anions is replaced by a second Et_3PO resulting in an anionic species. The single coordinated adduct was observed only in ^{31}P NMR spectroscopy and the ^{31}P chemical shift was recorded.

The **Figure 2.3** represents the molecular structure of $ZrCl_4$-$(OPEt_3)_2$ adduct, which also supports the previous comment that these metal halides often prefer to be in hexacoordinate system. A penta-coordinated compound is only possible if a bridging chloride coordinating ligand other than Et_3PO would take place in the trans position to the Et_3PO. It can also be an anionic chloride ligand with a counter cation and so the overall molecule is anionic or any coordinating solvent molecule occupying the trans position. The chemical shifts of double coordination adduct in a ^{31}P NMR spectroscopy of a mixture of both single and double coordination sites for Et_3PO would appear to move towards downfield region compared to a single coordination adduct. It is usually the values for a single coordination adduct with chemical shifts in the downfield region that was observed and considered as the experimentally acceptable values for the estimation of their Lewis acidity.

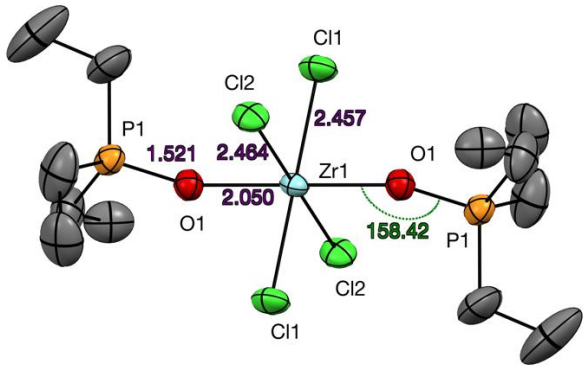

Figure 2.3. Displacement ellipsoids plot of (25% probability level) $ZrCl_4(OP(CH_2CH_3)_3)_2$. **(2C)** Superscripts denote symmetry-equivalent atoms.

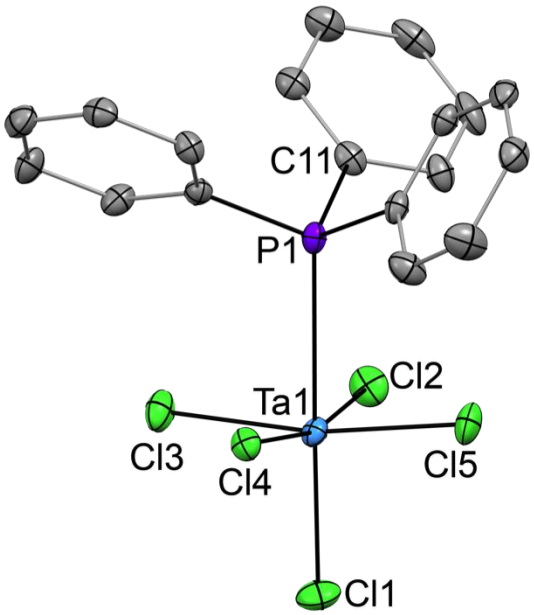

Figure 2.4. The displacement ellipsoid plot (50% probability) of the $TaCl_5 \cdot PPh_3$ adduct (**2D**). Hydrogen atoms are not shown. Selected distances (Å): Ta1–P1 = 2.792(1), Ta1–Cl1 = 2.303(1), Ta1–Cl2 = 1.316(1)

The $TaCl_5$–PPh_3 pair potentially represents the transition-metal based congener of borane-phosphine FLPs. Interestingly, the adduct $TaCl_5 \cdot PPh_3$ was isolated from the benzene solution containing the equimolar mixture of the metal halide and the phosphine. The crystal structure of this complex featured an elongated Ta–P distance of 2.792(1) Å, which belongs to the upper range of the reported Ta–PR_3 distances (2.459(8)–2.831(1) Å) for untethered phosphines. Incidentally, this adduct is the first structurally characterized trialkyl or triarylphosphine complex of a homoleptic tantalum(V) halide. The solution of the 1:1 mixture of $TaCl_5$ and PPh_3 in C_6D_6 indicated the persistence of the adduct with the sharp signal at 13 ppm in the ^{31}P NMR spectrum (**Figure 2.5**). However, we found that the formation of this moderately stable adduct does not preclude the unexpected reactivity reported below, i.e. the $TaCl_5$–PPh_3 system is a cooperative but not frustrated Lewis pair.[(49)]

On multiple occasions many vinyl imido complexes have been documented to form upon reactions of nitriles with Ti, V, and Ta alkylidenes and in the reactions of alkynes and Ti hydrazido complexes.[25-32] Importantly, results reported herein indicate that deprotonation of acetonitrile (pK_a = 31 in DMSO)[33] coordinated to $TaCl_5$ can occur even with the use of the relatively weak base PPh_3 (pK_a = 8 in CH_3CN).[34] In the majority of cases, deprotonation of N-coordinated acetonitrile resulted in the formation of a carbanion that has been shown to rearrange into the nucleophilic C-bound cyanomethyl group that can be subsequently attacked by electrophiles such as ketones or aldehydes.[35]

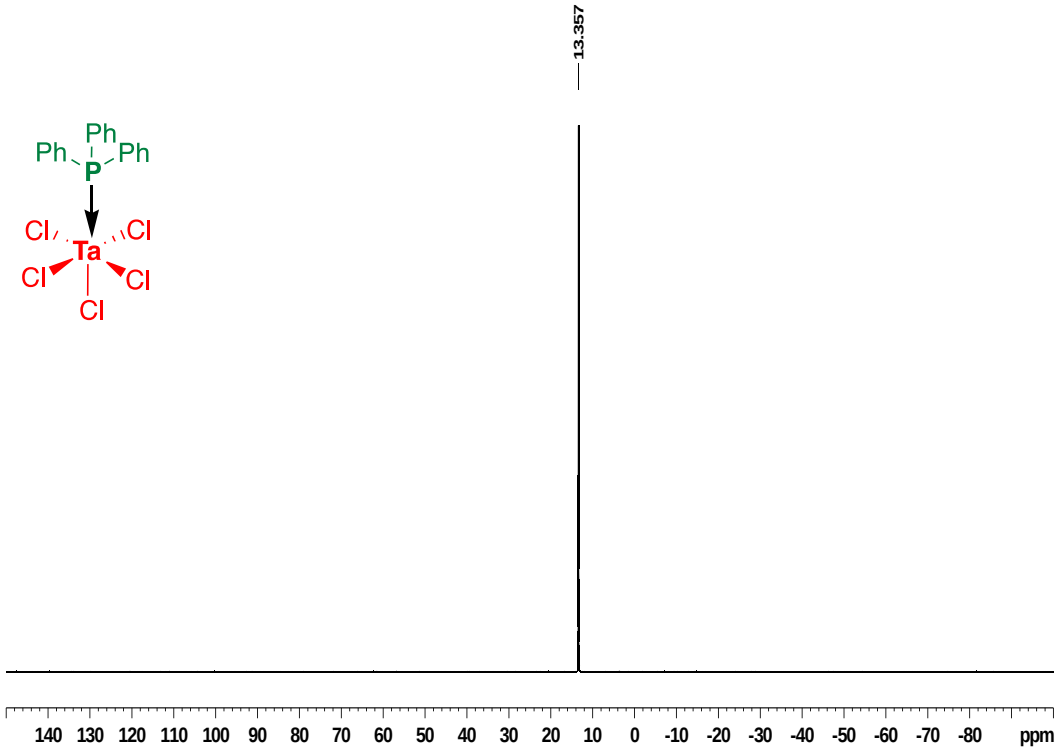

Figure 2.5 The $^{31}P\{^1H\}$ NMR spectrum of $TaCl_5 \cdot PPh_3$ in C_6D_6.

^{31}P NMR (121.5 MHz C_6D_6): δ 13.4

Encouraged by these results, we probed the reactivity of the $TaCl_5$–PPh_3 Lewis pair with another class of substrates containing relatively stable bonds. The activation of ethers and esters has recently attracted attention because of the presence of these functional groups in feedstocks of biological origin.[36] The reaction of the $TaCl_5$–PPh_3 pair with diethyl ether in a benzene solution led to the activation of the carbon-oxygen bond according to NMR spectral data. The sole organic product of this reaction was $[PPh_3Et]^+$ (**Scheme 2.2**) according to ^1H and ^{31}P NMR data. Therefore, the activation of diethyl ether proceeded twice with cleavage of both C–O bonds.

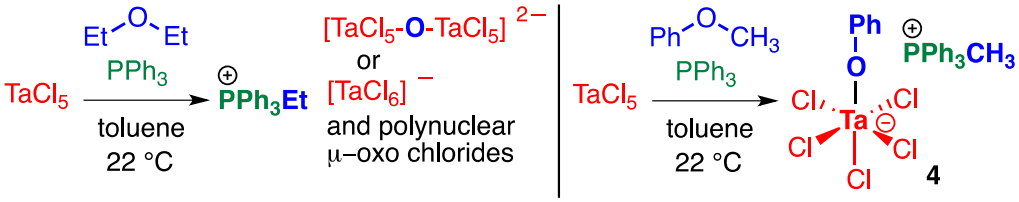

Scheme: 2.2 General synthesis of complexes with acetophenone and bisphenyl aldehyde with $TaCl_5/PPh_3$.

The fate of the oxygen atom is not firmly established at this moment as numerous attempts to identify the oxygen-containing product failed. It is likely that the oxo-bridged Ta(V) chloroanions such as $[(TaCl_5)O(TaCl_5)]^{2-}$ or higher nuclearity species were formed in the reaction.[37,38] Notably, this reaction proceeded at room temperature. This transformation may be considered as an S_N2-type reaction where the nucleophilicity of coordinated ether drastically increases upon coordination to the highly electron deficient and oxophillic Ta(V) center. While there are numerous examples of C–O bond activation in cyclic ethers such as THF,[18,39,40] the examples of the cleavage of C–O bonds of acyclic ethers and especially Et_2O under mild conditions are rare.[35,36] The related cationic zirconocene complexes with tethered phosphine ligands have been reported to activate

diethyl ether in a similar manner.[43] Importantly, $TaCl_5$ did not exhibit any reactivity towards diethyl ether without the presence of a Lewis base (PPh_3).[54]

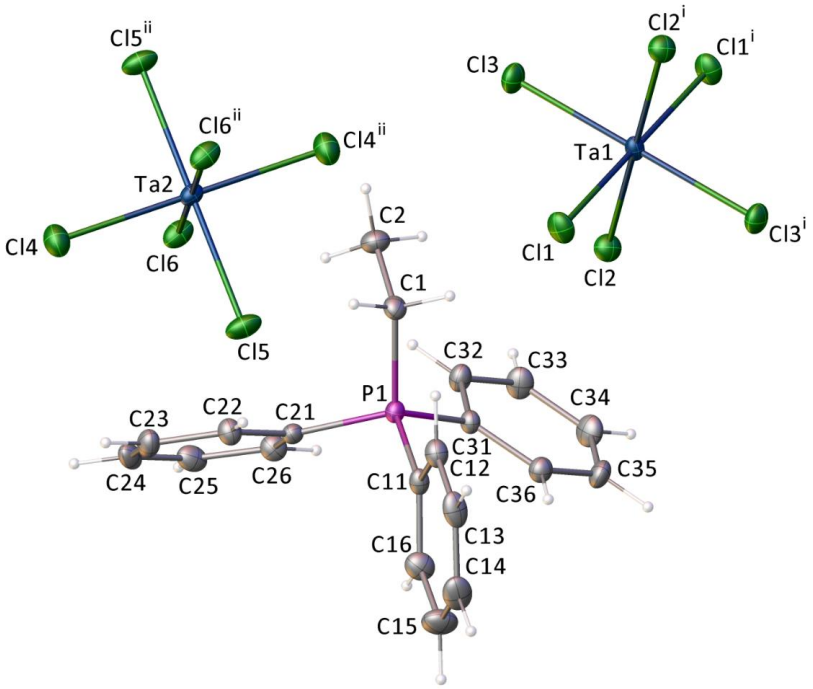

Figure 2.6: Displacement ellipsoids of $[P(CH_2CH_3)(C_6H_5)_3][TaCl_6]$ (**2E**) drawn at the 60% probability level. Both $TaCl_6^-$ anions are located on crystallographic inversion centers and therefore only half of each is present per cation. Selected distances (Å) and angles (°): P1–C1 = 1.8012(18), P1–C11 = 1.7948(18), P1–C1–C2 = 114.01(13), P1–C1–C11 = 108.84(9).

To further probe this type of C–O bond activation, we carried out the reaction of the $TaCl_5/PPh_3$ pair with anisole, PhOMe, in toluene at room temperature (**Scheme 2.2**). The facile reaction led to the formation of a single product according to ^1H and ^{31}P NMR data. It indicated that the bond of anisole was cleaved selectively between the methyl group carbon and the oxygen atom with the formation of the single $[PPh_3Me][TaCl_5(OPh)]$ product (**Figure 2.7**). The single crystal X-ray diffraction confirmed the proposed formulation. No reactivity between $TaCl_5$ and PhOMe was observed in the absence of a Lewis base. The cleavage of aryl-alkyl ethers has recently attracted renewed attention with

the studies of transformations promoted by late transition metal complexes through oxidative addition. In some cases, selective cleavage of either C(sp^2)–O or C(sp^3)–O bonds has been observed.[44-47]

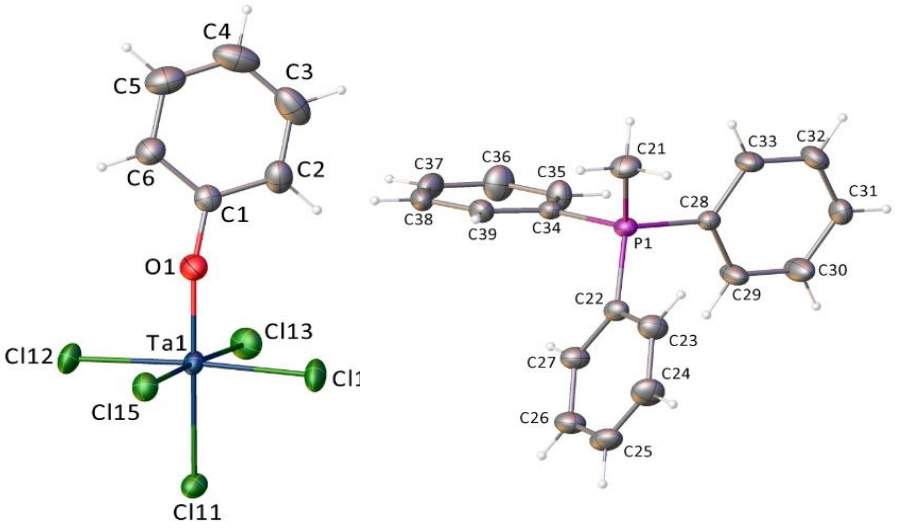

Figure 2.7: The displacement ellipsoid plot of $[PCH_3(C_6H_5)_3][TaCl_5(OC_6H_5)]\cdot(C_7H_8)_{0.25}$ (**2F**) (drawn at 50% probability level). Anion Ta1 and cation P1. Co-crystallized toluene disordered over a crystallographic inversion center are not shown. Selected distances (Å) and angles (°): Ta1–O1 = 1.848(2), O1–C1 = 1.349(3), P1–C21 =1.787(3), P1–C22 =1.798(3), Ta1–O1–C1 = 161.62(18), C21-P1-C22 = 109.94(13).

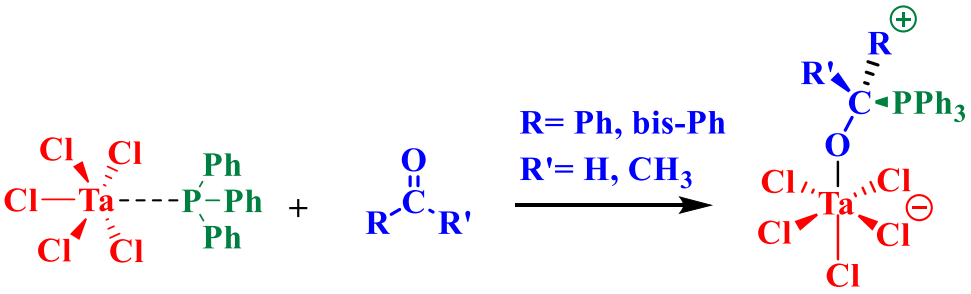

Scheme 2.3 General synthesis of complexes with acetophenone and bisphenyl aldehyde with $TaCl_5/PPh_3$.

The $TaCl_5/PPh_3$ CLP system in interaction with carbonyl groups (=CO) has been shown to activate both organic ketone and aldehyde groups (**Scheme 2.3**). For example,

the addition of 1 equivalent of acetophenone ($PhCOCH_3$) in a solution of 1 equivalent of PPh_3 and equimolar $TaCl_5$ in benzene, yields a product (**2G**) in abundance as spiky needle shaped crystals. Single-crystal X-ray diffraction reveals that the PPh_3 has coordinated to the acetophenone molecule at the carbon atom of the =CO functional group, by forming a stable P-C single bond and this unit is ligated to a $TaCl_5$ unit through the oxygen atom by forming an O-Ta single bond (**Figure 2.8**). As a result, the double bond between carbon and oxygen of carbonyl group has transformed into a single bond and the entire group is acting as an anionic ligand to the Ta metal center. The whole complex is zwitterionic with a cationic charge at the P atom and an anionic charge at the metal center. The Ta1-O1 distance in the crystal structure is 1.872(5) Å, which is representation of a single bond.

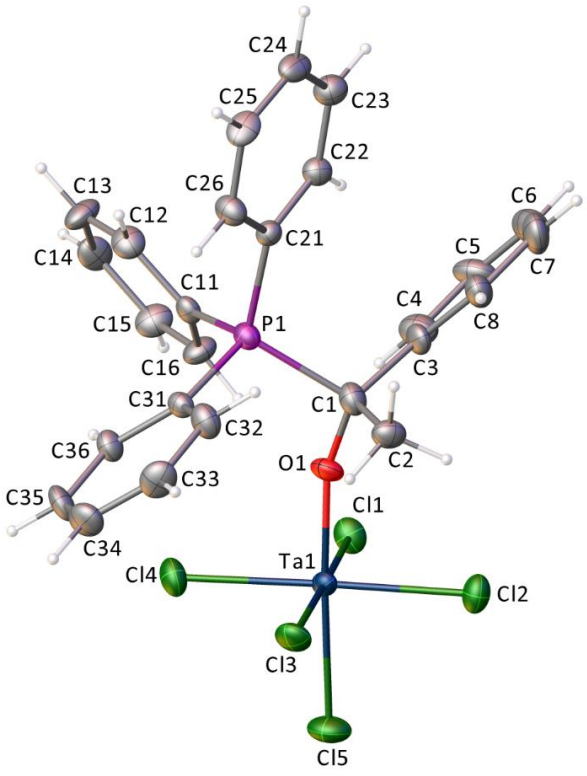

Figure 2.8 Displacement ellipsoid plots (60% probability) of the molecular structure of $TaCl_5(C_{26}H_{23}OP)$ (**2G**) Selected distances (Å) and angles (°): Ta1–O1 =1.872(5), O1–C1 =1.411(8), P1–C1 =1.912(6), C1–C2 =1.514(8), C1–C3 = 1.539(9), P1-C11 = 1.807(6), Ta1–O1–C1 = 158.3(4), P1-C1-O1 = 104.3(4).

In case of aldehyde 1 equivalent of 4-phenylbenzaldehyde ($C_6H_5C_6H_4CHO$) in a solution of 1 equivalent of PPh_3 and equimolar $TaCl_5$ in chlorobenzene, yields a product (**2H**) in abundance. Single-crystal X-ray diffraction reveals that the PPh_3 has coordinated to the at the carbon atom of the =CO functional group, by forming a stable P-C single bond and the oxygen atom by forming an O-Ta single bond (**Figure 2.9**). As a result, the double bond between carbon and oxygen of carbonyl group has transformed into a single bond. The whole complex is zwitterionic with a cationic charge at the P atom and an anionic charge at the metal center. The Ta1-O1 distance in the crystal structure is 1.8863(16) Å, which is within the range of a single bond and comparable to the compound **2G**.

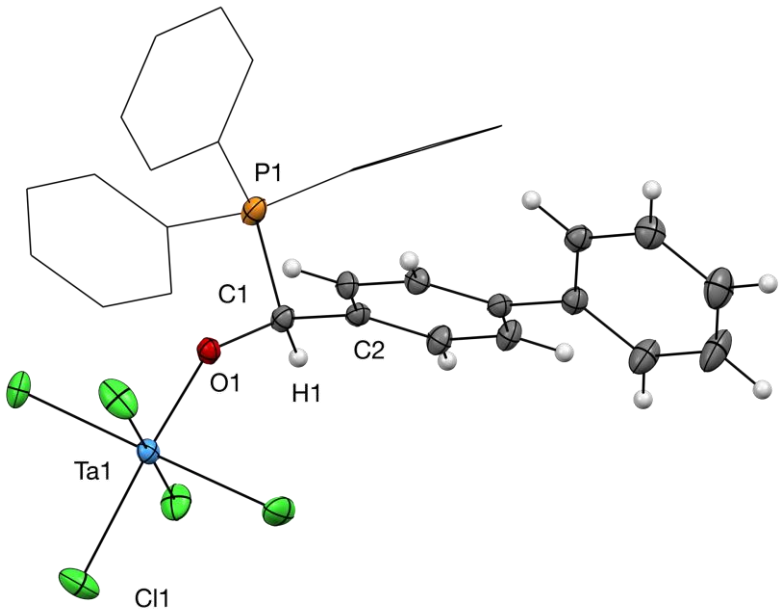

Figure 2.9 The displacement ellipsoid plot (50% probability) of $TaCl_5(OCH(C_{12}H_9)(P(C_6H_5)_3))\cdot(C_6H_5Cl)_{0.5}$ (**2H**). Co-crystallized disordered C_6H_5Cl solvent molecules are not shown here. Hydrogens in PPh_3 moiety are omitted for clarity. Selected distances (Å) and angles (°): Ta1–O1 =1.8863(16), O1–C1 =1.394(3), P1–C1 =1.865(2), C1–C2 =1.508(3), P1-C21 =1.793(2), Ta1–O1–C1 =145.05(14), P1-C1-O1 = 106.66(14).

Organoalkynes are another important substrate in organometallic synthetic chemistry. The $TaCl_5$-PPh_3 cooperative Lewis Pair can activate terminal alkyne. For example, two equivalents of PPh_3 and one equivalent $TaCl_5$ as a solution in toluene can activate phenylacetylene (**Scheme 2.4**).

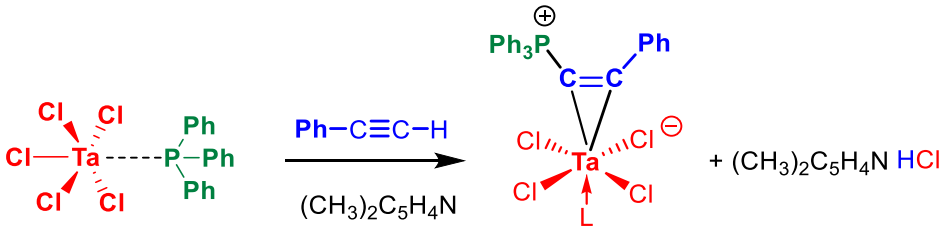

Scheme: 2.4 Reaction of phenyl acetylene with $TaCl_5/PPh_3$ Lewis pair.

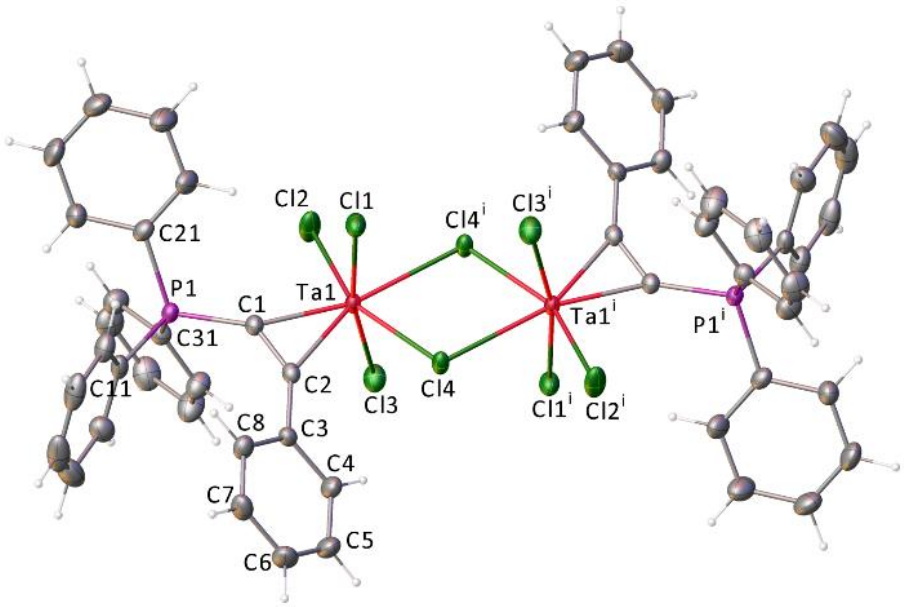

Figure 2.10: Displacement ellipsoid plot of the molecular structure of $Ta_2Cl_8(\eta^2$-$C_6H_5CCP(C_6H_5)_3)_2$ (**2I**) Displacement ellipsoids drawn at the 60% probability level. Selected distances (Å) and angles (°): Ta1-C1 =2.096(2), Ta1-C2 = 2.101(2), C1-C2 = 1.318(3), C2-C3 = 1.457(3), Ta1-Cl4 = 2.5258(5), Ta1-$Cl4^1$ = 2.6427(5), Ta1-C1-P1 = 148.13(13), C1-C2-Ta1 = 71.48(14), C1-Ta1-C2 = 36.59(8).

In presence of a base, lutidine the compound **2I** crystallizes as orange needles. Single crystal X-ray diffraction study shows an interesting structure, where the terminal hydrogen is deprotonated by one equivalent of PPh_3 and the anionic ligand can coordinate

to the Ta metal center. The triple bond of alkyne group can become a 4-electron donor ligand forming a cyclotrimer complex. The PPh_3 can coordinate to the α-carbon forming a P-C single bond (**Figure 2.10**).

In **table 2.2** a comparison between different bond distances and bond angles between some of the above-mentioned compounds shows that how the individual bonds may relate to each other. For example, the compounds formed by the activation of ethers (Et_2O, and anisole) and carbonyl compounds the C-O single bonds are all within the comparable ranges for a C-O single bond.

Table 2.2: Selected bond distances and bond angles of compounds **2E, 2F, 2G, 2H**

Compounds	bond distance(Å)			P-O bond Angles (°)	
	Ta-O	C-O	P-C	Ta-O-C	O-C-P
2E			1.8012(18)		
2F	1.848(2)	1.349(3)	1.787(3)	161.62(18)	
2G	1.872(5)	1.411(8)	1.912(6)	158.3(4)	104.3(4)
2H	1.8863(16)	1.394(3)	1.865(2)	145.05(14)	106.66(14)

In summary, the aforementioned results demonstrate the high potential of the $TaCl_5$-PPh_3 cooperative Lewis pair for the activation of strong bonds including C–H and C–O. The ability of the highly Lewis acidic Ta(V) center to coordinate and activate remote positions of a substrate through a bond rearrangement sequence, which is driven by the propensity of the metal center to form multiple bonds to a ligand, is the main distinguishing feature of this system. The $TaCl_5$–PPh_3 pair thus combines reactivity patterns of the frustrated Lewis pairs and "traditional" transition metal complexes. These results also demonstrate that even in the case of seemingly simple and well-understood systems, such as the $TaCl_5$–PPh_3 couple, a novel latent reactivity can be discovered. More examples of

unusual transformations can be anticipated as the utilization of transition metals as the Lewis acid or Lewis base components of frustrated or cooperative Lewis pairs is becoming increasingly studied.

2.3 Synthesis:

All synthetic manipulations were carried out either in a nitrogen-filled glovebox or on an air free dual-manifold Schlenk line, unless stated otherwise. The solvents were sparged with nitrogen, passed through activated alumina, and stored over activated 4 Å Linde-type molecular sieves. Benzene and chlorobenzene were distilled over CaH_2. $CDCl_3$, CD_2Cl_2, and CD_3CN were degassed and stored over activated 4 Å Linde-type molecular sieves. NMR spectra were recorded using Varian spectrometers and reported in δ (parts per million) and referenced to residual $^{1}H/^{13}C$ NMR signals of the deuterated solvent or an external 85% phosphoric acid (^{31}P (δ): 0.0 ppm) standard. *J* values are given in Hz. Midwest Microlab, Indianapolis, Indiana provided the elemental analysis results. $TaCl_5$ (Strem), Et_3PO, and PPh_3 were used as received.

Synthesis of $[Ta_2OCl_8(OP(CH_2CH_3)_3)_2][TaCl_5OP(CH_2CH_3)_3]$ (2A):

An equimolar solution of $TaCl_5$ and Et_3PO in chlorobenzene were gently mixed together in a 20 ml glass vial left unperturbed for overnight period. Crystalline products were formed, which was subjected to be studied by dissolving in deuterated benzene for NMR spectroscopy and submitted for X-ray crystallographic analysis.

Synthesis of $[NbCl_4(OP(CH_2CH_3)_3)_2]_2[Nb_4O_2Cl_{18}]\cdot C_6H_6$ (2B):

An equimolar solution of $NbCl_5$ and Et_3PO in benzene were gently mixed together in a 20 ml glass vial and stirred for 20 min. Crystalline products were formed from the

solution upon overnight standing, unperturbed. The crystals were collected and subjected to be studied by NMR spectroscopy and X-ray crystallographic analysis.

Synthesis of $ZrCl_4(OP(CH_2CH_3)_3)_2$) (2C):

An equimolar solution of $ZrCl_4$ and Et_3PO in methylene chloride were gently mixed together in a 20 ml glass vial and stirred for 20 min. Crystalline products were formed from the solution by slow evaporation method. The crystals were collected and subjected to be studied by NMR spectroscopy and X-ray crystallographic analysis.

Synthesis of $TaCl_5 \cdot PPh_3$ (2D)

A portion of PPh_3 (0.073 g, 0.279 mmol) was added to a solution of $TaCl_5$ (0.100 g, 0.279 mmol) in C_6D_6 (1 mL) and stirred for 1 hour producing a yellow solution. The solution was dried under vacuum and the residue was washed with hexanes, producing an orange powder (0.142 g, 82% yield). Single crystals for X-ray diffraction study were grown by a slow diffusion of hexane into a solution of the product in dichloromethane.

^{1}H NMR (300 MHz, C_6D_6): δ 7.69 (overlapping m, 6H, P*Ph*$_3$), 7.00 (overlapping m, 9H, P*Ph*$_3$). ^{31}P NMR (121.5 MHz C_6D_6): δ 13.4. ^{13}C NMR (75.5 MHz, C_6D_6): δ 134.6 (d, J_{PH} = 9 Hz, P*Ph*$_3$), 131.1 (d, J_{PH} = 2 Hz, P*Ph*$_3$), 130.4 (d, J_{PH} = 39 Hz, P*Ph*$_3$), 128.5 (d, J_{PH} = 10 Hz, P*Ph*$_3$). Calcd. for $TaCl_5PC_{18}H_{15}$: C, 34.84; H, 2.44 Found. C, 34.94; H, 2.54.

Synthesis of $[P(CH_2CH_3)(C_6H_5)_3][TaCl_6]$ (2E)

In a 20 mL glass vial, a solution of PPh_3 (0.286 g, 1.09 mmol) in Et_2O (4 mL) was added to a solution of $TaCl_5$ (0.200 g, 0.558 mmol) in Et_2O (2 mL) and gently shaken and left undisturbed. After 3 days the products were collected as colorless crystalline needles at the bottom of the vial, dried under vacuum and samples were prepared for characterization by NMR spectroscopy.

^{1}H NMR (300 MHz, CD_3CN): δ 7.89 (overlapping m, 15H, C-P*Ph*$_3$), 3.24 (dq, 2H, $^{2}J_{PH}$ = 13 Hz, $^{2}J_{HH}$ = 7.45 Hz, P–C*H*$_2$-CH$_3$), 1.31 (dt, 3H, $^{3}J_{PH}$ = 19.85 Hz, $^{2}J_{HH}$ = 7.5 Hz, P–CH$_2$-C*H*$_3$). ^{31}P NMR (121.5 MHz CD_3CN): δ 25.52. ^{13}C NMR (75.5 MHz, CD_3CN): δ 135.16 (d, J_{PH} = 3.2 Hz P*Ph*$_3$), 133.31 (d, J_{PH} = 10 Hz, P*Ph*$_3$), 130.34 (d, J_{PH} = 12 Hz, P*Ph*$_3$), 118.5 (d, P*Ph*$_3$), 15.89 (d, $^{2}J_{PH}$ = 53.2 Hz, P–C*H*$_2$-CH$_3$), 6.00 (d, $^{3}J_{PH}$ =5 Hz, P–CH$_2$-C*H*$_3$)

Synthesis of [PCH$_3$(C$_6$H$_5$)$_3$][TaCl$_5$(OC$_6$H$_5$)]·(C$_7$H$_8$)$_{0.25}$ (2F)

A portion of PPh_3 (0.286 g, 1.09 mmol) was added to a suspension of $TaCl_5$ (0.200 g, 0.558 mmol) in hexane (8 mL) in a 20 mL glass vial followed by addition of a portion of anisole (0.200 g, 1.849 mmol) and stirred for 30 mins that gives a light yellow oil as a separate layer at the bottom. The vial was left undisturbed. After 3 days the products were formed as yellowish crystals at the bottom of the vial. The crystals were submitted for X-ray crystallography and the vacuum dried samples were prepared for characterization by NMR spectroscopy.

^{1}H NMR (300 MHz, CD_2Cl_2): δ 7.79 (overlapping m, 15H, P*Ph*$_3$), 7.30 (overlapping m, 5H, P-O-C$_6$*H*$_5$) 2.81 (d, 3H, $^{3}J_{PH}$ = 13 Hz, P–C*H*$_3$).

^{31}P NMR (121.5 MHz CD_2Cl_2): δ 20.82. ^{13}C NMR (75.5 MHz, CD_2Cl_2): δ 135.63 (d, J_{PH} = 3 Hz, P*Ph*$_3$), 133 (d, J_{PH} = 10.72 Hz, P*Ph*$_3$), 130.67 (d, J_{PH} = 13 Hz, P*Ph*$_3$), 128.84 (s, P-O-C$_6$*H*$_5$), 123.71, 119.75 (s, P-O-C$_6$*H*$_5$), (s, P-O-C$_6$*H*$_5$), 118.4 (d, J_{PH} = 89 Hz P*Ph*$_3$), 10.1 (d, $^{2}J_{PH}$ = 59 Hz, P–C*H*$_3$).

Synthesis of TaCl$_5$(C$_{26}$H$_{23}$OP) (2G):

A portion of PPh_3 (0.036 g, 0.137 mmol) was added to a suspension of $TaCl_5$ (0.05 g, 0.140 mmol) in deuterated benzene (1 mL) in a 20 mL glass vial and stirred to prepare a

yellow solution. Into the solution acetophenone was directly added (0.1 g, 0.832 mmol) and stirred until yellow precipitate occurred from the solution. The vacuum dried samples were prepared for characterization by NMR spectroscopy. The crystals for X-ray crystallography were prepared by following same method from a solution of toluene. ^{1}H NMR (300 MHz, CD_2Cl_2): δ 7.79 (overlapping m, 15H, P*Ph*$_3$), 7.30 (overlapping m, 5H, P-C- C_6H_5) 2.75 (d, 3H, $^{3}J_{PH}$ = 16.8 Hz, P-C-C*H*$_3$). ^{31}P NMR (121.5 MHz CD_2Cl_2): δ 27.22.

Synthesis of $TaCl_5(OCH(C_{12}H_9)(P(C_6H_5)_3))\cdot(C_6H_5Cl)_{0.5}$ (2H)

A solution of 4-phenylbenzaldehyde (0.048 g, 0.263 mmol) in chlorobenzene (2mL) was added to a solution of $TaCl_5$ (0.1 g, 0.279 mmol) in chlorobenzene (2mL) in a 20 mL glass vial which gave a deep orange solution. A third solution of PPh_3 (0.078 g, 0.297 mmol) prepared in chlorobenzene (2 mL) was carefully added to the former solution mixture and left undisturbed for 3 days. Nice colorless crystals appeared at the bottom of the vial and it was submitted for characterization by X-ray crystallographic.

Synthesis of $Ta_2Cl_8(\eta^2\text{-}C_6H_5CCP(C_6H_5)_3)_2$ (2I)

A portion of PPh_3 (0.073 g, 0.279 mmol) was added to a solution of $TaCl_5$ (0.050 g, 0.140 mmol) in toluene and stirred for 10 min producing a yellow solution. Phenylacetylene (0.029 g, 0.279 mmol) was added directly to the previous solution. A portion of lutidine as a base was added to the reaction mixture and left undisturbed to crystallize. Orange needle shaped crystals were formed in a few days and characterized by single crystals for X-ray diffraction study.

X-Ray Structure Determination, $[Ta_2OCl_8(OP(CH_2CH_3)_3)_2][TaCl_5OP(CH_2CH_3)_3]$ (2A)

X-ray intensity data from a colorless wedge-shaped crystal were collected at 100(2) K using a Bruker D8 QUEST diffractometer equipped with a PHOTON-100 CMOS area

detector and an Incoatec microfocus source (Mo Kα radiation, λ = 0.71073 Å). The raw area detector data frames were reduced and corrected for absorption effects using the Bruker APEX3, SAINT+ and SADABS programs.[50, 51] Final unit cell parameters were determined by least-squares refinement of 9266 reflections taken from the data set. The structure was solved with SHELXT.[52] Subsequent difference Fourier calculations and full-matrix least-squares refinement against F^2 were performed with SHELXL-2017[52] using OLEX2.[53]

The compound crystallizes in the triclinic system. The space group *P*-1 (No. 2) was confirmed by structure solution. The asymmetric unit consists of two crystallographically independent but chemically similar $[Ta_2OCl_8(OP(CH_2CH_3)_3)_2]$ complexes and two crystallographically independent but chemically similar $[TaCl_5OP(CH_2CH_3)_3]$ complexes. One $-OP(CH_2CH_3)_3$ group of each $[Ta_2OCl_8(OP(CH_2CH_3)_3)_2]$ complex is disordered over two positions. The two components of each disordered group were restrained to be geometrically similar to the ordered $-OP(CH_2CH_3)_3$ group in each molecule using SHELX SAME instructions. Both $[TaCl_5OP(CH_2CH_3)_3]$ complexes are disordered and were modeled with two orientations each of both the $-TaCl_5$ and $-OP(CH_2CH_3)_3$ parts. The minor population $TaCl_5$ subunits of each complex were restrained to be geometrically similar to the major $TaCl_5$ components of the same complex (SAME). The $-OP(CH_2CH_3)_3$ groups were restrained to be similar to the $-OP(CH_2CH_3)_3$ group P3/O3/C31-C36 (SAME). Total occupancies for the two-component disorder assemblies were constrained to sum to one. Additional distance restraints of *d*(P-C) = 1.79(2) Å and *d*(C-C) = 1.54(2) Å were applied. All non-hydrogen atoms were refined with anisotropic displacement parameters except for disordered carbon atoms of the $[TaCl_5OP(CH_2CH_3)_3]$ complexes (isotropic). Hydrogen

atoms bonded to carbon were placed in geometrically idealized positions and included as riding atoms with *d*(C-H) = 0.99 Å and *U*iso(H) = 1.2*U*eq(C) for methylene hydrogen atoms, and *d*(C-H) = 0.98 Å and *U*iso(H) = 1.5*U*eq(C) for methyl hydrogens. The methyl hydrogens were allowed to rotate as a rigid group to the orientation of maximum observed electron density. The largest residual electron density peak in the final difference map is 2.16 $e^-/Å^3$, located 0.76 Å from Cl41.

X-Ray Structure Determination, $[NbCl_4(OP(CH_2CH_3)_3)_2]_2[Nb_4O_2Cl_{18}]\cdot C_6H_6$ (2B)

X-ray intensity data from a yellow plate crystal were collected at 100(2) K using a Bruker D8 QUEST diffractometer equipped with a PHOTON-100 CMOS area detector and an Incoatec microfocus source (Mo Kα radiation, λ = 0.71073 Å). The crystals become colorless and lose crystallinity in less than one hour in air, even under paratone-N oil. The raw area detector data frames were reduced and corrected for absorption effects using the Bruker APEX3, SAINT+ and SADABS programs.[50, 51] Final unit cell parameters were determined by least-squares refinement of 9366 reflections taken from the data set. The structure was solved with SHELXT.[52] Subsequent difference Fourier calculations and full-matrix least-squares refinement against F^2 were performed with SHELXL-2017[52] using OLEX2.[53]

The compound crystallizes in the triclinic system. The space group *P*-1 (No. 2) was confirmed by structure solution. The asymmetric unit consists of half each of two $[NbCl_4(OP(CH_2CH_3)_3)_2]^+$ cations, half of one $Nb_4O_2Cl_{18}^{2-}$ anion and half of one benzene molecule. All moieties are located on crystallographic inversion centers. All non-hydrogen atoms were refined with anisotropic displacement parameters. Hydrogen atoms were located in Fourier difference maps before being placed in geometrically idealized positions

and included as riding atoms with *d*(C-H) = 0.95 Å and *U*iso(H) = 1.2*U*eq(C) for aromatic hydrogen atoms, *d*(C-H) = 0.99 Å and *U*iso(H) = 1.2*U*eq(C) for methylene hydrogen atoms, and *d*(C-H) = 0.98 Å and *U*iso(H) = 1.5*U*eq(C) for methyl hydrogens. The methyl hydrogens were allowed to rotate as a rigid group to the orientation of maximum observed electron density. The largest residual electron density peak in the final difference map is 0.61 $e^-/Å^3$, located 0.81 Å from P1.

X-Ray Structure Determination, $ZrCl_4(OP(CH_2CH_3)_3)_2$) (2C)

Crystals formed as irregular colorless chunks, from which a suitably-size specimen was cleaved apart. Extensive fracturing and loss of single crystallinity was observed in crystals cooled to temperatures of *ca*. 220 K and below. Data were collected at 250(2) K, at which temperature the crystal remained intact in the diffractometer cold stream. X-ray intensity data were collected using a Bruker D8 QUEST diffractometer equipped with a PHOTON-100 CMOS area detector and an Incoatec microfocus source (Mo Kα radiation, λ = 0.71073 Å). The raw area detector data frames were reduced and corrected for absorption effects using the Bruker APEX3, SAINT+ and SADABS programs.[50, 51] Final unit cell parameters were determined by least-squares refinement of 9838 reflections taken from the data set. The structure was solved with SHELXT.[52] Subsequent difference Fourier calculations and full-matrix least-squares refinement against F^2 were performed with SHELXL-2017[52] using OLEX2.[53]

The compound crystallizes in the monoclinic system. The pattern of systematic absences in the intensity data was consistent with the space group $P2_1/c$, which was confirmed by structure solution. The asymmetric unit consists of half each of two crystallographically independent $ZrCl_4(OP(CH_2CH_3)_3)_2$ complexes. Both zirconium

complexes are located on crystallographic inversion centers. The ethyl carbon atoms of one -OP(CH_2CH_3)$_3$ group (P2, C21-C26) are disordered over two positions with a major population fraction of 0.56(1). Only the carbon atom positions are affected. The geometry of each PEt_3 disorder component was restrained to be similar to that of the ordered PEt_3 group P1/C11-C16 using SHELX instructions. Additional restraints on the U_{ij} parameters were applied to PEt_3 group carbon atoms using the enhanced rigid-bond restraint RIGU. All non-hydrogen atoms were refined with anisotropic displacement parameters. Hydrogen atoms bonded to carbon were placed in geometrically idealized positions and included as riding atoms with *d*(C-H) = 0.99 Å and *U*iso(H) = 1.2*U*eq(C) for methylene hydrogen atoms and *d*(C-H) = 0.98 Å and *U*iso(H) = 1.5*U*eq(C) for methyl hydrogens. The largest residual electron density peak in the final difference map is 0.89 $e^-/Å^3$, located 1.02 Å from H15A.

X-Ray Structure Determination, $TaCl_5 \cdot P(C_6H_5)_3$ (2D)

The compound crystallized as a dense thatch of yellow needles from which a suitable data crystal was cleaved apart. X-ray intensity data were collected at 100(2) K using a Bruker D8 QUEST diffractometer equipped with a PHOTON 100 CMOS area detector and an Incoatec microfocus source (Mo Kα radiation, λ = 0.71073 Å). The raw area detector data frames were reduced and corrected for absorption effects using the SAINT+ and SADABS programs. Final unit cell parameters were determined by least-squares refinement of 9821 reflections taken from the data set. The structure was solved by direct methods with SHELXT.[52] Subsequent difference Fourier calculations and full-matrix least-squares refinement against F^2 were performed with SHELXL-2014[52] using OLEX2.[53]

The compound crystallizes in the monoclinic system. The pattern of systematic absences in the intensity data was consistent with the space group $P2_1/c$, which was verified by structure solution. The asymmetric unit consists of one molecule. All non-hydrogen atoms were refined with anisotropic displacement parameters. Hydrogen atoms bonded to carbon were located in Fourier difference maps before being placed in geometrically idealized positions included as riding atoms with *d*(C-H) = 0.95 Å and *U*iso(H) = 1.2*U*eq(C). The largest residual electron density peak in the final difference map is 0.85 $e^-/Å^3$, located 0.1 Å from the tantalum atom.

X-Ray Structure Determination, $[P(CH_2CH_3)(C_6H_5)_3][TaCl_6]$ (2E)

X-ray intensity data from a colorless plate were collected at 100(2) K using a Bruker D8 QUEST diffractometer equipped with a PHOTON-100 CMOS area detector and an Incoatec microfocus source (Mo Kα radiation, λ = 0.71073 Å). The raw area detector data frames were reduced and corrected for absorption effects using the Bruker APEX3, SAINT+ and SADABS programs.[50,51] Final unit cell parameters were determined by least-squares refinement of 9722 reflections taken from the data set. The structure was solved with SHELXT.[52] Subsequent difference Fourier calculations and full-matrix least-squares refinement against F^2 were performed with SHELXL-2016[52] using OLEX2.[53]

The compound crystallizes in the triclinic system. The space group *P*-1 (No. 2) was confirmed by structure solution. The asymmetric unit consists of one $[P(CH_2CH_3)(C_6H_5)_3]^+$ cation and half each of two $TaCl_6^-$ anions. The $TaCl_6^-$ anions are located on crystallographic inversion centers. All non-hydrogen atoms were refined with anisotropic displacement parameters. Hydrogen atoms were located in Fourier difference maps before being placed in geometrically idealized positions and included as riding atoms with *d*(C-H) = 0.99 Å

and *U*iso(H) = 1.2*U*eq(C) for methylene hydrogen atoms, *d*(C-H) = 0.95 Å and *U*iso(H) = 1.2*U*eq(C) for aromatic hydrogen atoms and *d*(C-H) = 0.98 Å and *U*iso(H) = 1.5*U*eq(C) for methyl hydrogens. The methyl hydrogens were allowed to rotate as a rigid group to the orientation of maximum observed electron density. The largest residual electron density peak in the final difference map is 0.52 $e^-/Å^3$, located 0.90 Å from C31.

X-Ray Structure Determination of $[PCH_3(C_6H_5)_3][TaCl_5(OC_6H_5)]\cdot(C_7H_8)_{0.25}$ (2F)

X-ray intensity data from a colorless plate were collected at 100(2) K using a Bruker D8 QUEST diffractometer equipped with a PHOTON-100 CMOS area detector and an Incoatec microfocus source (Mo Kα radiation, λ = 0.71073 Å). The raw area detector data frames were reduced and corrected for absorption effects using the Bruker APEX3, SAINT+ and SADABS programs.[50,51] Final unit cell parameters were determined by least-squares refinement of 9674 reflections taken from the data set. The structure was solved by direct methods with SHELXT.[52] Subsequent difference Fourier calculations and full-matrix least-squares refinement against F^2 were performed with SHELXL-2014[3] using OLEX2.[53]

The compound crystallizes in the triclinic system. The space group *P*-1 (No. 2) was confirmed by structure solution. The asymmetric unit consists of two crystallographically independent $[PCH_3(C_6H_5)_3]+$ cations, two crystallographically independent $[TaCl_5(OC_6H_5)]^-$ anions and half of one toluene molecule, which is disordered over a crystallographic inversion center. All non-hydrogen atoms were refined with anisotropic displacement parameters. Hydrogen atoms bonded to carbon were located in Fourier difference maps before being placed in geometrically idealized positions and included as riding atoms with *d*(C-H) = 0.95 Å and *U*iso(H) = 1.2*U*eq(C) for aromatic hydrogen atoms

and *d*(C-H) = 0.98 Å and *U*iso(H) = 1.5*U*eq(C) for methyl hydrogens. The methyl hydrogens were allowed to rotate as a rigid group to the orientation of maximum observed electron density. Near the end of the refinement process, a very large residual electron density peak of 5.7 $e^-/Å^3$ was observed at 0.8 Å from Ta2. The magnitude of this peak is significantly larger than an ordinary heavy atom ripple peak. Assigning this peak as a minor tantalum component Ta2B and refining its occupancy factor along with that of Ta2 resulted in occupancies of Ta2/Ta2B = 0.97/0.03, which were within experimental error of summing to one. The difference map flattened to +1.7/-1.6 $e^-/Å^3$. The peak was interpreted as genuine and not as a crystallographic artefact arising from poor data quality or unresolved twinning. It is likely the result of disorder of the entire $TaCl_5(C_6H_5O)^-$ anion. However, only atomic parameters for the tantalum atom of the minor component (Ta2B) are reported; disorder of the lighter atoms could not be successfully modeled because of the combined effects of their smaller scattering factors and low population (~3%). The disordered toluene was refined anisotropically with rigid-bond restraints (RIGU) applied to the U_{ij} values. The six-membered ring was treated as a rigid hexagon. The largest residual electron density peak in the final difference map is 1.72 $e^-/Å^3$, located 0.72 Å from Ta1.

X-Ray Structure Determination, $TaCl_5(C_{26}H_{23}OP)$ (2G)

X-ray intensity data from a colorless spike were collected at 100(2) K using a Bruker D8 QUEST diffractometer equipped with a PHOTON 100 CMOS area detector and an Incoatec microfocus source (Mo Kα radiation, λ = 0.71073 Å).[50,51] The raw area detector data frames were reduced and corrected for absorption effects using the SAINT+ and SADABS programs.[51] Final unit cell parameters were determined by least-squares

refinement of 9920 reflections taken from the data set. The structure was solved by direct methods with SHELXT.[52] Subsequent difference Fourier calculations and full-matrix least-squares refinement against F^2 were performed with SHELXL-2014 using OLEX2.[53]

The compound crystallizes in the monoclinic system. The pattern of systematic absences in the intensity data was consistent with the space groups $P2_1$ and $P2_1/m$. Intensity statistics suggested an acentric structure. The space group $P2_1$ was eventually confirmed by structure solution, and subsequently checked with the ADDSYM program, which found no missed symmetyry elements.[4] The asymmetric unit consists of one molecule. All non-hydrogen atoms were refined with anisotropic displacement parameters. Hydrogen atoms were located in Fourier difference maps before being placed in geometrically idealized positions and included as riding atoms with *d*(C-H) = 0.95 Å and *U*iso(H) = 1.2*U*eq(C) for aromatic hydrogen atoms and *d*(C-H) = 0.98 Å and *U*iso(H) = 1.5*U*eq(C) for methyl hydrogens. The methyl hydrogens were allowed to rotate as a rigid group to the orientation of maximum observed electron density. The largest residual electron density peak in the final difference map is 1.20 $e^-/Å^3$, located 0.68 Å from the tantalum atom.

X-Ray Structure Determination, $TaCl_5(OCH(C_{12}H_9)(P(C_6H_5)_3))\cdot(C_6H_5Cl)_{0.5}$ (2H)

X-ray intensity data from a colorless plate crystal were collected at 100(2) K using a Bruker D8 QUEST diffractometer equipped with a PHOTON-100 CMOS area detector and an Incoatec microfocus source (Mo Kα radiation, λ = 0.71073 Å). The raw area detector data frames were reduced and corrected for absorption effects using the Bruker APEX3, SAINT+ and SADABS programs.[50,51] Final unit cell parameters were determined by least-squares refinement of 9688 reflections taken from the data set. The structure was

solved with SHELXT.[52] Subsequent difference Fourier calculations and full-matrix least-squares refinement against F^2 were performed with SHELXL-2017[52] using OLEX2.[53]

The compound crystallizes in the triclinic system. The space group *P*-1 (No. 2) was confirmed by structure solution. The asymmetric unit consists of one $TaCl_5(OCH(C_{12}H_9)(P(C_6H_5)_3$ complex and half of one chlorobenzene molecule, which is disordered about a crystallographic inversion center. The chlorobenzene is further disordered over two positions within the asymmetric unit. The total site occupancy of these two components was constrained to sum to 0.5 and refined to Cl1S/Cl2S = 0.220(8)/0.280(8). The C_6H_5Cl phenyl rings were refined as rigid hexagons with *d*(C-C) = 1.39 Å, and 1,2- and 1,3- distances to the chlorine atoms were restrained to appropriate values. All non-hydrogen atoms were refined with anisotropic displacement parameters except for disordered carbon atoms (isotropic). The anisotropic displacement parameters of the disordered chlorobenzene chlorine atoms were restrained to a spherical form using SHELX ISOR instructions. Hydrogen atoms bonded to carbon were placed in geometrically idealized positions and included as riding atoms with *d*(C-H) = 1.00 Å and *U*iso(H) = 1.2*U*eq(C) for methine hydrogen atoms and *d*(C-H) = 0.95 Å and *U*iso(H) = 1.2*U*eq(C) for aromatic hydrogen atoms. The largest residual electron density peak in the final difference map is 1.14 $e^-/Å^3$, located 0.96 Å from Cl2S.

X-Ray Structure Determination, $Ta_2Cl_8(\eta^2\text{-}C_6H_5CCP(C_6H_5)_3)_2$ (2I)

X-ray intensity data from a rough-textured orange needle were collected at 100(2) K using a Bruker D8 QUEST diffractometer equipped with a PHOTON-100 CMOS area detector and an Incoatec microfocus source (Mo Kα radiation, λ = 0.71073 Å). The raw area detector data frames were reduced and corrected for absorption effects using the

Bruker APEX3, SAINT+ and SADABS programs.[50,51] Final unit cell parameters were determined by least-squares refinement of 9054 reflections taken from the data set. The structure was solved with SHELXT.[52] Subsequent difference Fourier calculations and full-matrix least-squares refinement against F^2 were performed with SHELXL-2016[52] using OLEX2.[53]

The compound crystallizes in the monoclinic system. The pattern of systematic absences in the intensity data was consistent with the space group $P2_1/n$, which was confirmed by structure solution. The asymmetric unit consists of half of one $Ta_2Cl_8(\eta^2$-$C_6H_5CCP(C_6H_5)_3)_2$ complex, which is located on a crystallographic inversion center. All non-hydrogen atoms were refined with anisotropic displacement parameters. Hydrogen atoms were located in Fourier difference maps before being placed in geometrically idealized positions and included as riding atoms with *d*(C-H) = 0.95 Å and *U*iso(H) = 1.2*U*eq(C). The largest residual electron density peak in the final difference map is 1.05 $e^-/Å^3$, located 0.80 Å from Ta1.

Table 2.3 Crystallographic table for single crystal X-ray data for $M(Et_3PO)_x$ (M = Ta, Nb, Zr; x = 1 or 2), and $TaCl_5$-PPh_3 adduct.

CCDC				1552651
	$Ta(Et_3PO)_x$ **(2A)**	$Nb(Et_3PO)_2$ **(2B)**	$Zr(Et_3PO)_2$ **(2C)**	$TaCl_5$-PPh_3 **(2D)**
Empirical formula	$C_{18}H_{45}Cl_{13}O_4P_3Ta_3$	$C_{30}H_{66}Cl_{26}Nb_6O_6P_4$	$C_{12}H_{30}Cl_4O_2P_2Zr$	$C_{18}H_{15}Cl_5PTa$
Formula weight	1422.15	2125.86	501.32	620.47
Temperature/K	100(2)	100(2)	250(2)	100(2)
Crystal system	triclinic	triclinic	monoclinic	monoclinic
Space group	P-1	P-1	$P2_1/c$	$P2_1/c$
a/Å	15.2320(8)	10.9932(6)	13.1586(5)	9.6520(5)
b/Å	15.5592(8)	13.2306(7)	12.6599(5)	19.1580(8)
c/Å	19.9821(10)	13.3888(7)	14.0572(6)	11.2416(6)
α/°	106.360(2)	81.141(2)	90	90
β/°	105.357(2)	71.900(2)	101.0760(10)	91.2588(18)
γ/°	90.040(2)	89.208(2)	90	90
Volume/$Å^3$	4367.2(4)	1827.71(17)	2298.12(16)	2078.22(18)
Z	4	1	4	4
$\rho_{calc}g/cm^3$	2.163	1.931	1.449	1.983
μ/mm^{-1}	8.427	1.982	1.083	6.008
Crystal size/mm^3	0.06 × 0.06 × 0.04	0.32 × 0.2 × 0.04	0.38 × 0.32 × 0.26	0.22 × 0.08 × 0.06
Radiation	MoKα (λ = 0.71073)	MoKα (λ = 0.71073)	MoKα (λ = 0.71073)	MoKα (λ = 0.71073)
2Θ range for data collection/°	4.33 to 55.226	4.838 to 60.236	4.366 to 52.744	4.22 to 56.616
Reflections collected	149095	121994	82513	48257
Data/restraints/parameters	20240/480/927	10775/0/335	4705/60/233	5165/0/227

Goodness-of-fit on F^2	1.015	1.061	1.029	1.065
Final R indexes [I>=2σ (I)]	R_1 = 0.0426, wR_2 = 0.0871	R_1 = 0.0186, wR_2 = 0.0399	R_1 = 0.0479, wR_2 = 0.1169	R_1 = 0.0256, wR_2 = 0.0375
Final R indexes [all data]	R_1 = 0.0757, wR_2 = 0.0972	R_1 = 0.0253, wR_2 = 0.0415	R_1 = 0.0702, wR_2 = 0.1298	R_1 = 0.0350, wR_2 = 0.0391
Largest diff. peak/hole / e $Å^{-3}$	2.17/-2.66	0.61/-0.53	0.89/-0.59	0.85/-0.72

Table 2.4 Crystallographic table for single crystal X-ray data for compounds **2E, 2F, 2G, 2H, 2I.**

	Et_2O (2E)	**Anisole (2F)**	**Ketone (2G)**	**Aldehyde (2H)**	**Alkyne (2I)**
Empirical formula	$C_{20}H_{20}Cl_6PTa$	$C_{26.75}H_{25}Cl_5OPTa$	$C_{26}H_{23}Cl_5OPTa$	$C_{34}H_{27.5}Cl_{5.5}OPTa$	$C_{52}H_{40}Cl_8P_2Ta_2$
Formula weight	684.98	751.64	740.61	858.95	1372.28
Temperature/K	100(2)	100(2)	100(2)	100(2)	100(2)
Crystal system	triclinic	triclinic	monoclinic	triclinic	monoclinic
Space group	P-1	P-1	$P2_1$	P-1	$P2_1/n$
a/Å	9.5862(5)	11.9541(8)	10.1835(7)	9.9781(6)	10.3073(4)
b/Å	10.2413(5)	15.4467(10)	13.4242(9)	14.2420(8)	19.6313(7)
c/Å	14.5366(7)	16.0765(11)	10.1848(7)	14.6536(8)	12.1011(5)
α/°	70.630(2)	92.248(2)	90	61.5670(10)	90
β/°	73.145(2)	97.330(2)	108.551(2)	70.628(2)	96.3400(10)
γ/°	63.233(2)	102.399(2)	90	88.982(2)	90
Volume/$Å^3$	1185.22(11)	2868.8(3)	1319.97(16)	1702.70(17)	2433.63(16)
Z	2	4	2	2	2
$\rho_{calc}g/cm^3$	1.919	1.740	1.863	1.675	1.873
μ/mm^{-1}	5.386	4.372	4.749	3.733	5.035

Crystal size/mm^3	0.4 × 0.18 × 0.08	0.36 × 0.18 × 0.04	0.06 × 0.04 × 0.02	0.14 × 0.1 × 0.04	0.42 × 0.16 × 0.1
Radiation	MoKα (λ = 0.71073)	MoKα (λ = 0.71073)	MoKα (λ = 0.71073)	MoKα (λ = 0.71073)	MoKα (λ = 0.71073)
2Θ range for data collection/°	4.584 to 60.214	4.528 to 61.22	4.218 to 54.378	4.456 to 60.166	4.484 to 60.254
Reflections collected	52231	141230	50852	83798	117507
Data/restraints/parameters	6986/0/258	17603/45/655	5845/1/308	9979/16/396	7172/0/289
Goodness-of-fit on F^2	1.031	1.055	1.015	1.062	1.067
Final R indexes [I>=2σ (I)]	R_1 = 0.0181, wR_2 = 0.0326	R_1 = 0.0277, wR_2 = 0.0500	R_1 = 0.0288, wR_2 = 0.0443	R_1 = 0.0239, wR_2 = 0.0534	R_1 = 0.0212, wR_2 = 0.0417
Final R indexes [all data]	R_1 = 0.0285, wR_2 = 0.0348	R_1 = 0.0405, wR_2 = 0.0535	R_1 = 0.0429, wR_2 = 0.0463	R_1 = 0.0301, wR_2 = 0.0550	R_1 = 0.0274, wR_2 = 0.0432
Largest diff. peak/hole / e $Å^{-3}$	0.52/-0.63	1.72/-1.54	1.20/-0.70	1.14/-0.85	1.05/-0.53

References

1. S. J. K. Forrest, J. Clifton, N. Fey, P. G. Pringle, H. A. Sparkes, D. F. Wass, *Angew. Chem. Int. Ed.* **2015**, *54*, 2223–2227.
2. D. B. Grotjahn, D. A. Lev, *J. Am. Chem. Soc.* **2004**, *126*, 12232–12233.
3. L. Hintermann, A. Labonne, *Synthesis* **2007**, *2007*, 1121–1150.
4. F. Pohlki, S. Doye, *Chem. Soc. Rev.* **2003**, *32*, 104–114.
5. V. Lavallo, G. D. Frey, B. Donnadieu, M. Soleilhavoup, G. Bertrand, *Angew. Chem. Int. Ed.* **2008**, *47*, 5224–5228.
6. G. Kovács, A. Lledós, G. Ujaque, *Angew. Chem. Int. Ed.* **2011**, *50*, 11147–11151.
7. S. J. McLain, R. R. Schrock, P. R. Sharp, M. R. Churchill, W. J. Youngs, *J. Am. Chem. Soc.* **1979**, *101*, 263–265.
8. R. R. Schrock, J. D. Fellmann, *J. Am. Chem. Soc.* **1978**, *100*, 3359–3370.
9. B. C. Ankianiec, P. E. Fanwick, I. P. Rothwell, *J. Am. Chem. Soc.* **1991**, *113*, 4710–4712.
10. J. B. Diminnie, Z. Xue, *J. Am. Chem. Soc.* **1997**, *119*, 12657–12658.
11. L. R. Chamberlain, I. P. Rothwell, J. C. Huffman, *J. Am. Chem. Soc.* **1986**, *108*, 1502–1509.
12. D. R. Neithamer, R. E. LaPointe, R. A. Wheeler, D. S. Richeson, G. D. Van Duyne, P. T. Wolczanski, *J. Am. Chem. Soc.* **1989**, *111*, 9056–9072.
13. P. T. Wolczanski, *Polyhedron* **1995**, *14*, 3335–3362.
14. J. S. Figueroa, N. A. Piro, C. R. Clough, C. C. Cummins, *J. Am. Chem. Soc.* **2006**, *128*, 940–950.
15. J. S. Silvia, C. C. Cummins, *J. Am. Chem. Soc.* **2010**, *132*, 2169–2171.

16. A. J. Keane, P. Y. Zavalij, L. R. Sita, *J. Am. Chem. Soc.* **2013**, *135*, 9580–9583.

17. A. J. Keane, B. L. Yonke, M. Hirotsu, P. Y. Zavalij, L. R. Sita, *J. Am. Chem. Soc.* **2014**, *136*, 9906–9909.

18. F. Marchetti, G. Pampaloni, T. Repo, *Eur. J. Inorg. Chem.* **2008**, *2008*, 2107–2112.

19. R. Bini, C. Chiappe, F. Marchetti, G. Pampaloni, S. Zacchini, *Inorg. Chem.* **2010**, *49*, 339–351.

20. F. Marchetti, G. Pampaloni, *Chem Commun* **2012**, *48*, 635–653.

21. D. W. Stephan, *Acc. Chem. Res.* **2015**, *48*, 306–316.

22. A. M. Chapman, M. F. Haddow, D. F. Wass, *J. Am. Chem. Soc.* **2011**, *133*, 18463–18478

23. Beckett, M.A.; Brassington, D.S.; Coles, S.J.; Hursthouse, M.B.; Inorg.Chem.Commun., 2000, 3, 530.

24. Bandoli, G.; Bortolozzo, G.; Clemente, D. A.; Croatto, U.; and Panattoni, C.; J. Chem. Soc. **(A), 1970**, 2778-2780

25. K. M. Doxsee, J. B. Farahi, H. Hope, *J. Am. Chem. Soc.* **1991**, *113*, 8889–8898.

26. K. M. Doxsee, J. K. M. Mouser, *Organometallics* **1990**, *9*, 3012–3014.

27. W. Zhang, J. Yamada, K. Nomura, *Organometallics* **2008**, *27*, 5353–5360.

28. H. Tsurugi, T. Ohno, T. Kanayama, R. A. Arteaga-Müller, K. Mashima, *Organometallics* **2009**, *28*, 1950–1960.

29. F. Basuli, B. C. Bailey, L. A. Watson, J. Tomaszewski, J. C. Huffman, D. J. Mindiola, *Organometallics* **2005**, *24*, 1886–1906.

30. B. C. Bailey, A. R. Fout, H. Fan, J. Tomaszewski, J. C. Huffman, J. B. Gary, M. J. A. Johnson, D. J. Mindiola, *J. Am. Chem. Soc.* **2007**, *129*, 2234–2235.

31. U. J. Kilgore, C. A. Sengelaub, H. Fan, J. Tomaszewski, J. A. Karty, M.-H. Baik, D. J. Mindiola, *Organometallics* **2009**, *28*, 843–852.

32. J. D. Selby, C. D. Manley, M. Feliz, A. D. Schwarz, E. Clot, P. Mountford, *Chem. Commun.* **2007**, 4937–4939.

33. F. G. Bordwell, *Acc. Chem. Res.* **1988**, *21*, 456–463.

34. I. Kaljurand, A. Kütt, L. Sooväli, T. Rodima, V. Mäemets, I. Leito, I. A. Koppel, *J. Org. Chem.* **2005**, *70*, 1019–1028.

35. V. Y. Kukushkin, A. J. L. Pombeiro, *Chem. Rev.* **2002**, *102*, 1771–1802.

36. C. Li, X. Zhao, A. Wang, G. W. Huber, T. Zhang, *Chem. Rev.* **2015**, *115*, 11559–11624.

37. F. A. Cotton, R. C. Najjar, *Inorg. Chem.* **1981**, *20*, 1866–1869.

38. F. Marchetti, G. Pampaloni, S. Zacchini, *Polyhedron* **2016**, *115*, 99–104.

39. G. C. Welch, J. D. Masuda, D. W. Stephan, *Inorg. Chem.* **2006**, *45*, 478–480.

40. T. L. Breen, D. W. Stephan, *Inorg. Chem.* **1992**, *31*, 4019–4022.

41. M. H. Holthausen, T. Mahdi, C. Schlepphorst, L. J. Hounjet, J. J. Weigand, D. W. Stephan, *Chem. Commun.* **2014**, *50*, 10038.

42. F. Marchetti, G. Pampaloni, S. Zacchini, *Dalton Trans.* **2009**, 8096.

43. A. M. Chapman, M. F. Haddow, D. F. Wass, *J. Am. Chem. Soc.* **2011**, *133*, 18463–18478.

44. J. Cornella, C. Zarate, R. Martin, *Chem. Soc. Rev.* **2014**, *43*, 8081–8097.

45. G. A. Edouard, P. Kelley, D. E. Herbert, T. Agapie, *Organometallics* **2015**, *34*, 5254–5277.

46. M. E. van der Boom, S.-Y. Liou, Y. Ben-David, L. J. W. Shimon, D. Milstein, *J. Am. Chem. Soc.* **1998**, *120*, 6531–6541.

47. J. Choi, Y. Choliy, X. Zhang, T. J. Emge, K. Krogh-Jespersen, A. S. Goldman, *J. Am. Chem. Soc.* **2009**, *131*, 15627–15629.

48. J. Cornella, E. Gómez-Bengoa, R. Martin, *J. Am. Chem. Soc.* **2013**, *135*, 1997–2009.

49. Rahman, M. M.; Smith, M. D.; Amaya, J. A.; Makris, T. M.; Peryshkov, D. V. *Inorg. Chem.*, **2017**, *56*, 11798–11803.

50. APEX3 Version 2016.5-0 and SAINT+ Version 8.37A. Bruker AXS, Inc., Madison, Wisconsin, USA, 2016.

51. SADABS-2016/2: Krause, L., Herbst-Irmer, R., Sheldrick G.M. and Stalke D. *J. Appl. Cryst.* 2015, *48*, 3-10.

52. (a) SHELXT: Sheldrick, G.M. *Acta Cryst*. 2015, *A71*, 3-8. (b) SHELXL: Sheldrick, G.M. *Acta Cryst*. 2008, A64, 112-122.

53. OLEX2: a complete structure solution, refinement and analysis program. Dolomanov, O. V., Bourhis, L. J., Gildea, R. J., Howard J. A. K. and Puschmann, H. *J. Appl. Cryst.* **2009**, *42*, 339-341.

54. Rahman, M. M.; Smith, M.; Peryshkov, D. *Abstr. Pap.—Am. Chem. Soc., Div. Inorg. Chem.* **2018**, *256*, INORG 2984909.

Chapter 3

Formation of A Cationic Vinyl Imido Group Upon C-H Activation of Nitriles by Trialkylamines in Presence of $TaCl_5$.

Rahman, M. M.; Smith, M. D.; Peryshkov, D. V. *Inorg. Chem.*, **2016**, *55*, 5101–5103.

3.1 Introduction

High-valent group 5 (Nb, Ta) chlorides are dimeric molecular compounds, featuring six-coordinate metal centers. In solution, MX_5 halides form strong adducts with donor molecules; however, due to high Lewis acidity, the metal center tends to facilitate activation of the coordinated substrate. Ring-opening of cyclic ethers, deoxygenation of ketones, phosphine oxides, and sulfoxides by $NbCl_5$ and $TaCl_5$ under mild conditions have been recently reported.[1] Interestingly, CH_3CN adducts of both $NbCl_5$ and $TaCl_5$ are stable and have been isolated and structurally characterized.[2]

Herein, we report a new pathway of C–H activation of acetonitrile in the presence of the strong Lewis acid $TaCl_5$. We found that C–H bonds of acetonitrile become increasingly acidic upon the coordination to the metal center. This dramatic increase in acidity allowed deprotonation and subsequent attack by relatively weak nucleophiles triethylamine or diethylisopropylamine. The previously unknown rearrangement of a resulting nucleophilic carbanion into an electrophilic imido moiety and the subsequent reaction with a second equivalent of the amine resulted in the formation of cationic vinylimido complexes of Ta(V) (**Scheme 3.1**).

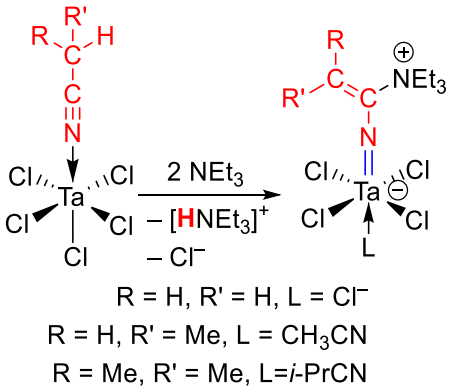

Scheme 3.1. The synthesis of zwitterionic vinylimido complexes of Ta(V) upon deprotonation of coordinated nitriles (MeCN, EtCN, *i*-PrCN)

3.2 Results and Discussion

The addition of 2 equiv. of NEt_3 to 1 equiv. of $TaCl_5$ in benzene solution containing 5 equiv. of CH_3CN at room temperature resulted in a quick color change from colorless to yellow. The analytically pure product was isolated as a yellow powder in 96% yield upon removal of volatiles from the reaction mixture. The single crystal X-ray diffraction revealed formation of an unexpected octahedral vinylimido complex $[HNEt_3][Ta\{NC(CH_2)NEt_3\}Cl_5]$ (**1**) (**Figure 3.1**). During the reaction with NEt_3, the second equivalent of the amine was incorporated in the imido group as a vinyl triethylammonium cation.

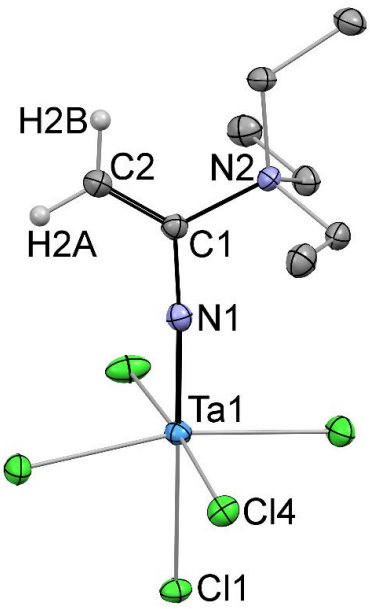

Figure 3.1 Displacement ellipsoid plot of $[HNEt_3][Ta\{NC(CH_2)NEt_3\}Cl_5]$ (**1**). (50% probability. Hydrogen atoms, except for the vinyl group, have been omitted for clarity. The $[HNEt_3]^+$ cation is not shown.)

The Ta1–N1 distance in the crystal structure is 1.797(2) Å, which clearly indicates the formation of a tantalum imido complex. The formal negative charge on the tantalum metal center led to a slight elongation of Ta=N bond; however, it is within a normal range

for the reported terminal imido complexes of Ta and Nb (1.61(1) – 1.812(6) Å).[3] The formation of a double bond between the carbon atoms of a parent acetonitrile molecule was confirmed by the short C1–C2 distance (1.325(4) Å). The N1, C1, C2, and N2 atoms are coplanar and the N1–C1–C2 angle is 125.3(3)°, which is consistent with sp^2 character of C1 atom. The N2–C1 bond length of 1.520(3) Å is congruous with the single bond assignment. The metal-chloride bond lengths differ significantly for Ta1–Cl1 (2.558(1) Å), which is located *trans*- to the imido group, and the other chloride ligands (Ta1–Cl2/Cl3/Cl4 distances are in the range from 2.411(1) to 2.433(1) Å).

The most characteristic feature of the ^{1}H NMR spectrum of **1** in CD_2Cl_2 is the presence of signals of protons belonging to the vinyl CH_2 group, which appear as two doublets at 4.63 and 4.85 ppm, ($^2J_{HH}$ = 2 Hz) corresponding to *cis*- and *trans*- orientations relative to the triethylammonium moiety. The use of CD_3CN as a substrate led to formation of $[DNEt_3][Ta\{NC(CD_2)NEt_3\}Cl_5]$, according to ^{1}H and ^{13}C NMR data ($^1J_{CD}$ = 20 Hz for the signal from the C=CD_2 group). A rather low value of kinetic isotope effect KIE = 1.54 was observed for the formation of **1** at room temperature when an equimolar mixture of CH_3CN and CD_3CN was employed.

To probe generality of this transformation, we employed other nitriles containing β-hydrogen atoms such as EtCN and (*i*-Pr)CN in reactions with NEt_3. In these cases, clean formation of analogous vinyl imido species was observed as indicated by the appearance of the characteristic signals in ^{1}H and ^{13}C NMR spectra of the reaction mixtures. The resulting zwitterionic Ta(V) vinylimido complexes **2** and **3** were isolated upon recrystallization as acetonitrile and isobutyronitrile adducts, respectively. Single crystal X-ray diffraction confirmed the expected structures

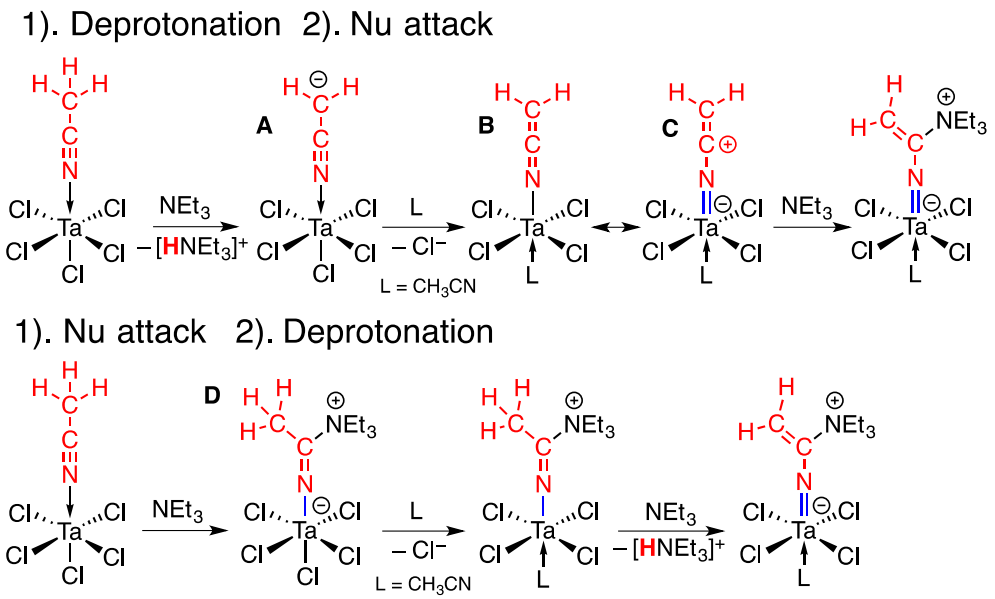

Scheme 3.2 Possible mechanisms of formation of zwitterionic vinyl imido complexes of Ta(V).

We propose the following sequence of bond rearrangements, which leads to the formation of **1** (**Scheme 3.1**). The acidity of C–H bonds of acetonitrile dramatically increases upon coordination to a strong Lewis acid $TaCl_5$, and it is deprotonated by an amine. The resulting anionic nitrile **A**, rearranges either into an electrophilic azaallene (**B**) or the imido group that bears a carbocation center (**C**). Our theoretical geometry optimization calculations of the deprotonated intermediate suggest the preference for the form **B** (**Figure 3.5**). The second amine molecule acts as a nucleophile and forms the cationic vinyl imido group in **1**. The replacement of one chloride ligand by a neutral nitrile can occur either at the deprotonation stage or when **1** has been formed. The replaced chloride ligand can form either $[HNEt_3]Cl$ or $[HNEt_3]TaCl_6$ salts. The complex **1** was isolated with the chloride in the *trans*- position to the imido group while the complexes **2** and **3** were isolated as nitrile adducts. We attribute this outcome to slight differences in relative solubilities of chloride- and nitrile- coordinated complexes with different imido groups in aromatic solvents. The subsequent deprotonation of the coordinated nitrile in **2**

or **3** was not observed, probably due to a decrease in the Lewis acidity of the metal center in comparison with parent $TaCl_5$ (**1** can be described as a 16-electron complex). The oxidation state of the metal center does not change during the reaction.

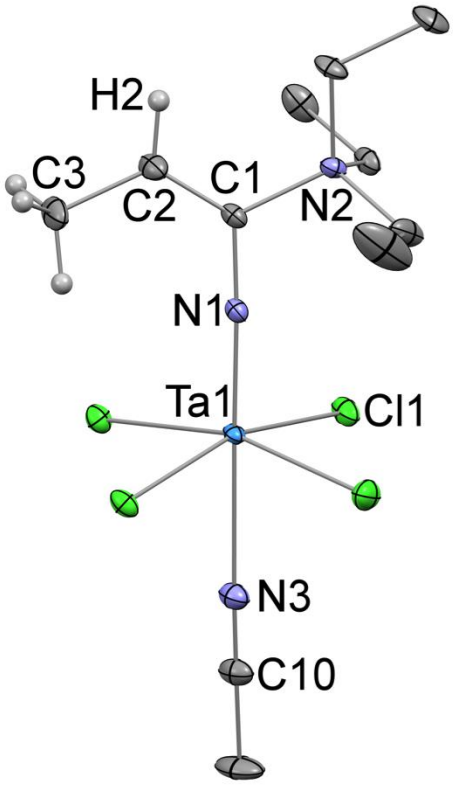

Figure 3.2 Displacement ellipsoid plot of $Ta\{NC(CHCH_3)NEt_3\}Cl_4(NCCH_3)$ (**2**). (50% probability. Hydrogen atoms, except for the vinyl group, have been omitted for clarity).

An alternative mechanism can be considered, consisting of the initial attack of the nucleophilic base Nu on the carbon atom of the CN group of the coordinated acetonitrile molecule with the formation of the feasible $Ta(NC(CH_3)Nu)Cl_5$ intermediate (**D)**, which undergoes deprotonation by the second equivalent of the base and the formation of the vinyl imido complex. The related amide $Re(NC(CH_3)PPh_2O)Cl_2(PPh_3)_2(CH_3CN)$ has been reported,[4] which bears some analogy to the hypothetical intermediate **D**. However, no deprotonation of the rhenium amide and formation of an imido group have been observed.

Our initial results suggest that the deprotonation is likely the first step in the transformation of nitriles reported herein. First, the reaction of $TaCl_5$ and 1 equiv of NEt_3 in CH_3CN produced only **1** according to ^1H NMR spectroscopy data with no traces of signals from the possible nucleophilic attack intermediate $Ta(NC(CH_3)NEt_3)Cl_5$. The reaction of $TaCl_5$ and 1 equiv of NEt_3 with CH_3CN in CD_2Cl_2 at –78 ºC overnight also led to observation of only **1** in ^1H NMR spectrum of the reaction mixture.

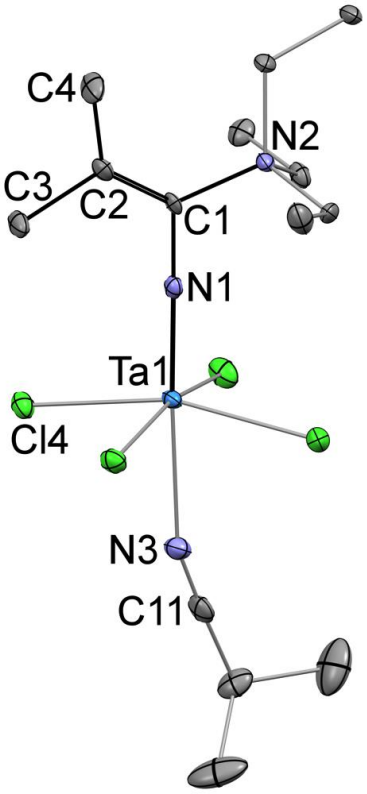

Figure 3.3 Displacement ellipsoid plot of $Ta\{NC(CMe_2)NEt_3\}Cl_4(NCHMe_2)$ (**3**). (50% probability. Hydrogen atoms have been omitted for clarity.)

Second, we conjectured that the increase in steric hindrance of both a nitrile substrate and an amine base would prevent the nucleophilic attack of the amine on the deprotonated intermediate **B** and shed a light on the pathway of the transformation. To probe this, we carried out the reaction of $TaCl_5$ and the Hunig's base $N(i\text{-}Pr)_2Et$ in presence

of excess (*i*-Pr)CN. ^{1}H NMR spectroscopy data and single crystal X-ray diffraction revealed the clean formation of the cationic vinyl imido complex [HN(*i*-Pr)$_2$Et][Ta{NCC(CH$_3$)$_2$C(CH$_3$)$_2$CN}Cl$_4$] (**4**), which, instead of the trialkylammonium fragment in **1**, contained the *C*-bound 1,1-dimethylcyano group (**Figure 3.4**).

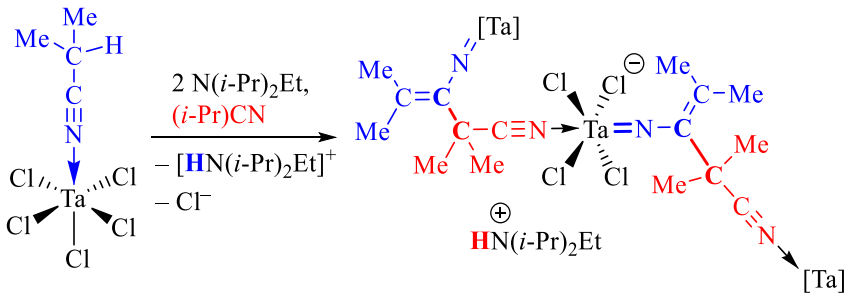

Scheme 3.3. The synthesis of [HN(*i*-Pr)$_2$Et][Ta{NC(CMe$_2$)CMe$_2$CN}Cl$_4$] vinyl imido coordination polymer (**4**)

Compound **4** crystallized as a coordination polymer with vinyl imido cyano groups bridging pairs of metal centers forming infinite chains. Ta1–N1 distance in the crystal structure is 1.775(2) Å, which reflects the presence of the tantalum imido moiety. The C1–C2 distance of 1.352(3) Å and the C1–C5 distance of 1.544(3) clearly indicate a double and a single C–C bonds, respectively. The Ta1–N2 distance of 2.371(2) Å corresponds to a coordinated nitrile group.

The synthesis of **4** particularly suggests that the deprotonation of the coordinated nitrile molecule is the first step of the reaction, which is followed by the formal nucleophilic attack of the metal-bound carbanion **A** on the metal-stabilized azaallene moiety **B**. The steric hindrance of the nitrile and the amine prevents the nucleophilic attack of the latter on **B** but does not prevent initial isobutyronitrile deprotonation. Notably, the formation of the C–C bond in **4** does not involve reduction, as it is often the case, but only deprotonation of two equivalents of the nitrile.

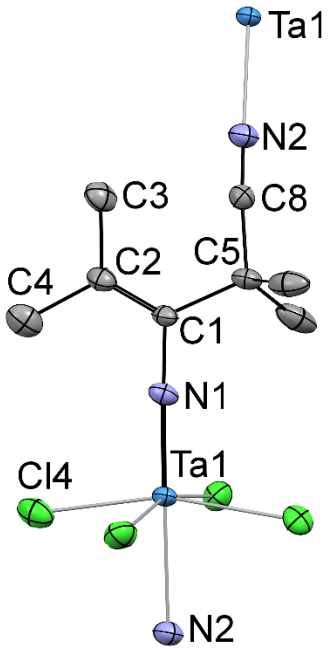

Figure 3.4 Displacement ellipsoid plot of [HN(*i*-Pr)$_2$Et][Ta{NC(CMe$_2$)CMe$_2$CN}Cl$_4$]·CH$_3$CN (**4**). (50% probability. Hydrogen atoms have been omitted for clarity. The [HN(*i*-Pr)$_2$Et]$^+$ cation and CH$_3$CN solvent molecules are not shown). Selected bond distances (Å) and angles (º): Ta1–N1 = 1.775(2), Ta1–N2 = 2.372(2), N1–C1 = 1.385(3), C1–C2 = 1.352(3), C1–C5 = 1.544(3), C8–N2 = 1.141(3), Ta1–N1–C1 = 174.2(2), N1–C1–C2 = 121.9(2).)

In the previously reported cases of metal-promoted deprotonation of acetonitrile, reactions with strong bases proceeded with a formation of a *nucleophilic* carbanion that could be attacked by electrophiles such as aldehydes or ketones. In contrast, in the system reported here, the deprotonation of the coordinated acetonitrile resulted in formation of a strong *electrophile* (either in the form of a carbanion or an azaallene) due to the rearrangement of a nitrile ligand to the imido group. It is likely that the propensity of the electron-deficient Ta(V) center to form imido complexes is one of the main driving forces to the emergence of the intermediate electrophile upon deprotonation. It appears that both Lewis acidity and the ability to form covalent double bonds to a nitrogen atom are

important. For comparison, a component of frustrated Lewis pairs (FLP), a strong Lewis acid $B(C_6F_5)_3$, has been reported to form an adduct with acetonitrile that is unreactive towards bases such as lutidine, even at elevated temperatures.[5a] The system reported herein is reminiscent of the recently reported FLPs containing cationic complexes of early transition metals by the virtue of the presence of a strong metal-centered Lewis acid ($TaCl_5$) and a strong base (NEt_3).[5b] Interestingly, Zr-based FLP systems have not been shown to deprotonate and activate alkylnitriles.[5c]

Related neutral vinyl imido groups have been reported to form upon insertion of nitriles into Ti, V, and Ta alkylidenes[6] and in the reactions of alkynes and Ti hydrazido complexes.[7] The enediimido species have been known to form upon reductive C–C coupling of acetonitrile by low-valent Ti, Mo, and W complexes.[8] To the best of our knowledge, this work is the first report of the formation of a metal imido complex by deprotonation of a coordinated nitrile.

In conclusion, a new type of a cationic vinyl imido ligand was selectively synthesized upon deprotonation of a coordinated nitrile by trialkylamine. The subsequent rearrangement of the deprotonated nitrile anion into electrophilic imido group is unprecedented. The extreme case of increased steric hindrance of both the substrate and the base led to C–C coupling of two resonance forms of the deprotonated nitrile. The exploration of the utility of this reaction for functionalization of nitriles is ongoing.

3.3 Experimental

All synthetic manipulations were carried out either in a nitrogen-filled drybox or on an air free dual-manifold Schlenk line, unless stated otherwise. The solvents were sparged with nitrogen, passed through activated alumina, and stored over activated 4 Å

Linde-type molecular sieves. Chloroform-d^3, dichloromethane-d^2, and acetonitrile-d^3 were degassed and stored over activated 4 Å Linde-type molecular sieves. NMR spectra were recorded using Varian spectrometers at 400 (^{1}H), 100 (^{13}C) and reported in δ (parts per million) and referenced to residual ^{1}H/^{13}C signals of a deuterated solvent. *J* values are given in Hz. Midwest Microlab, Indianapolis, Indiana provided the elemental analysis results. $TaCl_5$ (Strem) was used as received. NEt_3, N(*i*-Pr)$_2$Et, CH_3CN, CD_3CN, EtCN, and (*i*-Pr)CN were degassed by freeze-pump-thaw technique and stored over 4 Å Linde-type molecular sieves.

Synthesis of [HNEt$_3$][Ta{NCCH$_2$NEt$_3$}Cl$_5$] (1)

A portion of CH_3CN (0.057 g, 1.39 mmol, 5 equiv.) was added to a portion of $TaCl_5$ (0.100 g; 0.279 mmol) suspended in benzene (1 mL). The mixture was stirred for 30 min at room temperature resulting in formation of a pale yellow solution. A solution of NEt_3 (0.056 g; 0.56 mmol, 2 equiv.) in benzene (0.5 mL) was added dropwise to the reaction mixture, producing orange solution. Yellow precipitate formed within a minute after the addition. The reaction mixture was stirred for 12 h at room temperature. The volatiles were removed under vacuum producing analytically pure yellow solid, soluble in dichloromethane and sparingly soluble in chloroform (0.162 g, 0.267 mmol, 96% yield based on the amount of $TaCl_5$).

^{1}H NMR (CD_2Cl_2): δ 7.76 (s, 1H, *H*NEt$_3$), 4.88 (d, 1H, $^2J_{HH}$ = 2 Hz, (C=C*H*$_2$)N(CH$_2$CH$_3$)$_3$), 4.66 (d, 1H, $^2J_{HH}$ = 2 Hz, (C=C*H*$_2$)N(CH$_2$CH$_3$)$_3$), 3.62 (q, 6H, (C=CH$_2$)N(C*H*$_2$CH$_3$)$_3$), 3.26 (q, 6H, HN(C*H*$_2$CH$_3$)$_3$), 1.40 (t, 9H, N(CH$_2$C*H*$_3$)$_3$), 1.32 (t, 9H, N(CH$_2$C*H*$_3$)$_3$). ^{13}C NMR (CD_2Cl_2): δ 147.3 (*C*=CH$_2$), 101.3, (C=*C*H$_2$), 49.6

($N(CH_2CH_3)_3$), 44.7 ($N(CH_2CH_3)_3$), 6.4 ($N(CH_2CH_3)_3$), 5.7 ($N(CH_2CH_3)_3$). Calcd. for $C_{14}H_{33}Cl_5N_3Ta$: C, 27.95; H, 5.53; N, 6.98 Found. C, 27.67; H, 5.57; N, 6.88.

Synthesis of $Ta\{NCCHCH_3NEt_3\}Cl_4(CH_3CN)$ (2)

A portion of EtCN (0.123 g, 2.23 mmol, 8 equiv.) was added to a portion of $TaCl_5$ (0.500 g; 1.39 mmol) suspended in benzene (4 mL). The mixture was stirred for 5 min at room temperature resulting in formation of a yellow solution. A solution of NEt_3 (0.570 g; 5.58 mmol, 4 equiv.) in toluene (1 mL) was added dropwise to the reaction mixture, producing orange solution. Red oil separated from the reaction mixture and transformed into an orange precipitate within 20 minutes of stirring. The precipitate was filtered, washed with toluene (4 mL) and dried under vacuum producing the triethylammonium salt $[HNEt_3][Ta\{NCCHCH_3NEt_3\}Cl_5]$ (0.685 g, 1.11 mmol, 79% yield based on the amount of $TaCl_5$). Recrystallization from 1 mL of CH_3CN produced yellow crystalline solids of the acetonitrile adduct **2** (0.290 g, 0.558 mmol, 40% yield based on the amount of $TaCl_5$).

^1H NMR (CD_3CN): δ 5.12 (q, 1H, C=C(*H*)(CH_3)), 3.62 (q, $^3J_{HH}$ = 8 Hz, 6H, (C=C(H)CH_3)N(CH_2CH_3)$_3$), 2.56(d, $^3J_{HH}$ = 8 Hz, 3H, C=C(H)(CH_3)), 1.98 (s, 3H, CH_3CN), 1.21 (t, 9H, (C=C(H)CH_3)N(CH_2CH_3)$_3$). ^{13}C NMR (CD_3CN): δ 145.6 (*C*=C(H)(CH_3)), 117.5 (C=*C*(H)(CH_3)), 52.6 ($N(CH_2CH_3)_3$), 11.6 (C=C(H)(CH_3)), 8.4 ($N(CH_2CH_3)_3$). Calcd. for $C_{11}H_{22}Cl_4N_3Ta$: C, 25.45; H, 4.27; N, 8.09 Found. C, 25.09; H, 3.79; N, 8.15.

Synthesis of $[Ta\{NCC(CH_3)_2NEt_3\}Cl_4]((CH_3)_2CHCN)$ (3)

A portion of (*i*-Pr)CN (0.770 g; 11.2 mmol, 4 equiv.) was added to a portion of $TaCl_5$ (1.00 g, 2.79 mmol) suspended in toluene (10 mL). The mixture was stirred for 5 min at room temperature resulting in formation of a yellow solution. A solution of NEt_3

(1.130 g; 11.2 mmol, 4 equiv.) in toluene (1 mL) was added dropwise to the reaction mixture, producing orange solution. Red oil separated from the reaction mixture and transformed into a red precipitate within 10 minutes of stirring. The mixture was stirred for 18 h at room temperature. The precipitate was filtered, washed with 8 mL of toluene, and dried under vacuum producing orange powder. The crude product was dissolved in the mixture of 2 mL dichloromethane and 0.1 mL of (*i*-Pr)CN, and layered with 2 mL of toluene. The red crystalline solid was collected and washed with 1 mL of chloroform (0.521 g, 0.928 mmol, 33% yield based on the amount of $TaCl_5$).

^{1}H NMR (CD_2Cl_2): δ 3.75 (q, 6H, $(CH_3)(CH_3)C=CN(CH_2CH_3)_3$), 2.99 (sp, $^3J_{HH}$ = 8 Hz, 1H, $TaNCCH(CH_3)_2$), 2.83 (s, 3H, $(CH_3)(CH_3)C=CN(CH_2CH_3)_3$), 2.43 (s, 3H, $(CH_3)(CH_3)C=CN(CH_2CH_3)_3$), 1.41 (d, $^3J_{HH}$ = 8 Hz, 6H, $TaNCCH(CH_3)_2$), 1.32 (t, 9H, $(CH_3)(CH_3)C=CN(CH_2CH_3)_3$). ^{13}C NMR ($CD_2Cl_2$): δ 141.1 ($(CH_3)(CH_3)C=CN(CH_2CH_3)_3$), 128.0 ($TaNCCH(CH_3)_2$)), 125.0 ($(CH_3)(CH_3)C=CN(CH_2CH_3)_3$), 25.3 ($TaNCCH(CH_3)_2$), 21.6 ($(CH_3)(CH_3)C=CN(CH_2CH_3)_3$), 20.7 ($(CH_3)(CH_3)C=CN(CH_2CH_3)_3$), 19.0 ($TaNCCH(CH_3)_2$), 8.9 $(CH_3)(CH_3)C=CN(CH_2CH_3)_3$). Calcd. for $C_{14}H_{28}Cl_4N_3Ta$: C, 29.97; H, 5.03; N, 7.49 Found. C, 29.95; H, 4.93; N, 7.43.

Synthesis of [HN(*i*-Pr)$_2$Et][Ta{NC(CMe$_2$)CMe$_2$CN}Cl$_4$] (4)

A portion of (*i*-Pr)CN (0.160 g; 2.14 mmol, 4 equiv.) was added to a portion of $TaCl_5$ (0.20 g, 0.56 mmol) suspended in toluene (1 mL). The mixture was stirred for 5 min at room temperature resulting in formation of a yellow solution. A solution of N(*i*-Pr)$_2$Et (0.072 g; 0.56 mmol, 1 equiv.) in toluene (1 mL) was added dropwise to the reaction mixture, producing a red solution. Red oil separated from the reaction mixture and

transformed into a red precipitate within 10 minutes of stirring. The mixture was stirred for 18 h at room temperature. The precipitate was filtered, washed with 2 mL of toluene and 2 mL of dichloromethane, and dried under vacuum producing orange powder (0.270 g, 0.458 mmol, 81% yield based on the amount of $TaCl_5$). Single crystals for X-ray diffraction study were grown by a slow diffusion of toluene into a solution of the product in dichloromethane/acetonitrile mixture.

^{1}H NMR (CD_3CN): δ 6.28 (t, 1H, *H*N(*i*-Pr)$_2$Et), 3.68 (q, 2H, HN(*i*-Pr)$_2$C*H*$_2$CH$_3$), 3.16 (sp, 2H, HN(C*H*(CH$_3$)$_2$)$_2$Et), 2.60 (s, 1H, TaNC=C(C*H*$_3$)$_2$), 2.35 (s, 1H, TaNC=C(C*H*$_3$)$_2$), 1.75 (s, 6H, N≡CC(C*H*$_3$)$_2$, 1.32 (overlapping d and t, 15H, HN(CH(C*H*$_3$)$_2$)$_2$CH$_2$C*H*$_3$). Calcd. for $C_{16}H_{32}Cl_4N_3Ta$: C, 32.62; H, 5.47; N, 7.13 Found. C, 32.28; H, 5.19; N, 6.63.

Synthesis of [DNEt$_3$][Ta{NCCD$_2$NEt$_3$}Cl$_5$] (1-d)

A portion of CD_3CN (0.060 g, 1.4 mmol, 5 equiv.) was added to a portion of $TaCl_5$ (0.10 g; 0.28 mmol) suspended in benzene (4 mL). The mixture was stirred for 30 min at room temperature resulting in formation of a pale yellow solution. A solution of NEt_3 (0.056 g; 0.56 mmol, 2 equiv.) in benzene (0.5 mL) was added dropwise to the reaction mixture, producing orange solution. Yellow precipitate formed within a minute after the addition. The volatiles were removed under vacuum producing analytically pure yellow solid. (0.160 g, 0.266 mmol, 95% yield based on the amount of $TaCl_5$).

^{1}H NMR (CD_2Cl_2): δ 3.58 (q, 6H, (C=CD$_2$)N(C*H*$_2$CH$_3$)$_3$), 3.25 (q, 6H, DN(C*H*$_2$CH$_3$)$_3$), 1.37 (t, 9H, N(CH$_2$C*H*$_3$)$_3$), 1.29 (t, 9H, N(CH$_2$C*H*$_3$)$_3$). ^{13}C NMR (CD_2Cl_2): δ 147.8 (*C*=CD$_2$), 101.6 (quint. $^1J_{CD}$ = 20 Hz, C=*C*D$_2$), 49.2 (N(*C*H$_2$CH$_3$)$_3$), 44.3 (N(*C*H$_2$CH$_3$)$_3$), 6.9 (N(CH$_2$*C*H$_3$)$_3$), 5.3 (N(CH$_2$*C*H$_3$)$_3$).

The competitive formation of [HNEt$_3$][Ta{NCCH$_2$NEt$_3$}Cl$_5$] (1) and [DNEt$_3$][Ta{NCCD$_2$NEt$_3$}Cl$_5$] (1-d) from the equimolar mixture of CH$_3$CN and CD$_3$CN and NEt$_3$ as a limiting reactant.

An equimolar mixture of CH_3CN (0.23 g, 5.58 mmol, 10 equiv.) and CD_3CN (0.25 g, 5.58 mmol. 10 equiv.) in 1 ml of CD_2Cl_2 was added to a portion of a solid $TaCl_5$ (0.2 g; 0.56 mmol) and stirred for 30 m until it turned into a clear solution. A solution NEt_3 (0.028 g; 0.27 mmol, 0.5 equiv.) in 0.5 mL of CD_2Cl_2 was added dropwise producing a yellow solution. The product distribution (ratio of **1** vs. **1-d**) was determined using integral intensities of signals of the NCH_2CH$_3$ group (common for both **1** and **1-d**) and the Ta=NCCH_2 group (observed only for **1**) in the ^{1}H NMR spectrum of the reaction mixture.[9] The ratio P_H/P_D = 1.48 was found. Two independent experiments led to analogous results.

Calculation details for the deprotonated intermediate TaCl$_4$(CH$_3$CN)(CH$_2$CN)

The molecular structure was optimized in Spartan 10 using DFT B3LYP 6-31+G* basis. LANL2DZ effective core basis set was used for Ta.

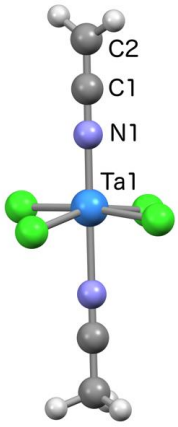

Figure 3.5. Optimized structure of deprotonated intermediate TaCl$_4$(CH$_3$CN)(CH$_2$CN).

Selected bond lengths:

Ta1–N1 1.940 Å

N1–C1 1.213 Å

C1–C2 1.317 Å

The list of atomic coordinates for $TaCl_4(CH_3CN)(CH_2CN)$ model:

Ta	-0.456883	0.148593	0.106519
N	-2.257664	0.699676	0.572131
Cl	0.542380	2.015817	1.142103
Cl	-0.264372	1.248121	-2.003491
Cl	0.022384	-1.154581	2.047698
Cl	-1.184833	-1.803453	-1.000113
C	-3.381881	1.041258	0.873785
C	-4.602509	1.411984	1.202037
H	-4.765393	2.331599	1.753497
H	-5.453475	0.799298	0.924697
N	1.669608	-0.514051	-0.437942
C	2.740647	-0.845975	-0.710521
C	4.091208	-1.264412	-1.052232
H	4.628380	-1.556389	-0.144471
H	4.622201	-0.439803	-1.537330
H	4.050201	-2.117681	-1.736367

X-Ray Structure Determination, $[HNEt_3][Ta\{NC(CH_2)NEt_3\}Cl_5]$ (1)

X-ray intensity data from an oval yellow plate crystal were collected at 100(2) K using a Bruker SMART APEX diffractometer (Mo Kα radiation, λ = 0.71073 Å).[10] The raw area detector data frames were reduced and corrected for absorption effects using the

SAINT+ and SADABS programs.[11] Final unit cell parameters were determined by least-squares refinement of 7825 reflections from the data set. The structure was solved by heavy-atom methods with SHELXS.[12] Subsequent difference Fourier calculations and full-matrix least-squares refinement against F^2 were performed with SHELXL-2014/1[12] using OLEX2.[13]

The compound crystallizes in the monoclinic space group $P2_1/c$ as determined by the pattern of systematic absences in the intensity data. The asymmetric unit consists of one formula unit. Non-hydrogen atoms were refined with anisotropic displacement parameters. Hydrogen atoms bonded to carbon were located in difference maps before being placed in geometrically idealized positions and included as riding atoms. The ammonium proton H3 was located in a difference map and refined freely. The largest residual electron density peak and hole in the final difference map are +1.71 and -0.48 $e^-/Å^3$, located 0.80 and 1.46 Å, respectively, from the tantalum atom.

X-Ray Structure Determination, Ta{NC(CHCH$_3$)NEt$_3$}Cl$_4$(NCCH$_3$) (2).

X-ray intensity data from a yellow block were collected at 100(2) K using a Bruker D8 QUEST diffractometer equipped with a PHOTON 100 CMOS area detector and an Incoatec microfocus source (Mo Kα radiation, λ = 0.71073 Å). The raw area detector data frames were reduced and corrected for absorption effects using the SAINT+ and SADABS programs.[11] Final unit cell parameters were determined by least-squares refinement of 9680 reflections taken from the data set. The structure was solved by Patterson methods with SHELXS.[12] Subsequent difference Fourier calculations and full-matrix least-squares refinement against F^2 were performed with SHELXL-2014[12] using OLEX2.[13]

The compound crystallizes in the orthorhombic system. The space groups *Pnma*

and *Pna*2_1 were consistent with the pattern of systematic absences in the intensity data; intensity statistics were inconclusive. Eventually the acentric group *Pna*2_1 (No. 33) was determined by achieving a reasonable and stable solution and refinement. The final model was checked with ADDSYM,[4] which found no missed symmetry elements. The asymmetric unit consists of one complex. All non-hydrogen atoms were refined with anisotropic displacement parameters. Hydrogen atoms were located in difference maps before being included as riding atoms. The absolute structure (Flack) parameter after the final refinement cycle was -0.013(3). The largest residual electron density peak in the final difference map is 0.87 $e^-/Å^3$, located 1.32 Å from the tantalum atom.

X-Ray Structure Determination, Ta{NC(CMe$_2$)NEt$_3$}Cl$_4$(NCCHMe$_2$) (3).

Crystals formed as densely intergrown yellow-orange blocks. Several crystals examined showed broad diffraction maxima and streaking in the area detector frames. The selected data crystal was an irregular fragment cleaved apart from the massive aggregation, and gave relatively sharp diffraction peaks. Some difficulty in indexing a reasonable unit cell was eventually determined to be caused by non-merohedral twinning. Using the Bruker Cell_Now program, all reflections from a set of 675 from the data crystal were indexed entirely to two domains with the reported unit cell parameters. The derived twin law, relating indices of one domain to those of the other, is (1 0 0 / 0 -1 0 / -0.427 0 -1). This corresponds to a rotation of 180° about the real-space [100] axis. X-ray intensity data were collected at 100(2) K using a Bruker D8 QUEST diffractometer equipped with a PHOTON 100 CMOS area detector and an Incoatec microfocus source (Mo Kα radiation, λ = 0.71073 Å). The raw area detector data frames were reduced and corrected for absorption effects using the SAINT+ and TWINABS programs. TWINABS also constructed SHELX HKLF-

4 and HKLF-5 format reflection files for solution and refinement, respectively. Final unit cell parameters were determined by least-squares refinement of 9841 reflections in the range $4.45° < 2\theta < 55.06°$ taken from both twin domains. The structure was solved by dual-space methods with SHELXT.[12] Subsequent difference Fourier calculations and full-matrix least-squares refinement against F^2 were performed with SHELXL-2014[12] using OLEX2.[13] The crystal is composed of nearly equal volumes of each twin domain, with the major fraction refining to 0.526(1).

The compound crystallizes in the monoclinic system. The pattern of systematic absences in the intensity data was uniquely consistent with the space group $P2_1/c$. The asymmetric unit consists of one complex. All non-hydrogen atoms were refined with anisotropic displacement parameters. Hydrogen atoms bonded to carbon were located in difference maps before being included as standard riding atoms. The largest residual electron density peak in the final difference map is 0.98 $e^-/Å^3$, located 0.87 Å from the tantalum atom.

X-Ray Structure Determination, [HN(*i*-Pr)$_2$Et][Ta{NC(CMe$_2$)CMe$_2$CN}Cl$_4$]·CH$_3$CN (4)

X-ray intensity data from an orange cube-shaped crystal were collected at 100(2) K using a Bruker D8 QUEST diffractometer equipped with a PHOTON 100 CMOS area detector and an Incoatec microfocus source (Mo Kα radiation, λ = 0.71073 Å). The raw area detector data frames were reduced and corrected for absorption effects using the SAINT+ and SADABS programs.[11] Final unit cell parameters were determined by least-squares refinement of 9431 reflections taken from the data set. The structure was solved by direct methods with SHELXT.[12] Subsequent difference Fourier calculations and full-

matrix least-squares refinement against F^2 were performed with SHELXL-2014[12] using OLEX2.[13]

The compound crystallizes in the tetragonal system. The pattern of systematic absences in the intensity data was uniquely consistent with the space group $I4_1/a$, which was confirmed by structure solution. The asymmetric unit consists of one $[TaCl_4(C_8H_{12}N_2)]$ polymeric repeat unit, one $HN(^iPr)_2(Et)$ cation and one acetonitrile molecule. The acetonitrile molecule is badly disordered and was modeled with four differently oriented components. The N-C and C-C distances were strongly restrained to maintain physically reasonable molecular geometries. The occupancies of the four individual components were constrained to sum to unity, and all component atoms were assigned a fixed isotropic displacement parameter of 0.10 Å^2. All other non-hydrogen atoms were refined with anisotropic displacement parameters. Hydrogen atoms were placed in geometrically idealized positions included as riding atoms with d(X-H) = 1.00 Å and U_{iso}(H) = 1.2U_{eq}(X) for CH and NH hydrogens, d(C-H) = 0.99 Å and U_{iso}(H) = 1.2U_{eq}(C) for methylene hydrogens, d(C-H) = 0.98 Å and U_{iso}(H) = 1.5U_{eq}(C) for methyl hydrogens. The methyl hydrogens were allowed to rotate as a rigid group to the orientation of maximum observed electron density except for the acetonitrile hydrogens, which were placed in arbitrary orientations and not allowed to rotate. The largest residual electron density peak in the final difference map is 0.74 e$^-$/Å^3, located 1.10 Å from H2SB, indicating the approximate nature of the disorder model.

Table 3.1 Crystallographic table for single crystal X-ray data for compounds **1, 2, 3,** and **4.**

CCDC	1500014	1500015	1500016	1500017
Compounds identifications	**1**	**2**	**3**	**4**
Empirical formula	$C_{14}H_{33}Cl_5N_3Ta$	$C_{11}H_{22}Cl_4N_3Ta$	$C_{14}H_{28}Cl_4N_3Ta$	$C_{18}H_{35}Cl_4N_4Ta$
Formula weight	601.63	519.06	561.14	630.25
Temperature/K	100(2)	100(2)	100(2)	100(2)
Crystal system	monoclinic	orthorhombic	monoclinic	tetragonal
Space group	$P2_1/c$	$Pna2_1$	$P2_1/c$	$I4_1/a$
a/Å	16.1004(12)	15.0296(8)	9.2314(4)	17.6001(6)
b/Å	10.5361(8)	8.6155(4)	15.3766(6)	17.6001(6)
c/Å	13.4658(10)	13.6508(7)	14.7811(6)	33.3526(13)
α/°	90	90	90	90
β/°	102.834(2)	90	97.673(2)	90
γ/°	90	90	90	90
Volume/$Å^3$	2227.2(3)	1767.61(15)	2079.35(15)	10331.4(8)
Z	4	4	4	16
$\rho_{calc}g/cm^3$	1.794	1.950	1.792	1.621
μ/mm^{-1}	5.537	6.814	5.800	4.680
Crystal size/mm^3	0.22 × 0.2 × 0.04	0.18 × 0.12 × 0.1	0.16 × 0.08 × 0.05	0.22 × 0.2 × 0.16
Radiation	MoKα (λ = 0.71073)	MoKα (λ = 0.71073)	MoKα (λ = 0.71073)	MoKα (λ = 0.71073)
2Θ range for data collection/°	2.594 to 54.206	5.42 to 60.178	4.452 to 55.108	4.334 to 56.636
Reflections collected	33354	52526	4875	103734

Data/restraints/parameters	4910/0/218	5189/1/178	4875/0/208	6440/13/266
Goodness-of-fit on F^2	1.044	1.126	1.261	1.036
Final R indexes [I>=2σ (I)]	R_1 = 0.0228, wR_2 = 0.0499	R_1 = 0.0127, wR_2 = 0.0308	R_1 = 0.0281, wR_2 = 0.0523	R_1 = 0.0205, wR_2 = 0.0421
Final R indexes [all data]	R_1 = 0.0287, wR_2 = 0.0529	R_1 = 0.0130, wR_2 = 0.0310	R_1 = 0.0320, wR_2 = 0.0531	R_1 = 0.0322, wR_2 = 0.0454
Largest diff. peak/hole / e $Å^{-3}$	1.71/-0.48	0.87/-0.47	0.98/-1.25	0.74/-0.67

REFERENCES

1. (a) Marchetti, F.; Pampaloni, G.; Repo, T. *Eur. J. Inorg. Chem.* **2008**, *2008*, 2107–2112 (b) Bini, R.; Chiappe, C.; Marchetti, F.; Pampaloni, G.; Zacchini, S. *Inorg. Chem.* **2010**, *49*, 339–351 (c) Marchetti, F.; Pampaloni, G.; Zacchini, S. *Dalton Trans.* **2007**, 4343–4349 (d) Bondi, R.; Marchetti, F.; Pampaloni, G.; Zacchini, S. *Polyhedron* **2015**, *100*, 192–198.
2. Willey, G. R.; Woodman, T. J.; Drew, M. *Polyhedron* **1997**, *16*, 351–353.
3. (a) Jayaratne, K. C.; Yap, G. P. A.; Haggerty, B. S.; Rheingold, A. L.; Winter, C. H. *Inorg. Chem.* **1996**, *35*, 4910–4920 (b) Bezler, H.; Strahle, J. *Z. Naturforsch., B: Anorg. Chem., Org. Chem.* **1979**, *34*, 1199 (c) Clegg, W.; Errington, R. J.; Hockless, D. C. R.; Redshaw, C. *Polyhedron* **1991**, *10*, 1959–1961 (d) Canich, J. A.; Cotton, F. A.; Duraj, S. A.; Roth, W. J. *Polyhedron* **1986**, *5*, 895–898 (e) Chao, Y.W.; Wexler, P. A.; Wigley, D. E. *Inorg. Chem.* **1990**, *29*, 4592–4594
4. Cowley, A. R.; Dilworth, J. R.; Nairn, A. K.; Robbie, A. J. *Dalton Trans.* **2005**, 680–693.
5. (a) Tran, S. D.; Tronic, T. A.; Kaminsky, W.; Heinekey, D. M.; Mayer, J. M. *Inorganica Chimica Acta* **2011**, *369*, 126–132 (b) Flynn, S. R.; Wass, D. F. *ACS Catal*., **2013**, *3*, 2574–2581 (c) Metters, O. J.; Forrest, S. J. K.; Sparkes, H. A.; Manners, I.; Wass, D. F. *J. Am. Chem. Soc.*, **2016**, *138*, 1994–2003.
6. (a) Doxsee, K. M.; Farahi, J. B.; Hope, H. *J. Am. Chem. Soc.,* **1991**, *113*, 8889–8898 (b) Zhang, W.; Yamada, J.; Nomura, K. *Organometallics* **2008**, *27*, 5353–5360. (c) Tsurugi, H.; Ohno, T.; Kanayama, T.; Arteaga-Müller, R. A.; Mashima, K. *Organometallics* **2009**, *28*, 1950–1960 (e) Basuli, F.; Bailey, B. C.; Watson, L. A.;

Tomaszewski, J.; Huffman, J. C.; Mindiola, D. J. *Organometallics* **2005**, *24*, 1886–1906 (f) Bailey, B. C.; Fout, A. R.; Fan, H.; Tomaszewski, J.; Huffman, J. C.; Gary, J. B.; Johnson, M. J. A.; Mindiola, D. J. *J. Am. Chem. Soc.* **2007**, *129*, 2234–2235. (g) Kilgore, U. J.; Sengelaub, C. A.; Fan, H.; Tomaszewski, J.; Karty, J. A.; Baik, M.-H.; Mindiola, D. J. *Organometallics* **2009**, *28*, 843–852.

7. Selby, J. D.; Manley, C. D.; Feliz, M.; Schwarz, A. D.; Clot, E.; Mountford, P. *Chem. Commun.* **2007**, 4937–3.
8. (a) Cotton, F. A.; Hall, W. T. *Inorg. Chem.* **1978**, *17*, 3525–3528 (b) Lopez, L. P. H.; Schrock, R. R.; Müller, P. *Organometallics* **2008**, *27*, 3857–3865. (c) Duchateau, R.; Williams, A. J.; Gambarotta, S.; Chiang, M. Y. *Inorg. Chem.* **1991**, *30*, 4863–4866. (d) Cross, J. L.; Garrett, A. D.; Crane, T. W.; White, P. S.; Templeton, J. L. *Polyhedron* **2004**, *23*, 2831–2840 (e) Tsai, Y.-C.; Stephens, F. H.; Meyer, K.; Mendiratta, A.; Gheorghiu, M. D.; Cummins, C. C. *Organometallics* **2003**, *22*, 2902–2913.
9. Simmons, E. M.; Hartwig, J. F. *Angew. Chem. Int . Ed.* **2012**, *51*, 3066 – 3072.
10. APEX3 Version 2016.5-0 and SAINT+ Version 8.37A. Bruker AXS, Inc., Madison, Wisconsin, USA, 2016.
11. SADABS-2016/2: Krause, L., Herbst-Irmer, R., Sheldrick G.M. and Stalke D. *J. Appl. Cryst.* 2015, *48*, 3-10.
12. (a) SHELXT: Sheldrick, G.M. *Acta Cryst*. 2015, *A71*, 3-8. (b) SHELXL: Sheldrick, G.M. *Acta Cryst*. 2008, A64, 112-122.
13. OLEX2: a complete structure solution, refinement and analysis program. Dolomanov, O. V., Bourhis, L. J., Gildea, R. J., Howard J. A. K. and Puschmann, H. *J. Appl. Cryst.* **2009**, *42*, 339-341.

Chapter 4

Activation of C–H Bonds of Alkyl- and Arylnitriles by The $TaCl_5$–PPh_3 Lewis Pair

Rahman, M. M.; Smith, M. D.; Amaya, J. A.; Makris, T. M.; Peryshkov, D. V. *Inorg. Chem.*, **2017**, *56*, 11798–11803.

4.1 Introduction

Activation of a substrate upon coordination to a metal center for a subsequent attack by a reagent, such as a nucleophilic base, is an important reaction pathway for many metal-promoted transformations. High Lewis acidity of a metal center is often found to facilitate both coordination and activation steps. Early transition metal complexes with low electron counts are strong Lewis acids, and they have been demonstrated to participate in a multitude of ligand activation reactions. Perhaps the simplest example of d^0 Group 5 compounds, their (Nb, Ta) chlorides and bromides, form strong adducts with donor molecules; however, due to high Lewis acidity, the metal center tends to promote activation of coordinated organic ligands. For example, ring-opening of THF, activation of benzylic C–H bonds, deoxygenation–dehydrohalogenation of aryl amides to form nitriles, decarboxylation of amino acids, and dehydration of ureas to form carbodiimides by $NbCl_5$ and $TaCl_5$ have been described.[1–7]

We recently reported that α-hydrogen atoms of nitriles in $TaCl_5$(RCN) (R = Me, Et, *i*-Pr) adducts become increasingly acidic and can be deprotonated by triethylamine and converted to vinylimido complexes upon subsequent nucleophilic attack.[8,40,41] In this article, we report facile activation of strong C–H bonds by the cooperative interaction of a highly Lewis acidic high-valent early transition metal halide, $TaCl_5$, and PPh_3 at room temperature. As an example, the coordination of benzonitrile to the strong Lewis acid $TaCl_5$ led to significant activation of the *para*- position of an aromatic ring of the ligand and allowed deprotonation even by the relatively weak base PPh_3. As a result, two activated benzonitrile fragments formed zwitterionic bimetallic enediimido complex through C=C double bond formation. This reactivity is patently different from the previously reported

activation of nitriles by late transition metal complexes, and it is also different from the reactivity of frustrated Lewis pairs (FLPs) with nitriles, which is normally limited to the formation of stable adducts.

4.2 Results and Discussion

The unexpected reactivity reported below as the independently prepared and isolated $TaCl_5 \cdot PPh_3$ reacted with nitriles in the same manner as a mixture of $TaCl_5$, a nitrile substrate, and PPh_3.

The unusual cooperative reactivity in this system was first demonstrated in the reaction of the $TaCl_5$–PPh_3 with benzonitrile, which does not contain α-hydrogen atoms, thus potentially leading to a different reaction outcome than the formation of a vinylimido group as it was the case with acetonitrile activation by the $TaCl_5$–NEt_3 system.[8] The addition of 1.14 equiv. of PPh_3 to a chlorobenzene solution containing 1 equiv. $TaCl_5$ and 1.1 equiv. of PhCN at room temperature led to the series of color changes from orange to dark brown to dark green to deep blue, finally producing white solid. Notably, the $^{31}P\{^1H\}$ NMR spectrum of the reaction mixture contained only a set of two doublets with J_{PP} = 3 Hz in 1:1 ratio at 22.8 and 22.4 ppm (**Figure 4.1b**) and a signal from excess PPh_3. The product was moderately soluble in $CHCl_3$ and CH_2Cl_2. The single crystal X-ray diffraction revealed the structure of an unexpected cationic imido complex $[TaCl_4\{NC(H)(PPh_3)C_6H_4(PPh_3)\}(NCC_6H_5)][TaCl_6]$ (**1**) (**Figure 4.1c**). The *para*- position of the aromatic ring of the starting benzonitrile ligand was substituted with the triphenylphosphonium cation. The nitrogen atom of the benzonitrile was converted to the imido functionality coordinated to the metal center (Ta≡N bond length is 1.777(3) Å). The carbon atom of the former benzonitrile in **1** is sp^3-hybridized with an additional hydrogen

atom and the second triphenylphosphonium cation. The tantalum metal center remained in the oxidation state +5. Another tantalum center formed the $[TaCl_6]^-$ counterion.

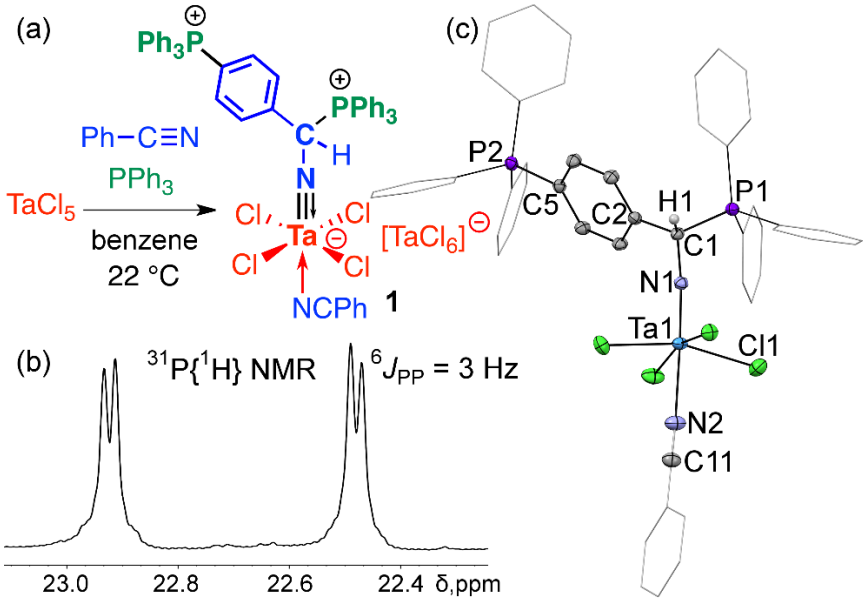

Figure 4.1 (a) Scheme of Reaction of $TaCl_5/PPh_3$ pair with benzonitrile with the formation of the Ta(V) imido complex $[TaCl_4\{NC(H)(PPh_3)C_6H_4(PPh_3)\}(NCC_6H_5)][TaCl_6]$ (**1**). (b) A fragment of the $^{31}P\{^1H\}$ NMR spectrum of **1** in CD_2Cl_2. (c) The displacement ellipsoid plot (50% probability) of **1**. The majority of hydrogen atoms and carbon atoms of triphenylphosphonium groups and the benzonitrile ligand are omitted for clarity. The $[TaCl_6]^-$ counterion and co-crystallized chlorobenzene solvent molecules are not shown. Selected distances (Å) and angles (°): Ta1–N1 = 1.777(3), Ta1–N2 = 2.380(3), C1–P1 = 1.865(3), C5–P2 = 1.795(3), C1–C2 = 1.516(4), and Ta1–N1–C1 = 170.8(2).

The formation of **1** is remarkable in regard to multiple aspects. First, the coordination of the benzonitrile ligand to the highly Lewis acidic $TaCl_5$ led to the significant activation of the *para*-hydrogen atom of the aromatic ring of the nitrile. The relatively weak base PPh_3 replaced that hydrogen atom, and another equivalent of PPh_3 scavenged it as a proton. The nitrile carbon atom then reacted with this transient $[HPPh_3]^+$ cation to complete the formation of **1**. Notably, this proton did not originate from a solvent, as the reaction in C_6D_6 did not lead to deuterium incorporation in the product.

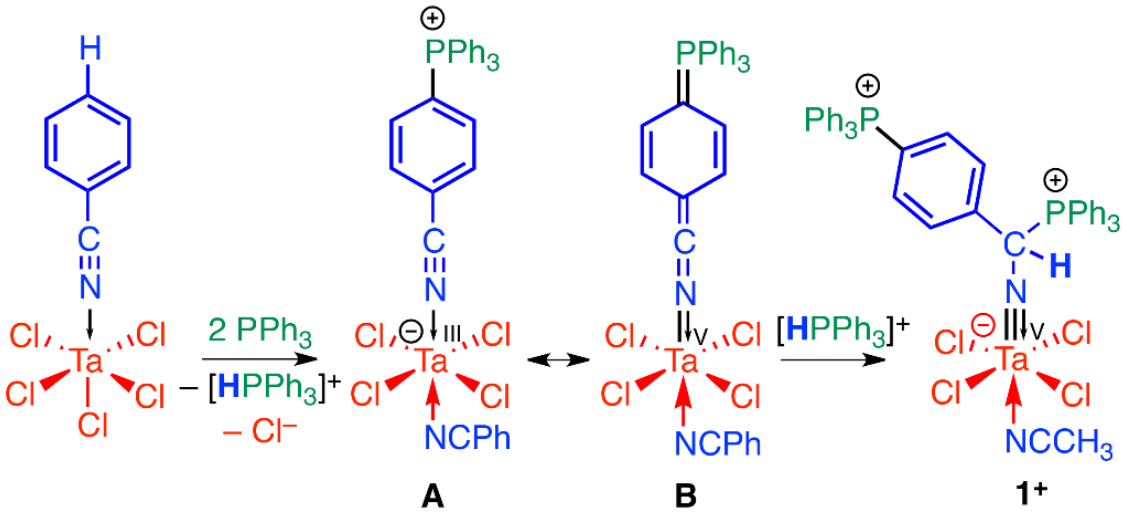

Scheme 4.1 The possible mechanism of the formation of $[TaCl_4\{NC(H)(PPh_3)C_6H_4(PPh_3)\}(NCC_6H_5)]^+$ (**1**$^+$) in the reaction of PhCN with the $TaCl_5$-PPh_3 Lewis pair.

Several possibilities can be considered for rearrangement of the intermediate formed after the substitution of the aromatic C–H bond with PPh_3. The phosphine acts as a two-electron reductant during this step. The resulting intermediate can be represented as a nitrile complex of Ta(III) (**A**) or, alternatively, as a complex of Ta(V) with a 1-azaallenylidene fragment conjugated with phosphoranylidene moiety (**B**) (**Scheme 4.1**). Both these resonance structures could be protonated at the former nitrile carbon atom to form the Ta(V) imido complex **1**. The geometry optimization calculations of the substituted intermediate suggest the preference for the form **B**, the high-oxidation state azaallenylidene complex of Ta, as evidenced by the calculated Ta–N distance of 1.966 Å corresponding to an anionic ligand rather than a coordinated nitrile. The N–C distance of 1.200 Å corresponding to a double bond and a relatively short C–P distance of 1.747 Å, corresponding to a phosphoranylidene (**Figure 4.2**).

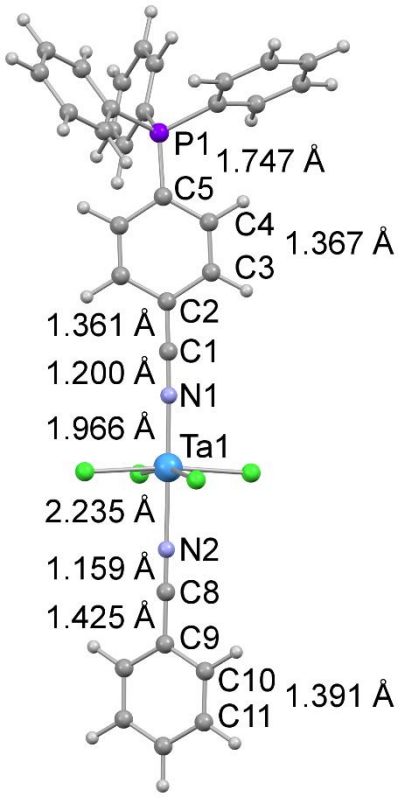

Figure 4.2 The DFT-optimized structure of the poposed substituted intermediate in the formation of **1.** Interatomic distances correspond to the formulation of the complex as a Ta(V) azaallenylidene.

Calculations have been performed using the ADF suite of programs at the PBE0/TZP level.

The orthogonal atomic coordinates of the optimized model are listed below

C -1.691913 -1.048547 0.456281

H -1.131656 -1.941626 0.712964

C -1.691913 -1.048547 0.456281

C -3.113595 1.295403 -0.190097

C -3.058350 -1.066979 0.462866

C -0.970402 0.156594 0.116595

C -1.747320 1.334278 -0.196808

C	-3.831811	0.101156	0.143772
H	-3.562122	-1.992409	0.731649
H	-1.228606	2.256766	-0.435278
H	-3.659937	2.202842	-0.429257
P	-5.569663	-0.014915	0.004007
C	-6.343298	1.635980	0.040259
C	-7.421981	4.219321	0.095029
C	-6.919309	2.135533	1.217061
C	-6.317410	2.439256	-1.112804
C	-6.849747	3.727696	-1.079849
C	-7.458712	3.421927	1.240082
H	-6.949116	1.523810	2.112854
H	-5.885442	2.062043	-2.035082
H	-6.819710	4.344109	-1.973632
H	-7.906139	3.800281	2.154516
H	-7.840397	5.221649	0.117356
C	-6.233776	-1.018532	1.384628
C	-7.240278	-2.455564	3.567063
C	-7.342100	-1.863481	1.223867
C	-5.628262	-0.904552	2.647813
C	-6.132556	-1.621648	3.732451
C	-7.842497	-2.575953	2.313688
H	-7.807862	-1.976943	0.250689

H	-4.756452	-0.269615	2.772860
H	-5.654612	-1.533254	4.703809
H	-8.697932	-3.232004	2.179646
H	-7.628704	-3.016494	4.412620
C	-6.159126	-0.799428	-1.552703
C	-6.995535	-2.020090	-3.929775
C	-5.265549	-1.584647	-2.295378
C	-7.473609	-0.619408	-2.017044
C	-7.887408	-1.229574	-3.200773
C	-5.687108	-2.195842	-3.476931
H	-4.240153	-1.705534	-1.958755
H	-8.169620	0.004940	-1.463321
H	-8.902964	-1.081341	-3.557262
H	-4.988409	-2.801446	-4.046901
H	-7.318456	-2.491116	-4.854020
C	0.390485	0.169314	0.101168
N	1.590488	0.162281	0.088427
Ta	3.555038	0.096015	0.044858
N	5.786705	0.000028	-0.021850
C	6.944109	-0.046031	-0.069359
C	8.366210	-0.106716	-0.127991
C	11.142522	-0.226391	-0.244362
C	9.122561	1.059556	0.087918

C	8.998678	-1.332963	-0.402732
C	10.387834	-1.383510	-0.457098
C	10.510671	0.990668	0.025766
H	8.617808	1.996632	0.298578
H	8.399597	-2.222132	-0.570070
H	10.882757	-2.326634	-0.668681
H	11.100351	1.887385	0.190608
H	12.226931	-0.273271	-0.289938
Cl	3.701057	-1.220464	-1.998355
Cl	3.730419	2.110636	-1.214167
Cl	3.918951	1.390329	2.071404
Cl	3.638579	-1.930823	1.297801

While the product of the reaction was the Ta(V) imido complex, a series of color changes during the synthesis might be indicative of the involvement of reduced Ta(IV) species. In order to probe whether reduction of Ta(V) to Ta(IV) played a major role in formation of **1**, samples were followed by EPR spectroscopy at different stages of the synthetic procedure. Spectra of the reaction mixture taken within minutes after mixing the reagents at room temperature displayed a nearly axial signal at g = 2.11 and 1.89, and a minor signal from free radical species at g = 2.0 (**Figure 4.3**).

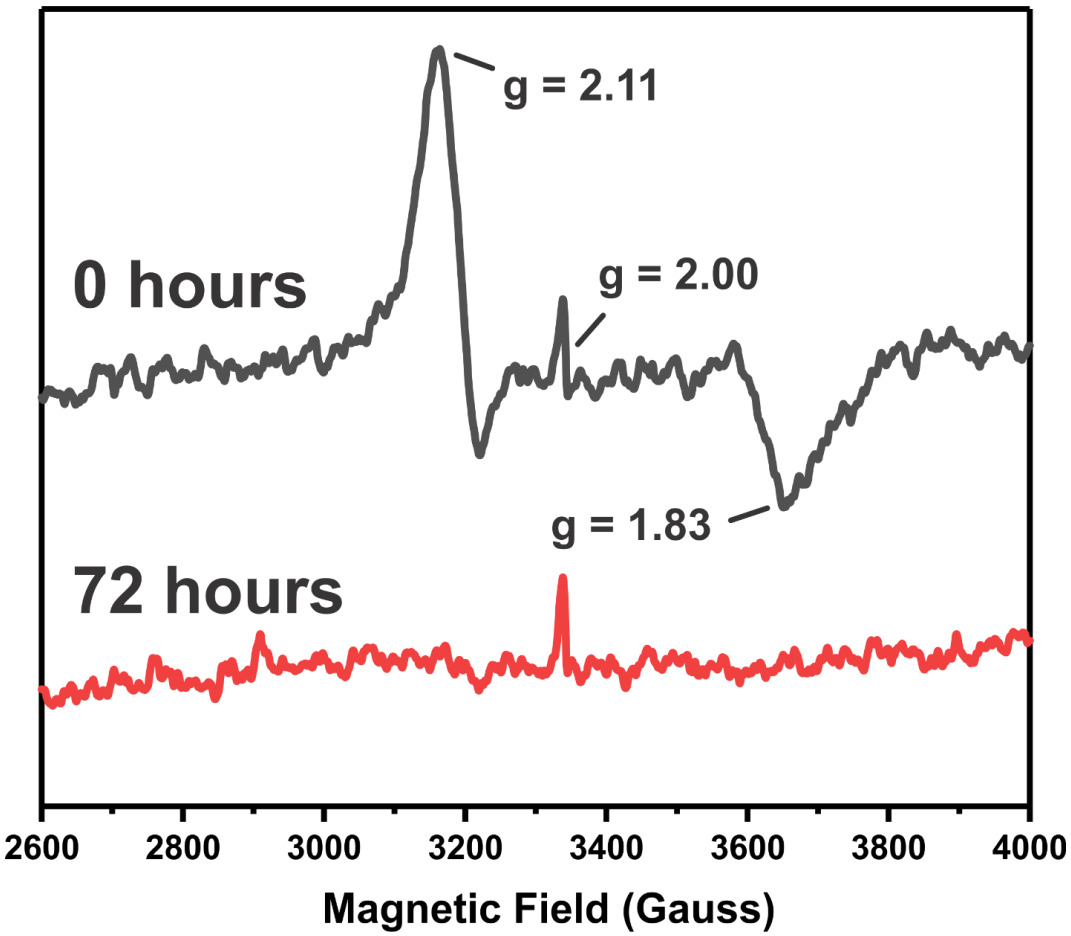

Figure 4.3 The EPR spectrum of the reaction mixture during the synthesis of **1** in CH_2Cl_2.

The former signal is diagnostic of a Ta(IV) species (S=1/2).[9] Double integration and comparison to a TEMPO spin standard of known concentration[10] indicated that these Ta(IV) paramagnetic species constituted only ~1 % of the total amount of Ta in the reaction mixture. While this unidentified reduced complex may be an intermediate in the formation of **1**, its low concentration suggests that it most likely corresponds to a very minor side reaction channel, which decays slowly to a diamagnetic species over the course of 72 hours.

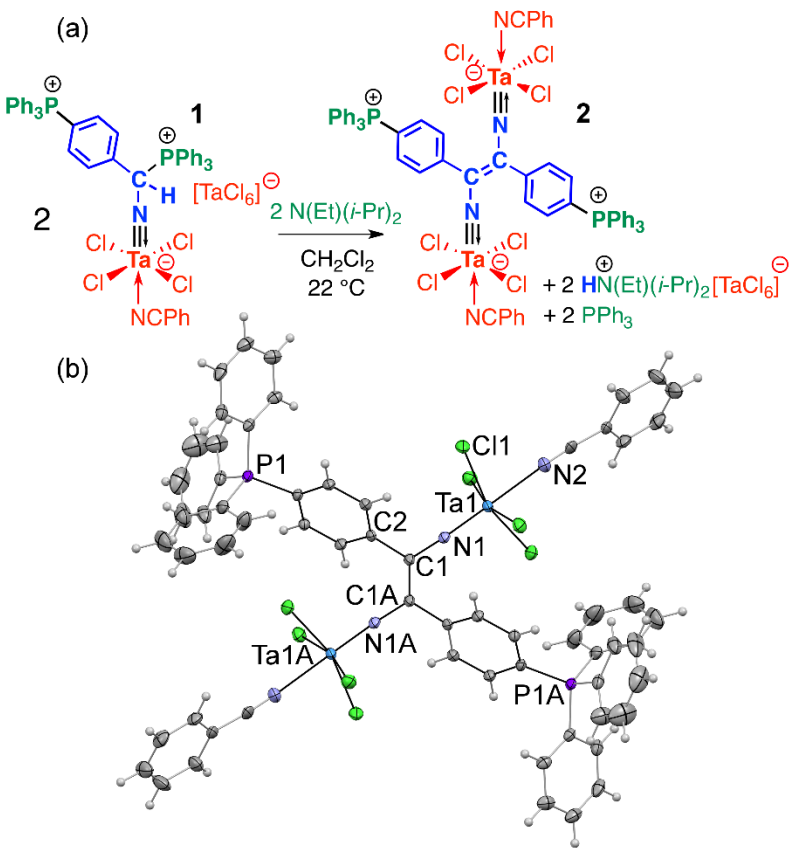

Figure 4.4 (a) Reaction of the Ta(V) imido complex **1** and Hunig's base with formation of the bimetallic Ta(V) enediimido complex $[TaCl_4\{NC(C_6H_4PPh_3)CC(PPh_3C_6H_4)CN\}TaCl_4](NCC_6H_5)_2$ (**2**). (b) The displacement ellipsoid plot (50% probability) of **2**. Co-crystallized CH_2Cl_2 solvent molecules are not shown. Selected distances (Å) and angles (°): Ta1–N1 = 1.780(2), Ta1–N2 = 2.345(2), N1–C1 = 1.369(3), C1–C1A = 1.370(4), C1–C2 = 1.493(3), Ta1–N1–C1 = 174.5(2).

The presence of a hydrogen atom at the carbon atom of the imido group (H1(C1) in the crystal structure of **1**, **Figure 4.1c**) prompted us to explore its reactivity with bases. This hydrogen atom is benzylic and also in the α-position with respect to the triphenylphosphonium cation, which would make it relatively acidic. Addition of excess Hunig's base to the pale-yellow solution of **1** in CD_2Cl_2 led to the color change to intense orange and the formation of a sparingly soluble orange-brown crystalline precipitate. The ^{31}P NMR spectrum of the reaction mixture indicated a gradual disappearance of two

doublets of **1** and the appearance of two singlets at 22.8 and –5.6 ppm. The signal at –5.6 ppm corresponded to free PPh_3.

The single crystal X-ray diffraction revealed the unusual structure of the C_{2h}-symmetric bimetallic imido complex $[TaCl_4\{NC(C_6H_4PPh_3)CC(PPh_3C_6H_4)CN\}TaCl_4](NCC_6H_5)_2$ (**2**, **Figure 4.4a**). The molecular structure of **2** is derived from that of **1** by formal deprotonation of the benzylic C–H bond in **1** by the amine base and the removal of the attached PPh_3 group. The imido functionality remained intact in **2** with the Ta1–N1 bond length of 1.780(2) Å. The C1–N1 distance is 1.369(3) Å, which corresponds to the single bond character. Two imido fragments of **1** that were initially derived from benzonitrile were coupled to each other in **2** through the formation of the C1=C1A double bond (1.370(4) Å) between the carbon atoms of the imido groups completing the formation of the bimetallic (E)-1,2-diphenyl-1,2-diimidoethylene complex. The structural parameters of **2** are clearly different from the possible diiminato/diazavinylidene formulation, which would exhibit the longer central single C–C bond, shorter C=N double bonds, and longer Ta–N iminato bonds. These two ligand formulations are not resonance structures as they differ by two electrons.

Notably, the conversion of **1** to **2** was also observed *in situ* starting from benzonitrile without isolation of **1** by the sequential addition of PPh_3 and $NEt(i\text{-}Pr)_2$ to the solution of $TaCl_5$ in dichloromethane containing several equiv. of benzonitrile. Thus, the dimerization of two activated nitrile moieties through C=C double bond was achieved by the use of the Lewis pair $TaCl_5$–PPh_3 followed by the reaction with an amine base.

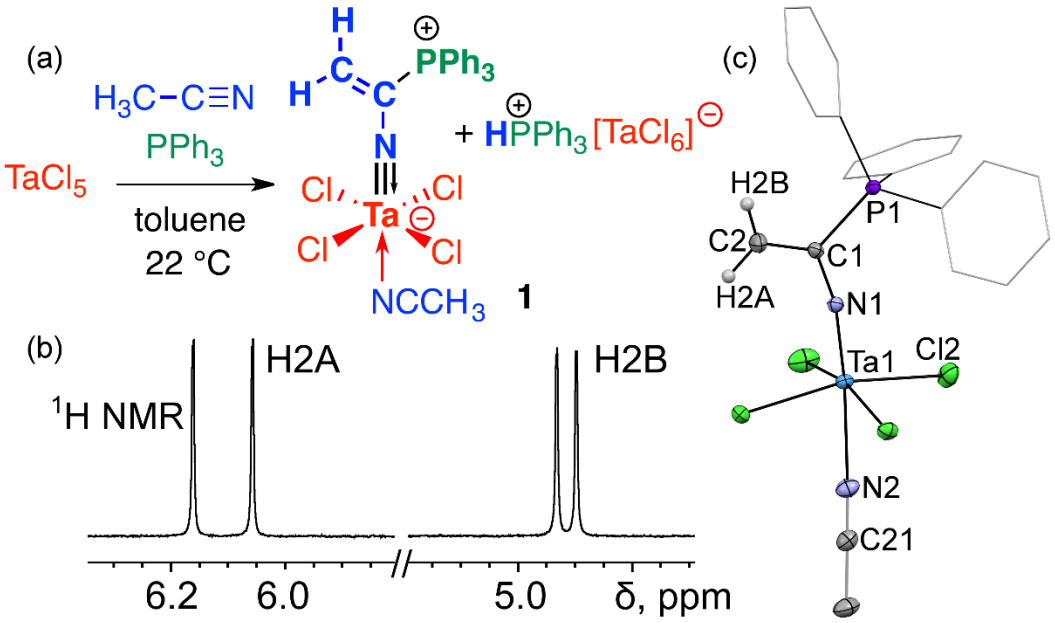

Figure 4.5 (a) Reaction of $TaCl_5/PPh_3$ pair with acetonitrile with the formation of the vinylimido Ta(V) complex $Ta\{NC(PPh_3)CH_2\}Cl_4(CH_3CN)$ (**3**). (b) A fragment of the ^1H NMR spectrum of **3** in CD_2Cl_2. (c) The displacement ellipsoid plot (50% probability) of **3**. The majority of hydrogen and carbon atoms of the triphenylphosphonium group and the acetonitrile ligand are omitted for clarity. The $[TaCl_6]^-$ counterion is not shown. Selected distances (Å) and angles (°): Ta1–N1 = 1.784(1), C1–C2 = 1.337(2), N1–C1 = 1.371(2), C1–P1 = 1.814(1), Ta1–N2 = 2.389(1), and Ta1–N1–C1 = 167.1(1).

The Ta1–N1 distance in the crystal structure is 1.784(1) Å, which indicates the formation of a tantalum imido complex. The formation of a double bond between the carbon atoms of a parent acetonitrile molecule was confirmed by the short C1=C2 distance (1.337(2) Å). The most characteristic feature of the ^1H NMR spectrum of **1** is the presence of signals of protons belonging to the vinyl CH_2 group, which appear as two doublets of doublets at 4.95 and 6.02 ppm ($^3J_{PH}$ = 13 Hz and $^3J_{PH}$ = 42 Hz, respectively, $^2J_{HH}$ = 0.8 Hz) corresponding to *cis*- and *trans*- orientations relative to the triphenylphosphonium moiety.

The $TaCl_5$–PPh_3 pair, similarly to its previously reported $TaCl_5$–NEt_3 counterpart,[8] is also capable of activation of alkylnitriles. The reaction of 2 equiv. of PPh_3 and 1 equiv.

of $TaCl_5$ in a dichloromethane solution containing excess CH_3CN at room temperature, which resulted in isolation of a zwitterionic vinyl imido complex $Ta\{NC(PPh_3)CH_2\}Cl_4(CH_3CN)$ (**3**, **Figure 4.5a**). One equivalent of PPh_3 acted as a base deprotonating acetonitrile while another equivalent incorporated as a nucleophile into the imido group. Notably, deprotonation of acetonitrile (pK_a = 31 in DMSO)[11] coordinated to $TaCl_5$ occurred with the use of the relatively weak base PPh_3 (pK_a = 8 in CH_3CN).[12]

The reaction of the $TaCl_5$–PPh_3 pair with succinonitrile, which possesses two nitrile groups and two α-hydrogen atoms that can be potentially deprotonated, in dichloromethane led to the selective formation of the bimetallic complex of Ta(V) featuring the *s-trans*-1,3-butadiene fragment and the *anti*- configuration of two imido groups at 1,4- positions, $(TaCl_4\{NC(PPh_3)CHCH(PPh_3)CN\}TaCl_4)(NCC_2H_4CN)_2$ (**4, Figure 4.6b**). The product exhibited low solubility in common organic solvents and precipitated from dichloromethane upon formation as a bright-orange microcrystalline powder. Suitable single crystals were analyzed by X-ray diffraction, which confirmed the double deprotonation of the starting nitrile and formation of two Ta(V) imido groups (**Figure 4.6c**). The complex possesses an idealized C_{2h}-symmetry with the *s-trans*- configuration of the butadiene fragment. The formally single bond C2–C2A is relatively short (1.436(4) Å) while the formally double bond C1=C2 is elongated (1.366(2) Å) indicating a degree of delocalization of the diene π-system. Interestingly, this delocalization may be partially extended to the conjugated imido groups as evidenced by the C1–N1 distance (1.360(2) Å) that is shorter than that in an analogous complex **3** (1.371(2) Å) and the Ta1≡N1 imido bond length of 1.796(2) Å that is longer than that in **3** (1.784(1) Å).

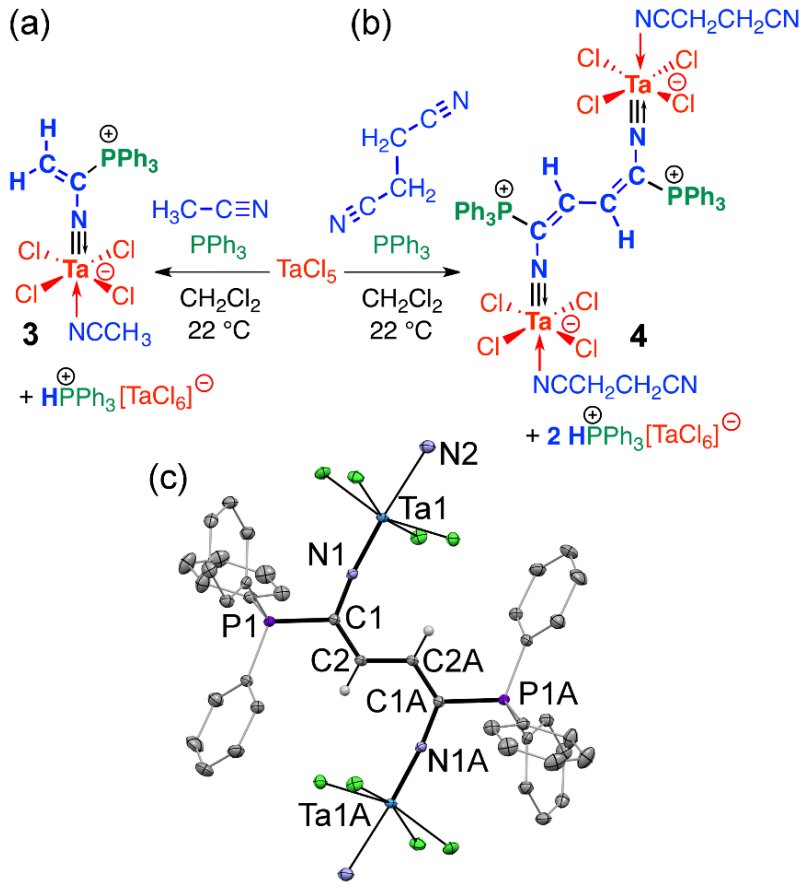

Figure 4.6 (a) Synthesis of the vinylimido Ta(V) complex Ta{NC(PPh$_3$)CH$_2$}Cl$_4$(CH$_3$CN) (**3**). (b) Synthesis of (TaCl$_4${NC(PPh$_3$)CHCH(PPh$_3$)CN}TaCl$_4$)(NCC$_2$H$_4$CN)$_2$, the bimetallic Ta(V) *anti*-1,4-diimido-*s*-*trans*-1,3-butadiene complex (**4**). (c) The displacement ellipsoid plot (50% probability) of **4**. (The majority of hydrogen atoms and carbon atoms of the succinonitrile ligand are omitted for clarity. Co-crystallized dichloromethane solvent molecules are not shown. Selected distances (Å) and angles (º): Ta1–N1 = 1.796(2), Ta1–N2 = 2.364(2), C1–P1 = 1.815(2), N1–C1 = 1.360(2), C1–C2 = 1.366(2), C2–C2A = 1.436(4), and Ta1–N1–C1 = 171.9(1)).

Activation of C–H bonds of benzonitrile by low-valent transition metal complexes has been reported to proceed through oxidative addition with often observed selectivity for *ortho*- positions.[13,14] In contrast, the activation mode reported herein proceeds through initial Lewis acid-Lewis base interaction with an indirect involvement of the Ta(V) metal center. The transformation of a phosphine to the phosphonium cation provides two electrons for the eventual conversion of a nitrile to the imido group. The propensity of the

electron-deficient Ta(V) center to form strong imido bonds is likely one of the main directing forces of this reaction. The combination of high Lewis acidity and the ability to form covalent multiple bonds to a nitrogen atom appears to be equally important for this reaction outcome. For comparison, the frustrated Lewis pair $B(C_6F_5)_3$–2,6-lutidine has been shown to form a simple borane-acetonitrile adduct with no further activation even at elevated temperatures.[15] Nitrile adducts $R–C{\equiv}N{\longrightarrow}B(C_6F_5)_3$ (R = CH_3, C_6H_5) have been shown to undergo hydrogenation to amine adducts in the presence of the $B(C_6F_5)_3$–$P(Mes)_3$ pair with the borane acting as a protecting group but no C–H bond activation of a nitrile has been observed under these conditions.[16,17] Notably, recently reported zirconocene-based FLP systems have not been shown to activate alkylnitriles or to form multiple metal-ligand bonds upon activation of any substrates.[18,19]

Previously reported instances of nitrile coupling proceeded through metal-centered reductive pathways. These reactions can lead to metallacycles and bridged bimetallic complexes. Cyclic products are formed by the reductive C–C coupling of two coordinated nitriles, often leading to five-membered metallacycles.[20–22] Two-electron reduction per two nitriles has been shown to result in the formation of the bridging diiminato ligand upon dimerization of nitriles adducts of low-valent metal centers.[23–27] This process involves reduction of a coordinated nitrile by a metal center with the formation of a radical, which then dimerizes with another equivalent of its congener to form the single C–C bond. Four-electron reduction of two nitrile ligands by low-valent Group 4–6 complexes led to formation of enediimido species related to **2**.[28–35] In those instances, the C=C double bond is formed between two nitriles, which may be considered as a stepwise reduction to first form a diazavinylidene moiety that is further reduced by two metal centers to form the

bridging enediimido group. The oxidation state of each metal center is thus increased by two. In the surprising case reported herein, all transformations appear to be driven by Lewis acid – Lewis/Brønsted base cooperative interactions where the phosphine base provides a pair of electrons, and the oxidation state of the Ta(V) metal center likely does not change in the process. The presence of high-valent Ta(V) favors the formation of the enediimido bridge with multiple metal-nitrogen bonds.

4.3 Conclusions

The aforementioned results demonstrate the high potential of the $TaCl_5$–PPh_3 cooperative Lewis pair for the cooperative activation of relatively strong aliphatic and aromatic C–H bonds. The ability of the highly Lewis acidic Ta(V) center to coordinate and activate remote positions of a substrate through a bond rearrangement sequence, which is driven by the propensity of the metal center to form multiple bonds to a ligand, is the main distinguishing feature of this system. The $TaCl_5$–PPh_3 pair thus combines reactivity patterns of "traditional" transition metal complexes and frustrated Lewis pairs. These results also demonstrate that even in the case of a seemingly simple and well-understood system, such as the $TaCl_5$–PPh_3 couple, novel latent reactivity can be discovered. More examples of unusual transformations can be anticipated as the utilization of transition metals as the Lewis acid or Lewis base components of frustrated or cooperative Lewis pairs is becoming increasingly studied.

4.4 Experimental Section

All synthetic manipulations were carried out either in a nitrogen-filled drybox or on an air free dual-manifold Schlenk line, unless stated otherwise. The solvents were sparged with nitrogen, passed through activated alumina, and stored over activated 4 Å Linde-type

molecular sieves. Benzene was distilled from CaH_2. $CDCl_3$, CD_2Cl_2, and CD_3CN were degassed and stored over activated 4 Å Linde-type molecular sieves. NMR spectra were recorded using Varian spectrometers and reported in δ (parts per million) and referenced to residual $^1H/^{13}C$ NMR signals of the deuterated solvent or an external 85% phosphoric acid (^{31}P (δ): 0.0 ppm) standard. *J* values are given in Hz. Midwest Microlab, Indianapolis, Indiana provided the elemental analysis results.

$TaCl_5$ (Strem) and PPh_3 were used as received. CH_3CN, CD_3CN, $NCCH_2CH_2CN$, C_6H_5CN, and $(i\text{-Pr})_2(Et)N$ were degassed by freeze-pump-thaw technique and stored over 4 Å Linde-type molecular sieves.

Synthesis of $[TaCl_4\{NC(H)(PPh_3)C_6H_4(PPh_3)\}(NCC_6H_5)][TaCl_6]$ (1)

A portion of benzonitrile (0.165 g, 1.60 mmol, 1.14 equiv.) was added to a portion of $TaCl_5$ (0.501 g, 1.40 mmol) partially dissolved in chlorobenzene (16 mL). The mixture was stirred until complete dissolution of solids. A solution of PPh_3 (0.406 g, 1.548 mmol, 1.1 equiv.) in chlorobenzene (4 mL) was added dropwise leading to a series of rapid color changes from orange to dark brown to dark green to deep blue within 5 minutes. Dark blue oil separated from the solution, which converted to colorless crystals upon standing overnight. The crystalline product was filtered and washed with benzene (3 × 4 mL) and dried under vacuum producing white powder (0.915 g, 0.632 mmol, 90% yield). ^1H NMR (400 MHz, CD_2Cl_2): δ 8.21 (benzyl C(*H*)PPh_3), 7.99–7.52 (overlapping m, $P(C_6H_5)_3$, -C_6H_4-). $^{31}P\{^1H\}$ NMR ($CDCl_3$): δ 22.8 (d, $^6J_{PP}$ = 3 Hz), 22.4 ($^6J_{PP}$ = 3 Hz). ^{13}C NMR (100 Mhz, CD_2Cl_2): δ 141.8 (dd, $^2J_{PC}$ = 3 Hz, $^4J_{PC}$ = 1 Hz, *ipso*- to benzyl C_6H_4), 135.9 (d, $^4J_{PC}$ = 3 Hz, *para*- $P(C_6H_5)_3$), 135.4 (d, $^4J_{PC}$ = 3 Hz, *para*- $P(C_6H_5)_3$), 135.2(d, $^2J_{PC}$ = 9 Hz, *ortho*- $P(C_6H_5)_3$), 134.5 (d, $^2J_{PC}$ = 10 Hz, *ortho*- $P(C_6H_5)_3$), 134.3-134.1 (overlapping C_6H_4,

NCC_6H_5), 132.8 (NCC_6H_5), 131.9 (dd, $^2J_{PC}$ = 18 Hz, $^4J_{PC}$ = 3 Hz, *meta*- to benzyl C_6H_4), 130.8 (d, $^3J_{PC}$ = 13 Hz, *meta*- P(C_6H_5)$_3$), 130.5 (d, $^3J_{PC}$ = 15 Hz, *meta*- P(C_6H_5)$_3$), 129.4 (NCC_6H_5), 118.9 (dd, $^1J_{PC}$ = 89 Hz, $^5J_{PC}$ = 2 Hz *ipso*- P-(C_6H_4)-), 119.1 (NCC_6H_5), 117.1 (d, $^1J_{PC}$ =88 Hz, *ipso*- P(C_6H_5)$_3$), 116.5 (d, $^1J_{PC}$ = 81 Hz, *ipso*- P(C_6H_5)$_3$), 73.0 (d, $^1J_{PC}$ = 50 Hz, benzyl *C*(H)PPh_3). Calcd. for $C_{50}H_{40}Cl_{10}N_2P_2Ta_2$: C, 41.50; H, 2.79; N, 1.94 Found. C, 41.62; H, 2.91; N, 1.68.

Synthesis of [$TaCl_4${NC($C_6H_4PPh_3$)C=C($PPh_3C_6H_4$)CN}$TaCl_4$](NCC_6H_5)$_2$ (2)

A portion of N(*i*-Pr)$_2$Et (0.059 g, 0.456 mmol, 7 equiv.) was added dropwise to a solution of **1**, (0.100 g, 0.069 mmol) in dichloromethane (2 mL). The mixture was stirred overnight at room temperature. A dark orange-brown crystalline precipitate was filtered and dried. Resulting brown precipitate was isolated, washed with dichloromethane (1 mL) and dried under vacuum (0.029 g, 0.018 mmol, 52%). The complex **2** is insoluble in common deuterated solvents such as CD_2Cl_2, THF-d_8, $CDCl_3$, and C_6D_6. $^{31}P\{^1H\}$ NMR (C_6H_5CN): δ 22.8. Calcd. for $C_{64}H_{48}Cl_8N_4P_2Ta_2$: C, 48.63; H, 3.06; N, 3.54 Found. C, 49.03; H, 3.52; N, 3.74.

Synthesis of Ta{NC(PPh_3)CH_2}Cl_4(CH_3CN) (3)

A portion of $TaCl_5$ (1.000 g; 2.79 mmol) was dissolved in the mixture of CH_3CN (0.50 g, 12 mmol) and CH_2Cl_2 (8 mL). A solution of PPh_3 (1.460 g; 5.56 mmol) in CH_2Cl_2 (4 mL) was added dropwise at room temperature. The solution color changed to yellow and a precipitate formed; the reaction mixture was stirred overnight at room temperature. The suspension was filtered yielding yellow filtrate. Slow addition of Et_2O (8 mL) caused formation of yellow powder. The precipitate was filtered, washed with Et_2O (5 mL) and dried under vacuum. The product was isolated as yellow solid (0.424 g, 0.636 mmol, 45%

yield). ^{1}H NMR (400 MHz, CD_2Cl_2): δ 7.79 (overlapping m, 15H, C-P*Ph*$_3$), 6.02 (dd, 1H, $^{3}J_{PH}$ = 42 Hz, $^{2}J_{HH}$ = 0.8 Hz, P–C=C*H*H), 4.95 (dd, 1H, $^{3}J_{PH}$ = 13 Hz, $^{2}J_{HH}$ = 0.8 Hz, P–C=CH*H*), 2.26 (s, 3H, Ta-NCC*H*$_3$). ^{31}P NMR (CD_2Cl_2): δ 19.4. ^{13}C (100 MHz, CD_2Cl_2): δ 143.5 (d, $^{1}J_{PC}$ = 89 Hz, P–*C*H=CH$_2$), 135.5 (d, P(*C*$_6$H$_5$)$_3$), 135.5 (d, P(*C*$_6$H$_5$)$_3$), 131.1 (d, $^{2}J_{PC}$ = 24.7 Hz, P–CH=*C*H$_2$), 130.6 (d, P(*C*$_6$H$_5$)$_3$), 118.52 (d, $^{1}J_{PC}$ = 87 Hz, P(*C*$_6$H$_5$)$_3$), 118.50 (CH$_3$*C*N), 3.5 (*C*H$_3$CN). Calcd. for $TaCl_4N_2PC_{22}H_{20}$: C, 39.67; H, 3.03; N, 4.20 Found. C, 39.69; H, 3.20; N, 3.86.

Synthesis of (TaCl$_4${NC(PPh$_3$)CHCH(PPh$_3$)CN}TaCl$_4$)(NCC$_2$H$_4$CN)$_2$ (4)

A portion of succinonitrile (0.100 g, 1.25 mmol, 4.5 equiv.) was added to a portion of $TaCl_5$ (0.100 g, 0.279 mmol) partially dissolved in dichloromethane (4 mL). The mixture was stirred for 1 hour at room temperature resulting in a pale-yellow solution. A solution of PPh_3 (0.146 g, 0.557 mmol, 2 equiv.) in dichloromethane (1 mL) was added dropwise, the mixture was stirred for 5 minutes and left undisturbed for slow crystallization overnight. The bright orange crystalline precipitate formed. This precipitate was washed twice with dichloromethane (2 × 2 mL) and dried under vacuum (0.046 g, 0.033 mmol, 47% yield). The product is not appreciably soluble in any common organic solvents (dichloromethane, chloroform, THF, benzene, toluene, acetonitrile), which precluded it complete spectral characterization. Calcd. for $C_{48}H_{40}Cl_8N_6P_2Ta_2$: C, 40.94; H, 2.86; N, 5.97 Found. C, 40.85; H, 2.72; N, 4.23.

Electron Paramagnetic Resonance study of formation of 1.

Samples for EPR contained Ta at a concentration of 75 mM in CH_2Cl_2 and were transferred anaerobically at the indicated timepoints during synthesis into sealed quartz tubes. Room temperature EPR spectra were collected on a Bruker EMX spectrometer at a

microwave frequency of 9.65 GHz, a modulation amplitude of 0.6 mT, and a microwave power of 6.35 mW. In order to quantify the amount of paramagnetic species present, the EPR signal was doubly integrated using Spincount software. The concentration of paramagnetic species was determined through comparison to a 1 mM sample of 2,2,6,6-tetramethyl-1-piperidinyloxy (TEMPO) in CH_2Cl_2.

X-Ray Structure Determination, of $[TaCl_4\{NC(H)(PPh_3)C_6H_4(PPh_3)\}(NCC_6H_5)][TaCl_6]\cdot 4(C_6H_5Cl)$ 1·$(C_6H_5Cl)_4$

X-ray intensity data from a colorless blocky crystal cleaved from a massive chunk were collected at 100(2) K using a Bruker D8 QUEST diffractometer equipped with a PHOTON-100 CMOS area detector and an Incoatec microfocus source (Mo Kα radiation, λ = 0.71073 Å). The raw area detector data frames were reduced and corrected for absorption effects using the Bruker APEX3, SAINT+ and SADABS programs.[36, 37] Final unit cell parameters were determined by least-squares refinement of 9625 reflections taken from the data set. The structure was solved with SHELXT.[38] Subsequent difference Fourier calculations and full-matrix least-squares refinement against F^2 were performed with SHELXL-2016[3] using OLEX2.[39]

The compound crystallizes in the triclinic system. The space group *P*-1 was confirmed by structure solution. The asymmetric unit consists of one $[TaCl_4(C_{43}H_{35}NP_2)(C_7H_5N)]^+$ cation, one $TaCl_6^-$ anion and four crystallographically independent chlorobenzene molecules. Two of the chlorobenzene molecules are disordered. Molecule Cl23/Cl24 occupies two positions with component occupancies of Cl23/Cl24 = 0.877(4)/0.123(4). Molecule Cl25/Cl26/Cl27 is disordered over three positions with occupancies Cl25/Cl26/Cl27 = 0.587(3)/0.239(2)/0.173(2). Total group occupancy was constrained to sum to one for both molecules. Each disorder component

was restrained to be geometrically similar to an ordered chlorobenzene molecule (Cl21) using SHELX SAME instructions (183 total restraints). Nearly superimposed atoms were given equal displacement parameters. The carbon atoms of the Cl25/Cl26/Cl27 disorder assembly were refined isotropically; all other non-hydrogen atoms were refined with anisotropic displacement parameters. Hydrogen atoms bonded to carbon were placed in geometrically idealized positions and included as riding atoms with *d*(C-H) = 1.00 Å and *U*iso(H) = 1.2*U*eq(C) for the methine hydrogen atom and *d*(C-H) = 0.95 Å and *U*iso(H) = 1.2*U*eq(C) for aromatic hydrogen atoms. The largest residual electron density peak in the final difference map is 2.84 $e^-/Å^3$, located 0.82 Å from Ta2. This likely arises from a heavy atom Fourier 'ripple' and not a disorder component of the $TaCl_6^-$ anion, as the occupancy of Ta2 remained at 100% upon trial refinements.

X-Ray Structure Determination of $[TaCl_4\{NC(C_6H_4PPh_3)C=C(PPh_3C_6H_4)CN\}TaCl_4](NCC_6H_5)_2\cdot 2(CH_2Cl_2)$ $2\cdot(CH_2Cl_2)_2$

X-ray intensity data from an orange rhombic plate were collected at 100(2) K using a Bruker D8 QUEST diffractometer equipped with a PHOTON-100 CMOS area detector and an Incoatec microfocus source (Mo Kα radiation, λ = 0.71073 Å). The raw area detector data frames were reduced and corrected for absorption effects using the Bruker APEX3, SAINT+ and SADABS programs.[36, 37] Final unit cell parameters were determined by least-squares refinement of 9644 reflections taken from the data set. The structure was solved with SHELXT.[38] Subsequent difference Fourier calculations and full-matrix least-squares refinement against F^2 were performed with SHELXL-2016[3] using OLEX2.[39]

The compound crystallizes in the monoclinic system. The pattern of systematic absences in the intensity data was consistent with the space groups *C*2/*c* and *Cc*, the former of which was confirmed by structure solution. The asymmetric unit in *C*2/*c* consists of half

of one $(TaCl_4(C_7H_5N))_2(C_{50}H_{38}N_2P_2)$ complex located on a crystallographic inversion center, two non-coordinated benzonitrile molecules and one dichloromethane molecule. The benzonitrile ligand coordinated to Ta1 (atoms N2, C11-C17) is disordered over two closely spaced positions with occupancies A/B = 0.60(1)/0.40(1). Both non-coordinated benzonitrile molecules are disordered about symmetry elements such that only half of each is present per asymmetric unit. Benzonitrile N21S, C21S-C27S is disordered about a two-fold axis of rotation and N31S, C31S-C37S is disordered about a crystallographic inversion center. Atoms of each non-coordinated benzonitrile molecules were refined with half-occupancy with their C_6 rings fitted to a rigid hexagon with *d*(C-C) = 1.39 Å. Further 1,3- and 1,4-C-C and C-N distances involving the CN group were applied to maintain chemically reasonable geometries. The dichloromethane disorder was modeled with three components having occupancies A/B/C = 0.542(3)/0.291(3)/0.167(3), which were constrained to sum to one. Minor CH_2Cl_2 component geometries were restrained to be similar to that of the major with SHELX SAME instructions. All non-hydrogen atoms were refined with anisotropic displacement parameters except for the minor CH_2Cl_2 disorder component (isotropic). Disordered, partially occupied atoms which are nearly superimposed in the asymmetric unit were given equal anisotropic displacement parameters. A RIGU restraint was applied to atoms of benzonitrile N21S-C27S. Hydrogen atoms bonded to carbon were located in Fourier difference maps before being placed in geometrically idealized positions and included as riding atoms with *d*(C-H) = 0.95 Å and *U*iso(H) = 1.2*U*eq(C) for aromatic hydrogen atoms and *d*(C-H) = 0.99 Å and *U*iso(H) = 1.2*U*eq(C) for methylene hydrogens. The largest residual electron density peak in the final difference map is 1.09 $e^-/Å^3$, located 0.70 Å from Ta1.

X-Ray Structure Determination, $Ta\{NC(PPh_3)CH_2\}Cl_4(CH_3CN)$

X-ray intensity data from a colorless plate crystal were collected at 100(2) K using a Bruker D8 QUEST diffractometer equipped with a PHOTON 100 CMOS area detector and an Incoatec microfocus source (Mo Kα radiation, λ = 0.71073 Å).[36] The raw area detector data frames were reduced and corrected for absorption effects using the SAINT+ and SADABS programs.[1] Final unit cell parameters were determined by least-squares refinement of 9644 reflections taken from the data set. The structure was solved by direct methods with SHELXT.[2] Subsequent difference Fourier calculations and full-matrix least-squares refinement against F^2 were performed with SHELXL-2014[2] using OLEX2.[3]

The compound crystallizes in the monoclinic system. The pattern of systematic absences in the intensity data was consistent with the space group $P2_1/n$. The asymmetric unit consists of one complex. All non-hydrogen atoms were refined with anisotropic displacement parameters. Hydrogen atoms bonded to carbon were located in difference maps before being included as riding atoms. The largest residual electron density peak in the final difference map is 0.44 $e^-/Å^3$, located 0.65 Å from C15.

X-Ray Structure Determination of $(TaCl_4\{NC(PPh_3)CHCH(PPh_3)CN\}TaCl_4)(NCC_2H_4CN)_2 \cdot 6(CH_2Cl_2)$ $4\cdot(CH_2Cl_2)_6$

The compound crystallized as rough-textured orange needles which decompose rapidly (< 1 min) under oil. X-ray intensity data were collected at 100(2) K using a Bruker D8 QUEST diffractometer equipped with a PHOTON-100 CMOS area detector and an Incoatec microfocus source (Mo Kα radiation, λ = 0.71073 Å). The raw area detector data frames were reduced and corrected for absorption effects using the Bruker APEX3, SAINT+ and SADABS programs.[1,2] Final unit cell parameters were determined by least-

squares refinement of 9198 reflections taken from the data set. The structure was solved with SHELXT.[3] Subsequent difference Fourier calculations and full-matrix least-squares refinement against F^2 were performed with SHELXL-2016[3] using OLEX2.[4]

The compound crystallizes in the triclinic system. The space group *P*-1 (No. 2) was confirmed by structure solution. The asymmetric unit consists of half of one $[TaCl_4(C_4H_4N_2)]_2(C_{40}H_{32}N_2P_2)$ complex, which is located on a crystallographic inversion center, and three independent dichloromethane molecules. The $C_4H_4N_2$ ligand of the tantalum complex is disordered over two conformations, with the Ta-bound nitrogen atom N2 common to both components. Like C-N and C-C bonds of this ligand were restrained to be similar in length using SHELX SADI restraints, and nearly superimposed atoms (C3A/C3B) were refined with common displacement parameters. The component occupancies refined to A/B = 0.645(5)/0.355(5). One dichloromethane molecule (C3S/Cl5S/Cl6S and C4S/Cl7S/Cl8S) is disordered over two closely spaced positions with occupancies of 0.47(1) and 0.53(1). All non-hydrogen atoms were refined with anisotropic displacement parameters. Hydrogen atoms bonded to carbon were in general located in Fourier difference maps before being placed in geometrically idealized positions and included as riding atoms with *d*(C-H) = 0.95 Å and *U*iso(H) = 1.2*U*eq(C) for aromatic hydrogen atoms and *d*(C-H) = 0.99 Å and *U*iso(H) = 1.2*U*eq(C) for methylene hydrogens. The largest residual electron density peak in the final difference map is 1.14 $e^-/Å^3$, located 0.81 Å from Cl4S.

Table 4.1 Crystallographic table for single crystal X-ray data for compounds **1, 2, 3, and 4.**

CCDC	1552650	1552652	1425233	1552649
	PhCN imide (1)	Dimer-PhCN (2)	Acetonitrile imide (3)	Succinonitrile imide (4)
Empirical formula	$C_{74}H_{60}Cl_{14}N_2P_2Ta_2$	$C_{80}H_{62}Cl_{12}N_6P_2Ta_2$	$C_{22}H_{20}Cl_4N_2PTa$	$C_{54}H_{52}Cl_{20}N_6P_2Ta_2$
Formula weight	1897.38	1956.59	666.12	1917.85
Temperature/K	100(2)	100(2)	100(2)	100(2)
Crystal system	triclinic	monoclinic	monoclinic	triclinic
Space group	P-1	C2/c	$P2_1/n$	P-1
a/Å	13.3462(5)	18.7629(7)	13.4508(5)	9.5641(4)
b/Å	14.6409(5)	21.1353(8)	12.4085(5)	14.4806(7)
c/Å	20.9335(8)	20.2433(7)	14.6118(5)	14.8145(7)
α/°	88.0420(10)	90	90	65.608(2)
β/°	77.4990(10)	98.3720(10)	96.696(2)	73.443(2)
γ/°	69.5100(10)	90	90	88.441(2)
Volume/$Å^3$	3736.9(2)	7942.1(5)	2422.14(16)	1781.46(15)
Z	2	4	4	1
$\rho_{calc}g/cm^3$	1.686	1.636	1.827	1.788
μ/mm^{-1}	3.513	3.245	5.058	3.904
Crystal size/mm^3	0.24 × 0.16 × 0.1	0.38 × 0.22 × 0.1	0.14 × 0.12 × 0.06	0.32 × 0.1 × 0.05
Radiation	MoKα (λ = 0.71073)	MoKα (λ = 0.71073)	MoKα (λ = 0.71073)	MoKα (λ = 0.71073)
2Θ range for data collection/°	4.246 to 60.44	4.358 to 60.266	4.318 to 60.146	4.468 to 60.328
Reflections collected	185326	145852	147204	88025

Data/restraints/parameters	22164/184/890	11698/66/553	7111/0/273	10520/22/448
Goodness-of-fit on F^2	1.015	1.025	1.093	1.043
Final R indexes [I>=2σ (I)]	R_1 = 0.0373, wR_2 = 0.0778	R_1 = 0.0272, wR_2 = 0.0494	R_1 = 0.0131, wR_2 = 0.0279	R_1 = 0.0206, wR_2 = 0.0411
Final R indexes [all data]	R_1 = 0.0542, wR_2 = 0.0834	R_1 = 0.0457, wR_2 = 0.0546	R_1 = 0.0159, wR_2 = 0.0290	R_1 = 0.0262, wR_2 = 0.0427
Largest diff. peak/hole / e $Å^{-3}$	2.84/-1.48	1.09/-1.17	0.44/-0.57	1.14/-0.98

References

(1) Marchetti, F.; Pampaloni, G.; Repo, *Eur. J. Inorg. Chem.* **2008**, *2008*, 2107–2112.

(2) Bini, R.; Chiappe, C.; Marchetti, F.; Pampaloni, G.; Zacchini, S *Inorg. Chem.* **2010**, *49*, 339–351.

(3) Marchetti, F.; Pampaloni, G. *Chem. Commun.* **2012**, *48*, 635–653.

(4) Bortoluzzi, M.; Hayatifar, M.; Marchetti, F.; Pampaloni, G.; Zacchini, S. *Inorg. Chem.* **2015**, *54*, 4047–4055.

(5) Solari, E.; Floriani, C.; Chiesi-Villa, A.; Rizzoli, C. *J. Chem. Soc., Chem. Commun.* **1991**, *13*, 841–843.

(6) Boyd, P. D. W.; Glenny, M. G.; Rickard, C. E. F.; Nielson, A. J. *Polyhedron* **2011**, *30*, 632–637.

(7) Aresta, M.; Dibenedetto, A.; Stufano, P.; Aresta, B. M.; Maggi, S.; Pápai, I.; Rokob, T. A.; Gabriele, B. *Dalton Trans.* **2010**, *39*, 6985–6992.

(8) Rahman, M. M.; Smith, M. D.; Peryshkov, D. V. *Inorg. Chem.* **2016**, *55*, 5101–5103.

(9) Nguyen, A. I.; Blackmore, K. J.; Carter, S. M.; Zarkesh, R. A.; Heyduk, A. F. *J. Am. Chem. Soc.* **2009**, *131*, 3307–3316.

(10) Mangion, I.; Liu, Y. Z.; Reibarkh, M.; Williamson, R. T.; Welch, C. J. *J. Org. Chem.* **2016**, *81*, 6937–6944.

(11) Bordwell, F. G. *Acc. Chem. Res.* **1988**, *21*, 456–463.

(12) Kaljurand, I.; Kütt, A.; Sooväli, L.; Rodima, T.; Mäemets, V.; Leito, I.; Koppel, I. A. *J. Org. Chem.* **2005**, *70*, 1019–1028.

(13) Chotana, G. A.; Rak, M. A.; Smith, M. R. *J. Am. Chem. Soc.* **2005**, *127*, 10539–10544.

(14) Swartz, B. D.; Brennessel, W. W.; Jones, W. D. C−CN vs C−H *Organometallics* **2011**, *30*, 1523–1529.

(15) Tran, S. D.; Tronic, T. A.; Kaminsky, W.; Michael Heinekey, D.; Mayer, J. M. *Inorganica Chim. Acta* **2011**, *369*, 126–132.

(16) Chase, P. A.; Welch, G. C.; Jurca, T.; Stephan, D. W. *Angew. Chem. Int. Ed.* **2007**, *46*, 8050–8053.

(17) Chase, P. A.; Jurca, T.; Stephan, D. W. *Chem. Commun.* **2008**, *14*, 1701–1703.

(18) Chapman, A. M.; Haddow, M. F.; Wass, D. F. *J. Am. Chem. Soc.* **2011**, *133*, 18463–18478.

(19) Metters, O. J.; Forrest, S. J. K.; Sparkes, H. A.; Manners, I.; Wass, D. F. *J. Am. Chem. Soc.* **2016**, *138*, 1994–2003.

(20) Becker, L.; Arndt, P.; Jiao, H.; Spannenberg, A.; Rosenthal, U. *Angew. Chem. Int. Ed.* **2013**, *52*, 11396–11400.

(21) Becker, L.; Strehler, F.; Korb, M.; Arndt, P.; Spannenberg, A.; Baumann, W.; Lang, H.; Rosenthal, U. *Chem. Eur. J.* **2014**, *20*, 3061–3068.

(22) Dai, Q. X.; Seino, H.; Mizobe, Y. *Organometallics* **2014**, *33*, 3652–3655.

(23) De Boer, E. J. M.; Teuben, J. H. *J. Organomet. Chem.* **1978**, *153*, 53–57.

(24) Young, C. G.; Philipp, C. C.; White, P. S.; Templeton, J. L. *Inorg. Chem.* **1995**, *34*, 6412–6414.

(25) Tsai, Y.-C.; Stephens, F. H.; Meyer, K.; Mendiratta, A.; Gheorghiu, M. D.; Cummins, C. C. *Organometallics* **2003**, *22*, 2902–2913.

(26) Tsai, Y.-C.; Johnson, M. J. A.; Mindiola, D. J.; Cummins, C. C.; Klooster, W. T.; Koetzle, T. F. *J. Am. Chem. Soc.* **1999**, *121*, 10426–10427.

(27) Burford, R. J.; Piers, W. E.; Parvez, M. *Eur. J. Inorg. Chem.* **2013**, *2013*, 3826–3830.

(28) Finn, P. A.; King, M. S.; Kilty, P. A.; McCarley, R. E. *J. Am. Chem. Soc.* **1975**, *97*, 220–221.

(29) Cotton, F. A.; Hall, W. T. *Inorg. Chem.* **1978**, *17*, 3525–3528.

(30) Cotton, F. A.; Hall, W. T. *J. Am. Chem. Soc.* **1979**, *101*, 5094–5095.

(31) Lopez, L. P. H.; Schrock, R. R.; Müller, P. *Organometallics* **2008**, *27*, 3857–3865.

(32) Duchateau, R.; Williams, A. J.; Gambarotta, S.; Chiang, M. Y. *Inorg. Chem.* **1991**, *30*, 4863–4866.

(33) Cross, J. L.; Garrett, A. D.; Crane, T. W.; White, P. S.; Templeton, J. L. *Polyhedron* **2004**, *23*, 2831–2840.

(34) Becker, L.; Arndt, P.; Spannenberg, A.; Rosenthal, U. *Chem. Eur. J.* **2014**, *20*, 12595–12600.

(35) Farrell, W. S.; Yonke, B. L.; Reeds, J. P.; Zavalij, P. Y.; Sita, L. R. *Organometallics* **2016**, *35*, 1132–1140.

(36) APEX3 Version 2016.5-0 and SAINT+ Version 8.37A. Bruker AXS, Inc., Madison, Wisconsin, USA, 2016.

(37) SADABS-2016/2: Krause, L., Herbst-Irmer, R., Sheldrick G.M. and Stalke D. *J. Appl. Cryst.* 2015, *48*, 3-10.

(38) SHELXT: Sheldrick, G.M. *Acta Cryst*. 2015, *A71*, 3-8. (b) SHELXL: Sheldrick, G.M. *Acta Cryst*. 2008, A64, 112-122.

(39) OLEX2: a complete structure solution, refinement and analysis program. Dolomanov, O. V., Bourhis, L. J., Gildea, R. J., Howard J. A. K. and Puschmann, H. *J. Appl. Cryst.* 2009, *42*, 339-341.

(40) Rahman, M. M.; Peryshkov, D.; *Abstr. Pap.—Am. Chem. Soc., Div. Inorg. Chem.* **2016**, *251*, INORG 2593815.

(41) Rahman, M. M.; Peryshkov, D. *Abstr. Pap.—Am. Chem. Soc., Div. Inorg. Chem.* **2017**, *254*, INORG 2825889.

Chapter 5

Imido Group Interchange in Reactions of Zwitterionic Tantalum(V) Vinylimido Complexes and Nitriles.

Rahman, M. M.; Smith, M. D.; Peryshkov, D. V. *Organometallics*, **2018**, *37*, 2945-2949.

5.1 Introduction

Somewhat surprisingly, imido groups bound to high-valent transition metals are often stable towards nitriles and, in fact, a number of nitrile adducts of metal imido complexes have been characterized.[1-8] At the same time, examples of imido group reactivity with nitriles have also been documented. For instance, Mountford and co-workers reported an addition of acetonitrile to a Ti=N^{t}Bu imido group to afford a doubly deprotonated N-tert-butylacetamidinate ligand (**Scheme 5.1**).[9] Interestingly, this transformation is reversible upon heating. Doxsee and co-workers reported that vinylimido complexes of Ti(IV) coupled through a formally [4+2] cycloaddition reaction with pivalonitrile or 1-adamantylnitrile to afford diazatitanacyclohexadienes (**Scheme 5.1**).[10]

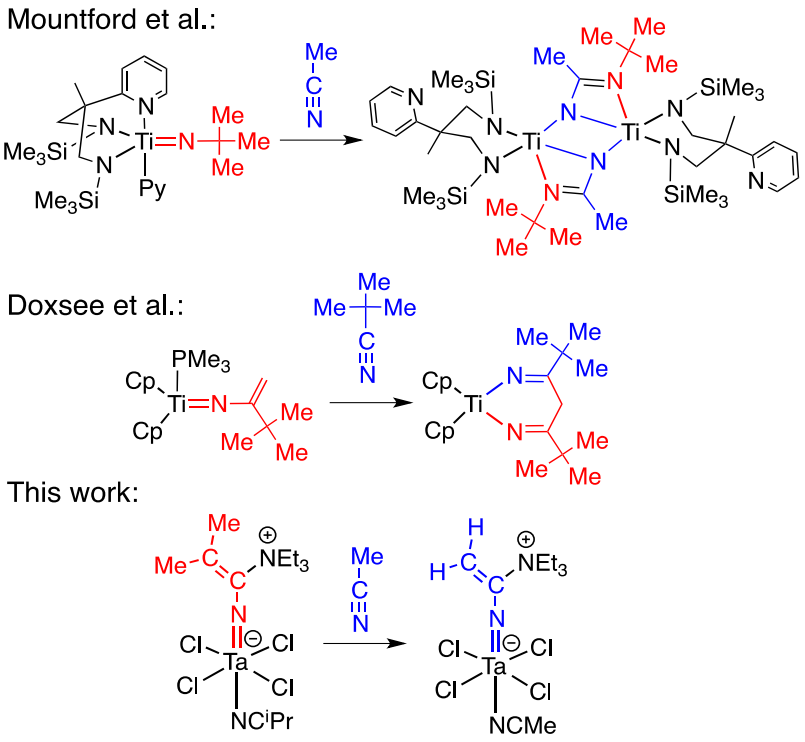

Scheme 5.1. Examples of reactivity of imido complexes of early transition metals with nitriles.

Recently, we reported a novel activation mode of alkylnitriles coordinated to $TaCl_5$ in the presence of the weakly nucleophilic base, NEt_3.[11,16] This process resulted in the formation of a series of zwitterionic vinylimido complexes of Ta(V) through the initial deprotonation of the coordinated nitrile, bond rearrangement governed by electrophilicity of the Ta(V) center, and the subsequent nucleophilic attack on the coordinated azaallene intermediate. These novel vinylimido complexes possess multiple potential reaction centers: the imido functionality, the vinyl group, and the cationic tetraalkylammonium fragment. Furthermore, facile ligand exchange was observed at the coordination site trans- to the imido group at the metal center. Herein we report an unusual reactivity of these imido complexes with alkylnitriles that resulted in the complete imido group interchange under mild conditions (**Scheme 5.2**).

5.2 Results and Discussion

Heating a solution of the imido complex derived from isobutyronitrile $[Ta(NCCMe_2\{NEt_3\})Cl_4](^iPrCN)$ (**1-^{i}Pr**[11]) in the presence of excess MeCN at 40 ºC in CD_2Cl_2 for 2 days resulted in the clean conversion to a vinylimido complex derived from acetonitrile $[Ta(NCCH_2\{NEt_3\})Cl_4](MeCN)$ (**1-Me**[11]). The progress of the reaction can be easily tracked by ^{1}H NMR spectroscopy as characteristic singlets from two inequivalent methyl groups of **1-^{i}Pr** gradually disappear and two doublets from the vinylimido group of **1-Me** grow in intensity (**Figure 5.1**). No intermediates were observed in the spectra of the reaction mixture. The conversion is quantitative according to ^{1}H NMR data. The net outcome of the reaction is the interchange of the vinylimido group, including the migration of NEt_3 and the formation of free isobutyronitrile ^{i}PrCN, which was observed in the ^{1}H NMR spectrum of the crude mixture. An analogous metathesis reaction proceeded in the

reaction of **1-^{i}Pr** and excess of propionitrile EtCN similarly producing the vinylimido complex [Ta(NCCHMe{NEt_3})Cl_4](EtCN) (**Figure 5.3**).

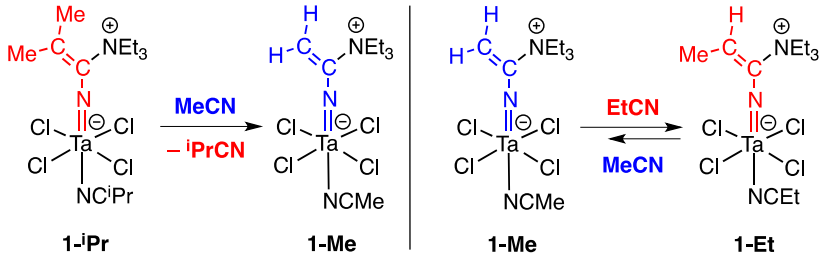

Scheme 5.2. Imido group interchange in zwitterionic Ta(V) vinylimido complexes.

The imido exchange reaction was found to proceed in both directions in the case of the MeCN/EtCN pair. Heating the imido complex **1-Me** with excess (2 equiv.) of propionitrile EtCN in CD_2Cl_2 at 45 ºC for 2 days led to the quantitative formation of **1-Et** and free MeCN according to ^{1}H NMR data (**Figure 5.4**). At the same time, the reverse transformation of **1-Et** to **1-Me** under similar conditions was found to be sluggish resulting in ca. 50% conversion after 2 weeks at 50 ºC according to ^{1}H NMR spectroscopy (see (**Scheme 5.2, Figure 5.5** for the ^{1}H NMR spectrum of the reaction mixture). The starting imido complex **1-Et**, as synthesized from $TaCl_5$ and EtCN at a room temperature, consists of a mixture of two isomers in a ratio Z : E = 1 : 4 − 6 (we found that this ratio varies depending on recrystallization conditions). The less abundant (and presumably less stable) Z isomer with the cis- mutual orientation of the methyl and triethylammonium groups reacts with acetonitrile at a significantly higher rate that the E isomer. Furthermore, only the E isomer of **1-Et** formed in the reaction of **1-^{i}Pr** and EtCN.

We propose that the transformation of **1-^{i}Pr** to **1-Me** proceeds through the complete imido group interchange, in other words, the nitrogen of the incoming nitrile becomes a part of the new imido group. Elimination of triethylamine from the starting vinylimido

group is likely the first step of the transformation (**Scheme 5.3**). The resulting coordinated azaallene fragment readily deprotonates the incoming nitrile molecule, especially if the nitrile ligand is coordinated to a metal center. This deprotonation may also happen through "shuttling" of a proton by the released triethylamine. The following rearrangement of the new deprotonated nitrile and nucleophilic attack by the amine proceeds analogously through the azaallene intermediate as during the formation of these zwitterionic vinylimido species.

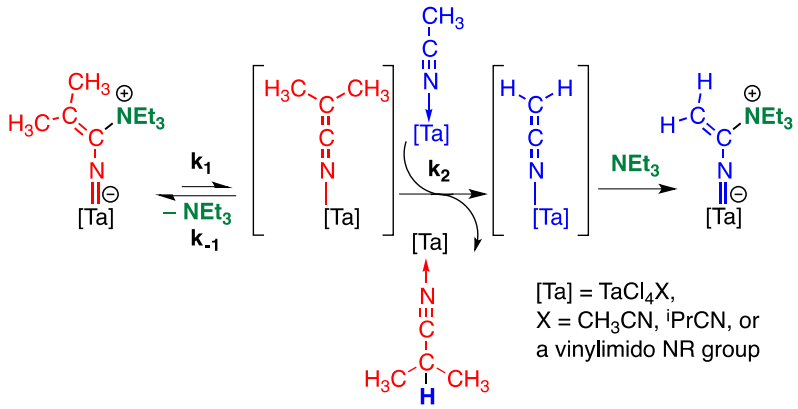

Scheme 5.3 Proposed mechanism of imido group interchange on the example of the 1-^{i}Pr to 1-Me conversion**.**

To support the proposed mechanism of the imido group exchange we conducted a set of experiments with the observations listed below. First, the imido group metathesis occurred only with nitriles containing α-hydrogen atoms; for instance, pivalonitrile did not participate in an exchange reaction. Second, the reaction of $[Ta(NCCH_2\{NEt_3\})Cl_5]^-$ (**1-Me'**) complex with excess CD_3CN in CD_2Cl_2 at 40 ºC led to the formation of a deuterated imido complex $[Ta(NCCD_2\{NEt_3\})Cl_5]^-$ (**1-Me'-d^2**) and the appearance of the signal from CD_2HCN in the ^{1}H NMR spectrum of the reaction mixture (**Scheme 5.4, Figures 5.6 and 5.7**). This observation is congruous with the proton transfer from the incoming nitrile (CD_3CN) to the starting imido group ($Ta{=}NCCH_2\{NEt_3\}$) resulting in its conversion to a

nitrile (initially to CDH_2CN, which is likely to participate further in the imido interchange, eventually yielding CD_2HCN).

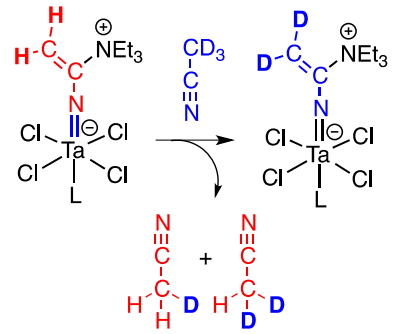

Scheme 5.4. Evidence of a proton transfer from a nitrile to an imido group on the example of the 1-Me' to 1-Me'-d^2 conversion.

Finally, we attempted to carry out the replacement of triethylammonium moiety of the imido group by another neutral nucleophile (**Scheme 5.5, Figure 5.8**). The vinylimido complex **1-Me** reacted with PPh_3 at 45 ºC in CD_2Cl_2 for 2 d with no other nitrile present. As expected, the reaction cleanly produced a new vinylimido complex $[Ta(NCCH_2\{PPh_3\})Cl_4](MeCN)$ **2-Me** by the exchange of NEt_3 and PPh_3 nucleophiles. We have independently prepared this imido complex in the direct reaction of MeCN and the $TaCl_5{\cdot}PPh_3$ adduct.[12]

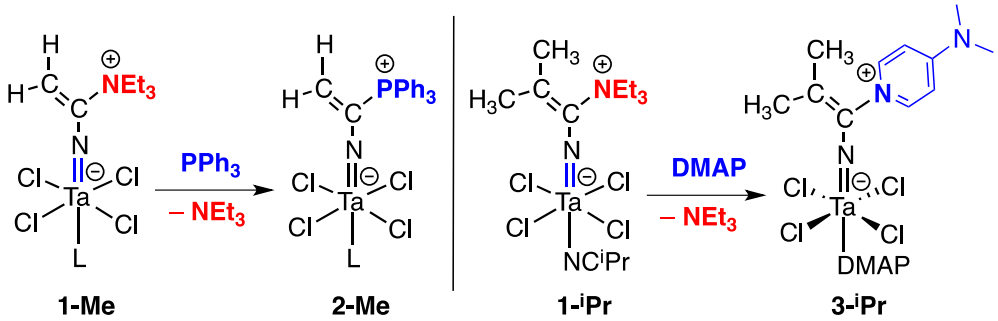

Scheme 5.5 Replacement of the ammonio group by triphenylphosphine (left, 2-Me) or DMAP (right, 3-^{i}Pr) in the zwitterionic vinylimido complex 1-^{i}Pr**.**

Similarly, the vinylimido complex **1-^{i}Pr** reacted with an excess of DMAP in CD_2Cl_2 at room temperature. Within 15 min, exchange of amine to pyridine at the imido group produced an orange crystalline solid [Ta(NCCMe$_2${DMAP})Cl$_4$](DMAP) (**3-^{i}Pr**). This interchange reaction opens the way for functionalization of these imido complexes with a broader range of nucleophilic groups as this DMAP-containing imido complex could not be obtained in the direct reaction of $TaCl_5$(^{i}PrCN) and DMAP, which produced a simple unreactive adduct $TaCl_5$(DMAP) instead. These nucleophile exchange reactions of vinylimido complexes particularly suggest that the elimination of triethylamine from the starting vinylimido group is the first step of the overall interchange transformation.

The single crystal X-ray diffraction experiment for a sample of **3-^{i}Pr** confirmed the expected molecular structure with the zwitterionic vinylimido group (**Figure 5.1**). The interatomic distances and angles are within typical ranges for the linear imido group at the Ta(V) center (Ta1≡N1 = 1.783(3) Å, Ta1≡N1–C1 = 169.2(2)º) and the carbon-carbon double bond of the vinylimido fragment (C1=C2 = 1.339(5) Å).

The kinetics of the imido group interchange reaction was probed through initial rate studies with variable concentrations of an imido complex and a nitrile at 40 ºC in dichloromethane (**Figures 5.11 and 5.12**). The rate of conversion of **1-^{i}Pr** to **1-Et** was found to be the first order in the starting imido complex. At the same time, no dependence of the rate of the reaction on the concentration of propionitrile was found. Addition of 12 equiv. of NEt_3 to the reaction mixture resulted in the slower reaction progression. Addition of 8 equiv. of pivalonitrile also caused a significantly slower reaction rate. Similarly, the conversion of **1-^{i}Pr** to **1-Me** was found to exhibit the first order kinetics in the **1-^{i}Pr** imido complex and the zero order in acetonitrile. A comparison of reaction rates of **1-^{i}Pr** with

CH_3CN and **1-^{i}Pr** with CD_3CN revealed the value of the kinetic isotope effect of 1.5. The reaction of **1-^{i}Pr** with EtCN was significantly faster than its reaction with MeCN (k_{obs}(**1-Et**)/ k_{obs}(**1-Me**) = 4.2).

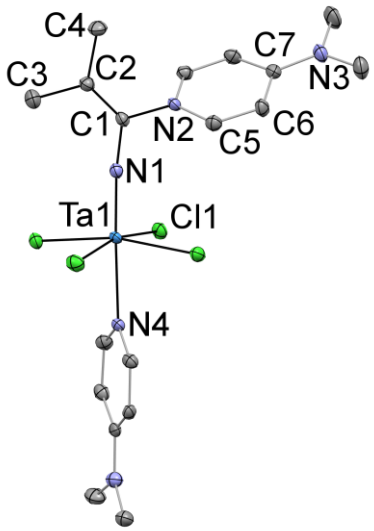

Figure 5.1. Displacement ellipsoid plot (50% probability) of **3-^{i}Pr**. Hydrogen atoms have been omitted for clarity. Selected bond distances (Å) and angles (º): Ta1–N1 = 1.783(3), Ta1–N4 = 2.361(3), N1–C1 = 1.374(4), C1–C2 = 1.339(5), C1−N2 = 1.459(4), Ta1–N1–C1 = 169.2(2), N2–C1–C2 = 120.3(3).

These observations are compatible with the proposed mechanism shown in **Scheme 5.3**. The release of triethylamine from the starting vinylimido group is a slow reversible step of the reaction. This step is inhibited by added NEt_3. Notably we were able to intercept the azaallene intermediate (not observed) in reactions with PPh_3 or DMAP (**Figures 5.1, 5.9, and 5.10**). Deprotonation of the coordinated nitrile by this intermediate is a faster step which is congruent with the apparent independence of the overall reaction rate on a nitrile concentration and the absence of the significant primary isotope effect. Deprotonation of an incoming nitrile is likely to occur only if it is coordinated to a tantalum center as these alkylnitriles do not react with NEt_3 without $TaCl_5$ present. This proposal is consistent with inhibition of the reaction in the presence of pivalonitrile that also coordinates to the metal

center but lacks α-hydrogen atoms and therefore cannot be deprotonated and transformed to an imido group. Therefore, the second step is likely bimolecular in tantalum as it involves an interaction of the azaallene intermediate and a nitrile complex and does not depend on the concentration of a nitrile. The rate below can be derived using the steady-state approximation:

$$\frac{-d[\mathbf{1\text{-}\ ^{i}Pr}]}{dt} = \frac{k_1[\mathbf{1\text{-}\ ^{i}Pr}]k_2[\mathbf{1\text{-}\ ^{i}Pr}]}{k_{-1}[\mathrm{NEt_3}] + k_2[\mathbf{1\text{-}\ ^{i}Pr}]}$$

However, if the proton transfer step is fast, the overall reaction rate would appear as the first order in the starting imido concentration under conditions used in our experiments. This is also consistent with the absence of the primary isotope effect for breaking C-H bonds of acetonitrile. In other words, if $k_2 >> k_1$ then the derived rate law can be simplified and appears to be the first order in the starting imido:

$$\frac{-d[\mathbf{1\text{-}\ ^{i}Pr}]}{dt} = \frac{k_1[\mathbf{1\text{-}\ ^{i}Pr}]}{k_{-1}[\mathrm{NEt_3}]}$$

Attempts to study kinetics of this transformation at higher temperatures in tetrachloroethane proved to be inconclusive due to formation of multiple products including insoluble species. We were able to identify one of these products due to its characteristic ^{1}H NMR spectra features as one containing vinylimidocyanoalkyl group, featuring two isobutyronitrile-based fragments coupled through a C–C bond (**Scheme 5.6**). An analogous complex has been prepared earlier by deprotonation of isobutyronitrile by a sterically hindered Hunig's base N(^{i}Pr)$_2$Et in the presence of $TaCl_5$, which led to the subsequent C–C bond formation between deprotonated intermediates.[25] We also observed the appearance of signals from this vinylimidocyanoalkyl group during heating of **1-^{i}Pr** in CD_2Cl_2 at 45 ºC for 4 days with no other nitrile present (except a coordinated ^{i}PrCN ligand

in the starting imido complex (**Figure 5.13**). Under the conditions reported herein, the elimination of NEt_3 from the starting imido in **1-^{i}Pr** can lead to the bimolecular coupling of the nucleophilic deprotonated nitrile and the electrophilic azaallene intermediate at higher temperatures resulting in the C–C coupling reaction similarly to the independent synthesis mentioned above.

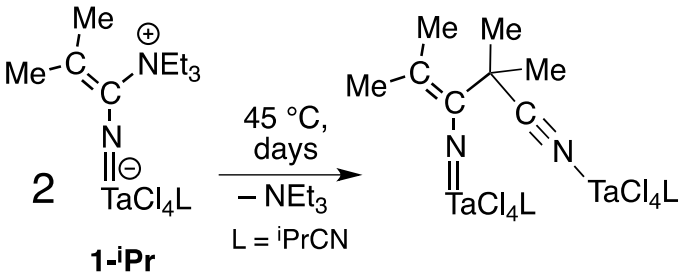

Scheme 5.6. The prevalent decomposition pathway for the vinylimido complex 1-^{i}Pr upon prolonged heating without an added nitrile.

5.3 Conclusions

Imido groups bound to high-valent transition metals are often stable towards nitriles as evidenced by a large number of reported nitrile adducts of metal imido complexes. The reactivity of zwitterionic vinylimido complexes of Ta(V) with nitriles described above is different from the reactions of nitriles with related vinylimido complexes of Ti(IV) or any other early transition metal imido species. Instead of previously reported cycloaddition reactions, in the case presented herein, elimination of the amine and subsequent proton transfer from a nitrile substrate to the former vinylimido fragment led to the formation of a new imido group. This is the first example of the reaction of an imido complex with a nitrile that results in the formation of a new imido group and a free nitrile in a metathesis-type transformation. Furthermore, the cationic group on the imido ligand can be replaced with other nucleophiles, which was demonstrated by NEt_3 to PPh_3 and NEt_3 to DMAP exchange reactions.

5.4 Experimental Section

All synthetic manipulations were carried out either in a nitrogen-filled drybox or on an air free dual-manifold Schlenk line.[27] Solvents were sparged with nitrogen, passed through activated alumina, and stored over activated 4 Å Linde-type molecular sieves. Chloroform-d^3, dichloromethane-d^2, and acetonitrile-d^3 (Cambridge Isotope Laboratories) were degassed and stored over activated 4 Å Linde-type molecular sieves. NMR spectra were recorded using Varian spectrometers at 400 MHz (^{1}H) and 100 MHz (^{13}C) and reported in δ (parts per million) and referenced to residual ^{1}H/^{13}C signals of a deuterated solvent or an external 85% phosphoric acid (^{31}P (δ): 0.0 ppm) standard. Midwest Microlab, Indianapolis, Indiana provided the elemental analysis results.

$TaCl_5$ (Strem) was used as received. NEt_3, CH_3CN, CD_3CN, EtCN, and ^{i}PrCN were degassed by freeze-pump-thaw technique and stored over 4 Å Linde-type molecular sieves. Starting **1-^{i}Pr**, **1-Me**, and **1-Et** were synthesized according to the previously published procedure.[25]

A typical imido group interchange experiment involved an addition of excess nitrile (2 to 30 equiv.) to a solution of a vinylimido complex of Ta(V) in CD_2Cl_2 in an NMR tube with a J. Young valve. Reaction temperature varied from 22 ºC to 50 ºC; reaction time varied from 15 min. to 2 weeks. Reaction progress was monitored by ^{1}H NMR spectroscopy.

Conversion of 1-^{i}Pr to 1-Me

This known compound[25] formed in the imido group interchange reaction. In a typical reaction, **1-^{i}Pr** was dissolved in CD_2Cl_2 and transferred into an NMR tube with the J. Young valve under nitrogen. Excess of MeCN was added. The solution was heated at 40

ºC for 2 days. During that time, at least 95% of the **1-^{i}Pr** was converted into **1-Me** according to ^{1}H NMR spectroscopy.

Conversion of 1-^{i}Pr to 1-Et

This known compound[25] formed in the imido group interchange reaction. In a typical reaction, **1-^{i}Pr** was dissolved in CD_2Cl_2 and transferred into an NMR tube with the J. Young valve under nitrogen. Excess of EtCN was added. The solution was heated at 45 ºC for 1 day. During that time, at least 99% of the **1-^{i}Pr** was converted into **1-Et** according to ^{1}H NMR spectroscopy.

Conversion of 1-Me to 1-Et

This known compound[25] formed in the imido group interchange reaction. In a typical reaction, **1-Me** was dissolved in CD_2Cl_2 and transferred into an NMR tube with the J. Young valve under nitrogen. Excess of EtCN was added. The solution was heated at 45 ºC for 2 days. During that time, at least 99% of the **1-Me** was converted into **1-Et** according to ^{1}H NMR spectroscopy.

Conversion of 1-Et to 1-Me

This known compound[25] formed in the imido group interchange reaction. In a typical reaction, **1-Et** was dissolved in CD_2Cl_2 and transferred into an NMR tube with the J. Young valve under nitrogen. Excess of MeCN was added. The solution was heated at 50 ºC for 2 weeks. During that time, at least 50% of the **1-Et** was converted into **1-Me** according to ^{1}H NMR spectroscopy.

Conversion of 1-Me to 2-Me

This known compound[26] formed in the imido group interchange reaction. In a typical reaction, **1-Me** (0.040g, 0.007 mmol) was dissolved in CD_2Cl_2 and transferred into

an NMR tube with the J. Young valve under nitrogen. A portion of PPh_3 (0.035 g, 0.013 mmol, 2 equiv) was added. The solution was heated at 45 ºC for 2 days. During that time, at least 99% of the **1-Me** was converted into **2-Me** according to ^{1}H NMR spectroscopy.

Conversion of 1-^{i}Pr to 3-^{i}Pr

A portion of **1-^{i}Pr** (50 mg, 0.09 mmol) was dissolved in 2 mL of CH_2Cl_2. A solution of DMAP (0.021 mg, 0.17 mmol, 2 equiv) in CH_2Cl_2 (2 mL) was added. Within 15 min at room temperature, an orange precipitate formed. The precipitate was filtered, washed with 1 mL CH_2Cl_2, and dried under vacuum (0.021 g, 0.03 mmol, 24 %). **^{1}H NMR (400 MHz, CD_2Cl_2):** δ 8.87 (d, 2H, $^3J_{HH}$ = 7 Hz, $NC_5\mathit{H}_4N(CH_3)_2$), 8.26 (d, 2H, $^3J_{HH}$ = 7 Hz, $NC_5\mathit{H}_4N(CH_3)_2$), 6.80 (d, 2H, $^3J_{HH}$ = 7 Hz, $NC_5\mathit{H}_4N(CH_3)_2$), 6.52 (d, 2H, $^3J_{HH}$ = 7 Hz, $NC_5\mathit{H}_4N(CH_3)_2$), 3.25 (s, 6H, $NC_5H_4N(C\mathit{H}_3)_2$), 3.05 s, 6H, $NC_5H_4N(C\mathit{H}_3)_2$), 2.69 (s, 3H, $NC{=}C(C\mathit{H}_3)_2$), 2.05 (s, 3H, $NC{=}C(C\mathit{H}_3)_2$). **^{13}C (100 MHz, CD_2Cl_2):** δ 154.7 ($TaNC{=}\mathit{C}(CH_3)_2$), 151.4 ($N\mathit{C}_5H_4N(CH_3)_2$), 142.1 ($N\mathit{C}_5H_4N(CH_3)_2$), 129.8 ($TaN\mathit{C}{=}C(CH_3)_2$), 125.2 ($N\mathit{C}_5H_4N(CH_3)_2$), 123.8 ($N\mathit{C}_5H_4N(CH_3)_2$), 106.5 ($N\mathit{C}_5H_4N(CH_3)_2$), 105.5 ($N\mathit{C}_5H_4N(CH_3)_2$), 40.2 ($NC_5H_4N(\mathit{C}H_3)_2$), 39.0 ($NC_5H_4N(\mathit{C}H_3)_2$), 18.0 ($TaNC{=}C(\mathit{C}H_3)_2$), 17.7 ($TaNC{=}C(\mathit{C}H_3)_2$). Calcd. for $C_{18}H_{26}Cl_4N_5Ta$: C, 34.04; H, 4.13; N, 11.03. Found C, 34.38; H, 4.02; N, 11.35.

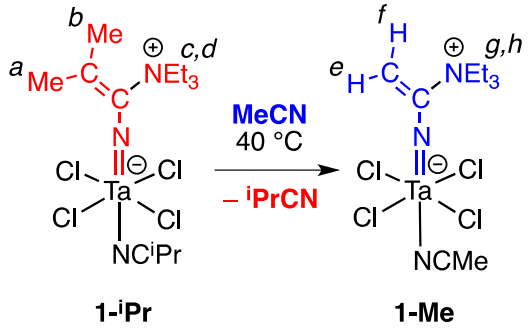

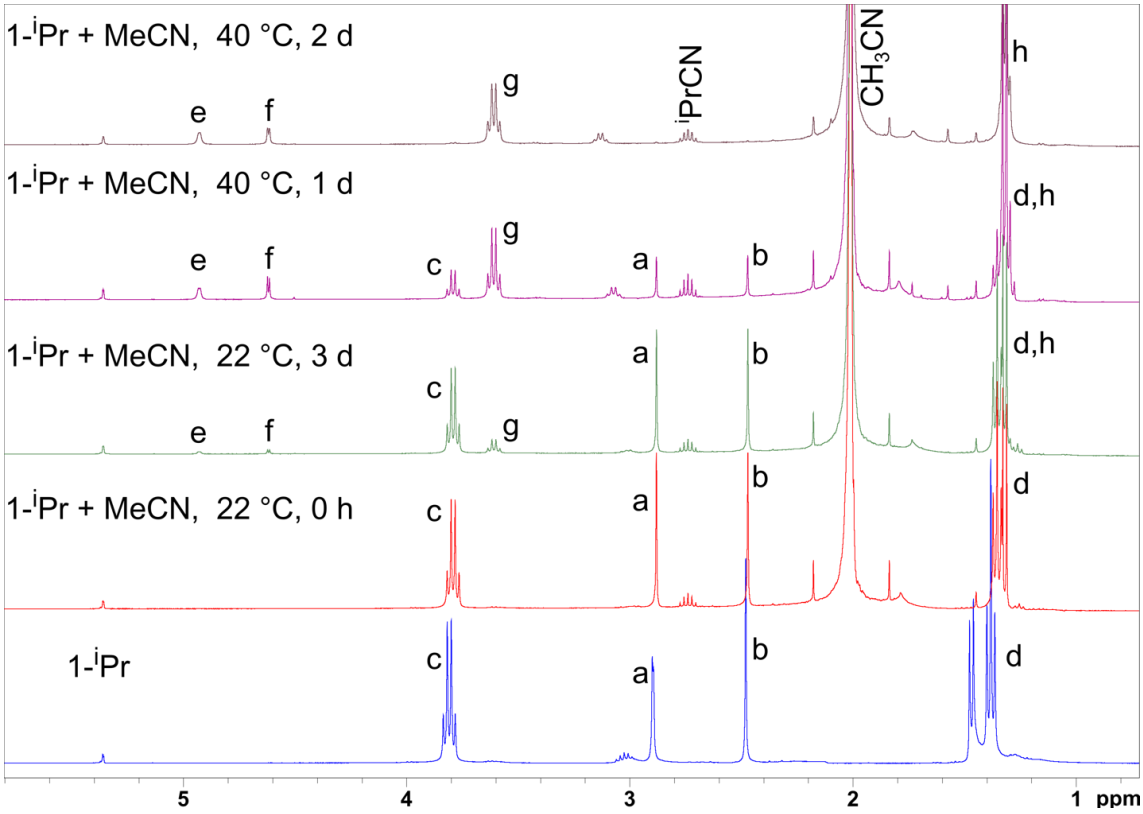

Figure 5.2 ^{1}H NMR spectra of a mixture of **1-^{i}Pr** and excess MeCN. Notice the disappearance of the signals from **1-^{i}Pr** and the emergence of the signals from **1-Me** during the conversion.

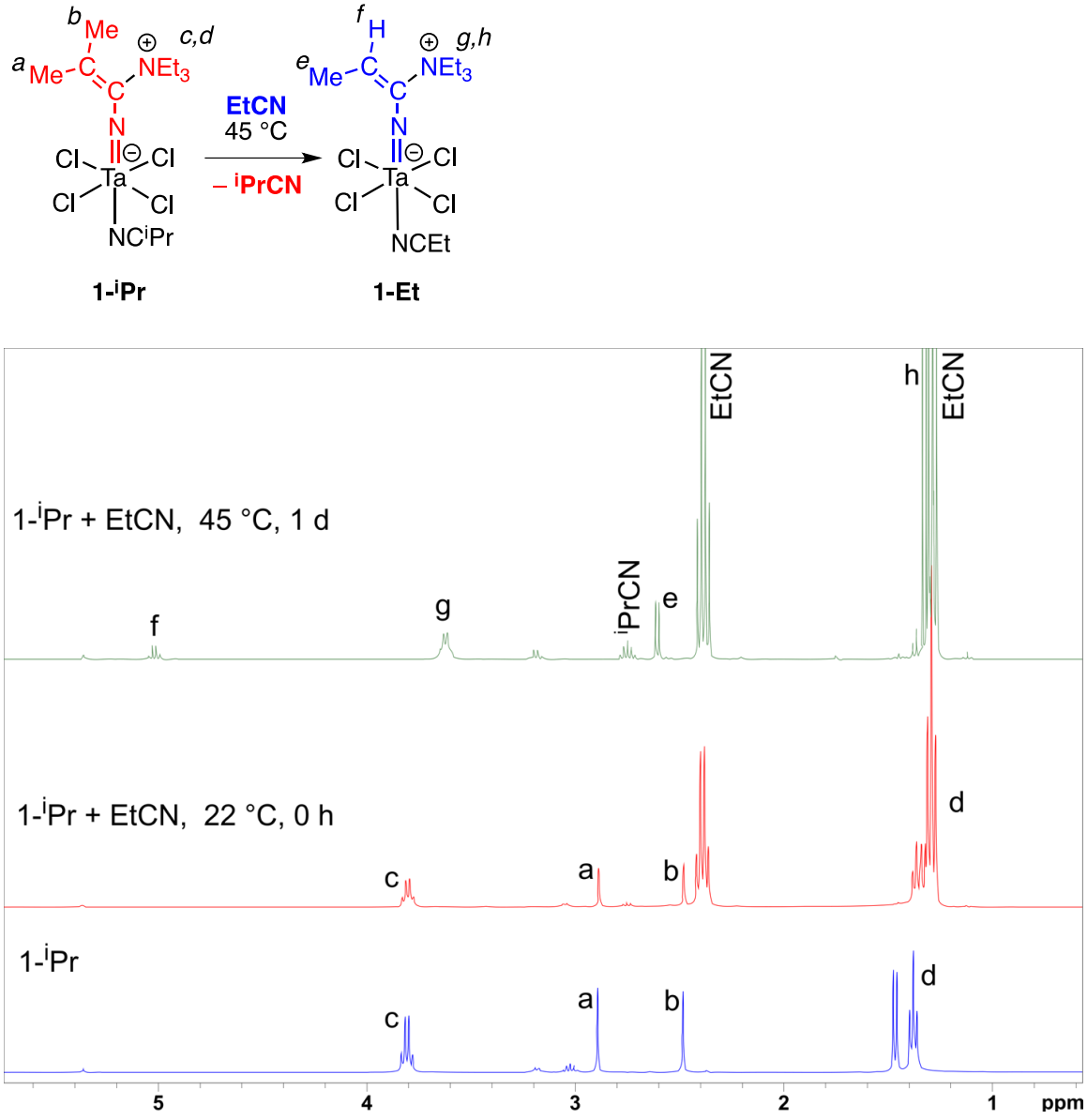

Figure 5.3 ^{1}H NMR spectra of a mixture of **1-^{i}Pr** and excess EtCN. Notice the disappearance of the signals from **1-^{i}Pr** and the emergence of the signals from **1-Et** during the conversion.

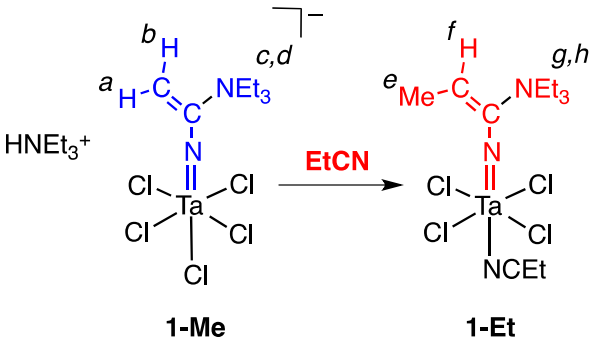

1-Me **1-Et**

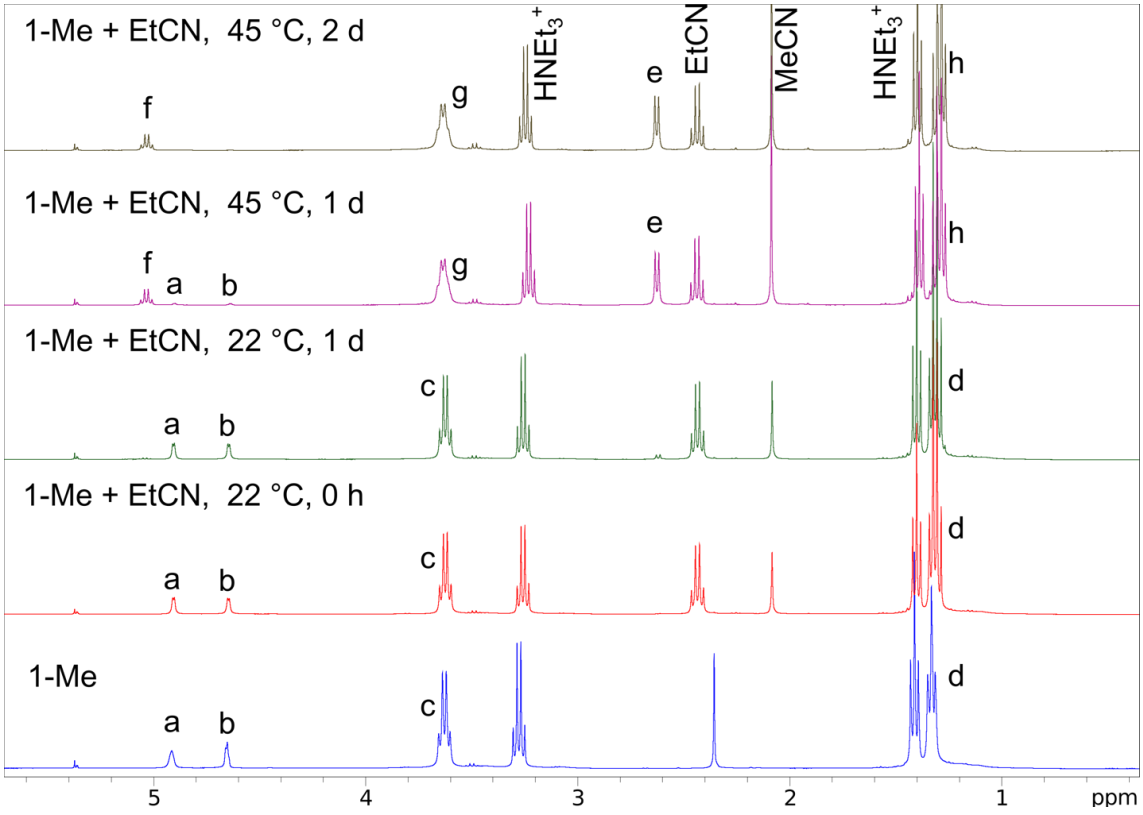

Figure 5.4 ^{1}H NMR spectra of a mixture of **1-Me** and excess EtCN. Notice the disappearance of the signals from **1-Me** and the emergence of the signals from **1-Et** during the conversion. The presence of $HNEt_3Cl$ is due to an equilibrium between $[Ta(NCCH_2\{NEt_3\})Cl_4](MeCN)]$ and $[Ta(NCCH_2\{NEt_3\})Cl_5](HNEt_3)]$ in CH_3CN.[1]

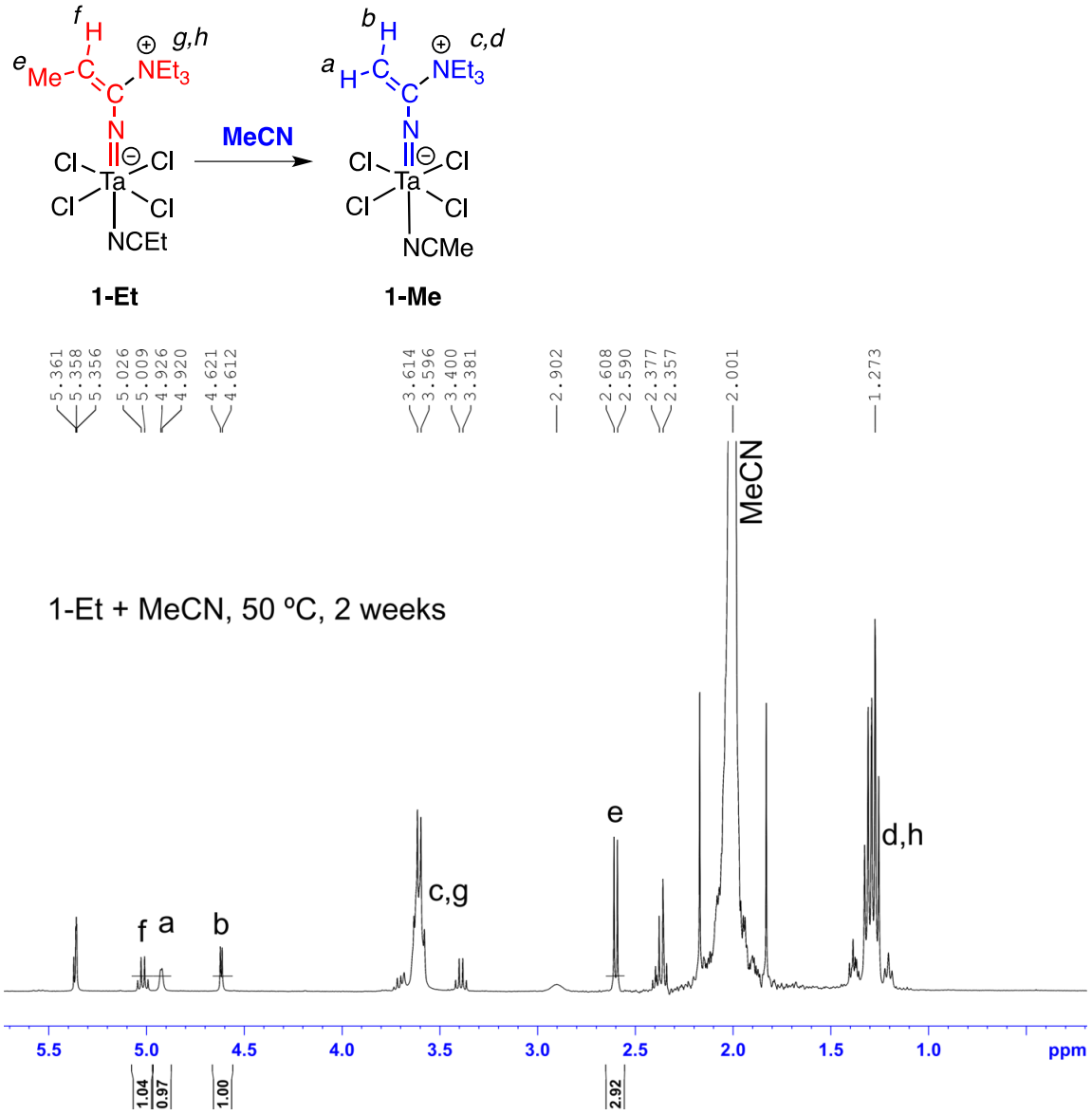

Figure 5.5 The ^{1}H NMR spectrum of a mixture of **1-Et** and excess MeCN after heating for 2 weeks at 50 ºC. Notice the presence of signals from both **1-Et** and **1-Me**.

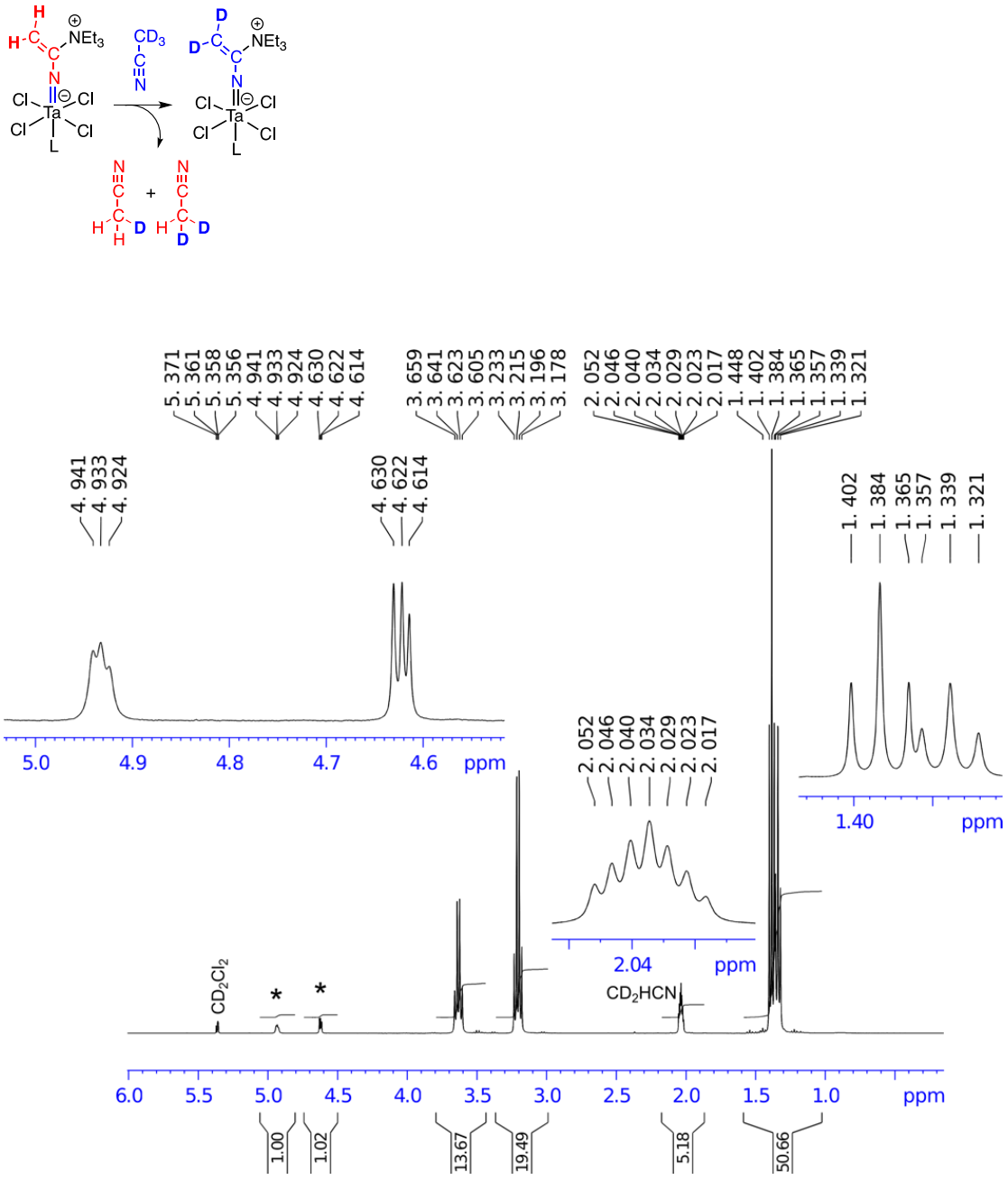

Figure 5.6 The ^{1}H NMR spectrum of a mixture of **1-Me** and 5 equiv. CD_3CN after heating at 40 ºC (partial conversion). Notice the appearance of a signal from C**D**$_2$HCN. Asterisks denote signals from the vinylimido group in Ta{NC=C**H**(**D**)NEt$_3$}Cl$_4$(CD_3CN) and the remaining Ta{NC=C**H**$_2$NEt$_3$}Cl$_4$(CD_3CN).

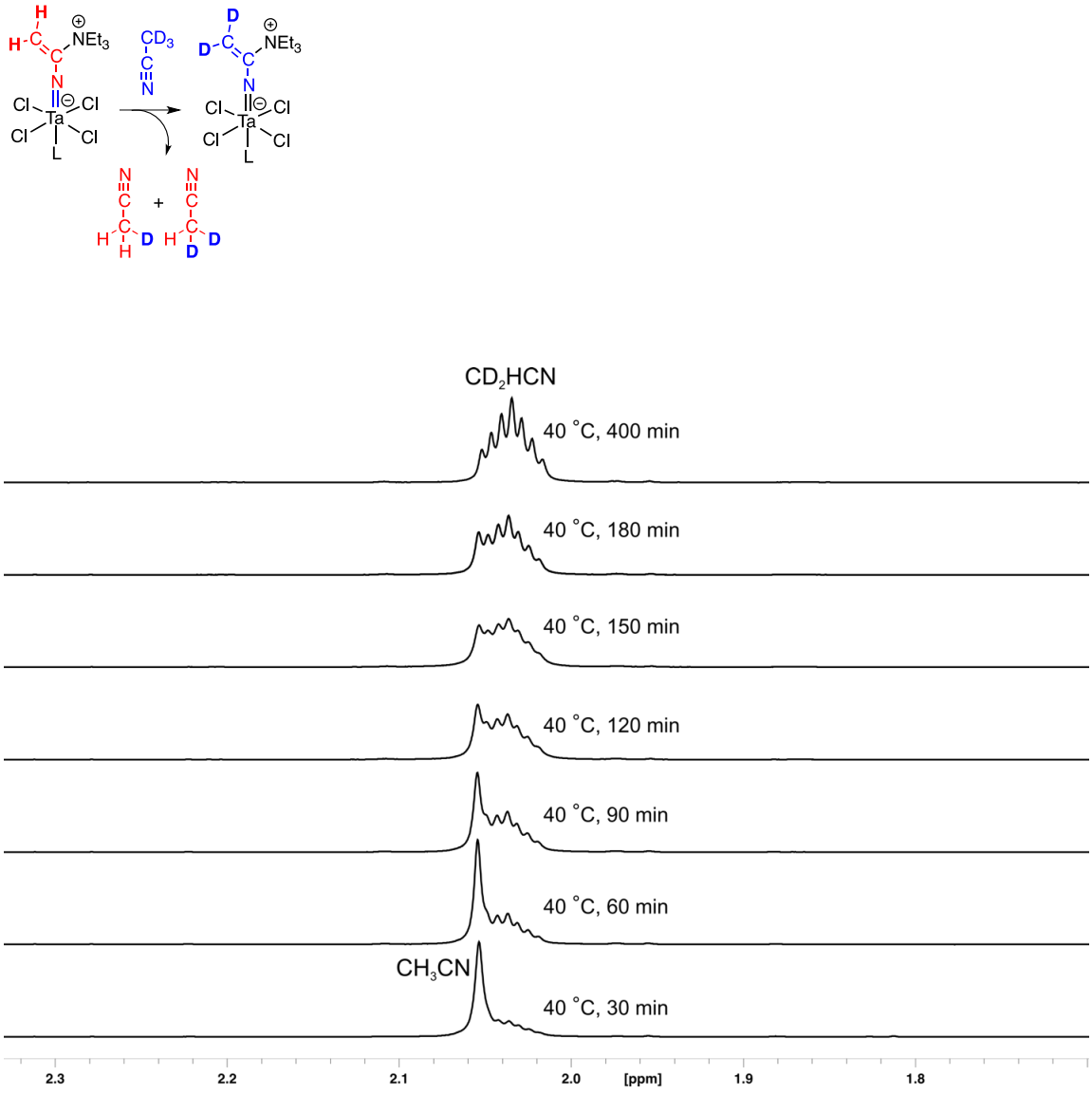

Figure 5.7 Fragments of ^{1}H NMR spectra of a mixture of **1-Me** and 5 equiv. CD_3CN after heating at 40 ºC. Notice the gradual appearance of a signal from C**D**$_2$HCN.

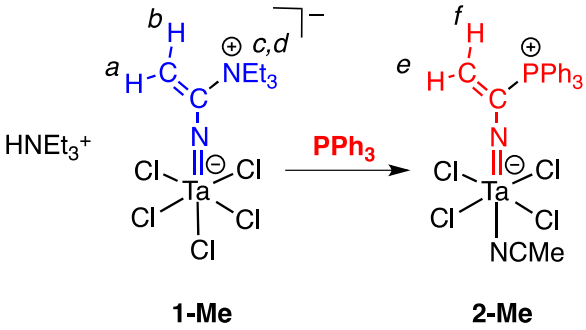

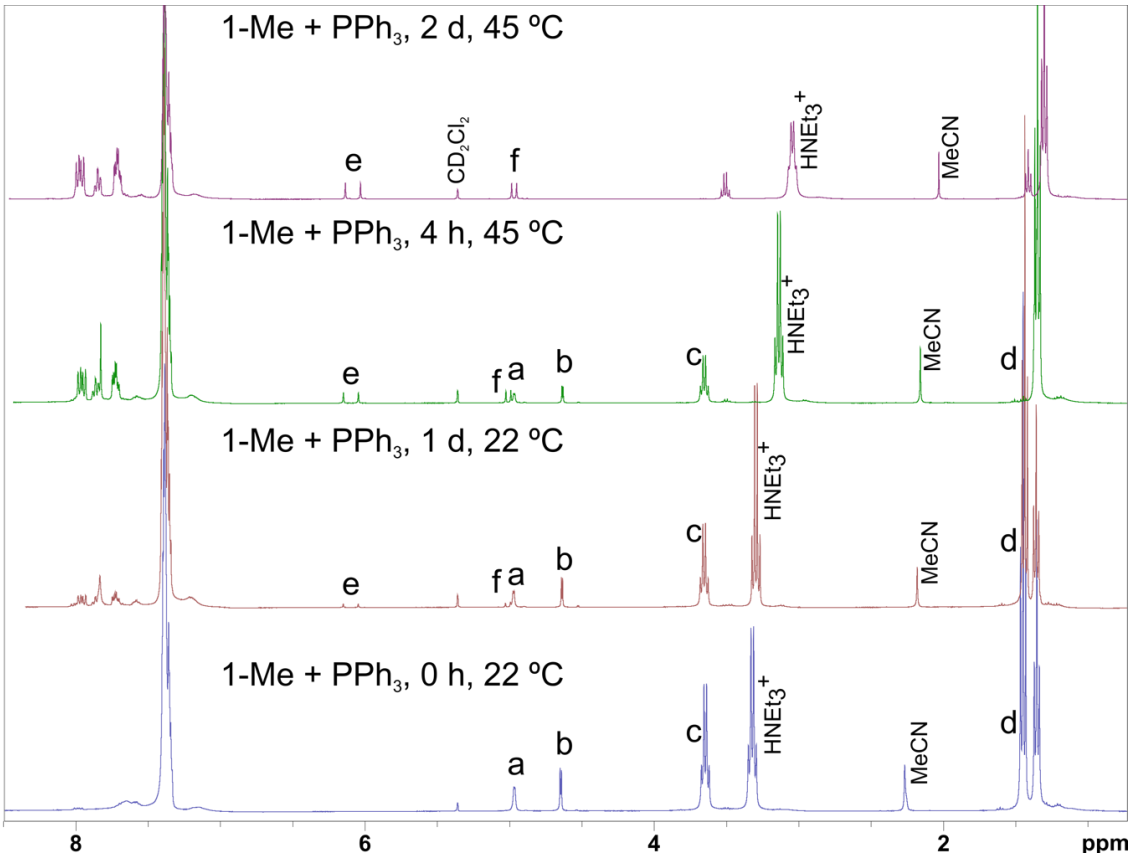

Figure 5.8 ^{1}H NMR spectra of a mixture of **1-Me** and excess PPh_3. Notice the disappearance of the signals from **1-Me** and the emergence of the signals from **2-Me** during the conversion. The presence of $HNEt_3Cl$ is due to an equilibrium between $[Ta(NCCH_2\{NEt_3\})Cl_4](MeCN)]$ and $[Ta(NCCH_2\{NEt_3\})Cl_5](HNEt_3)]$ in CH_3CN.[1]

.

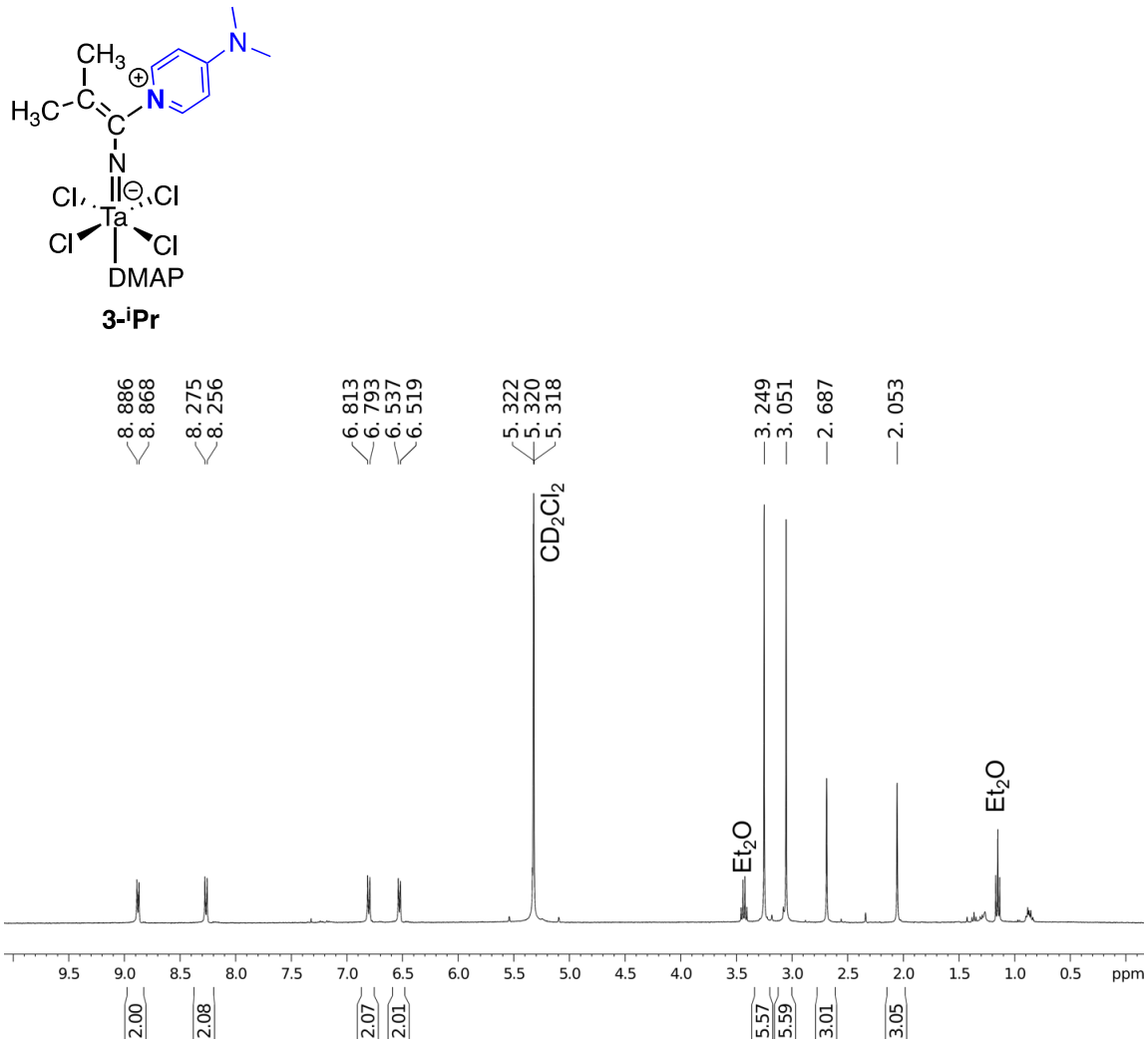

Figure 5.9 The ^{1}H NMR spectrum of **3-^{i}Pr** in CD_2Cl_2.

^{1}H NMR (400 MHz, CD_2Cl_2): δ 8.87 (d, 2H, $^{3}J_{HH}$ = 7 Hz, $NC_5H_4N(CH_3)_2$), 8.26 (d, 2H, $^{3}J_{HH}$ = 7 Hz, $NC_5H_4N(CH_3)_2$), 6.80 (d, 2H, $^{3}J_{HH}$ = 7 Hz, $NC_5H_4N(CH_3)_2$), 6.52 (d, 2H, $^{3}J_{HH}$ = 7 Hz, $NC_5H_4N(CH_3)_2$), 3.25 (s, 6H, $NC_5H_4N(CH_3)_2$), 3.05 s, 6H, $NC_5H_4N(CH_3)_2$), 2.69 (s, 3H, $NC=C(CH_3)_2$), 2.05 (s, 3H, $NC=C(CH_3)_2$).

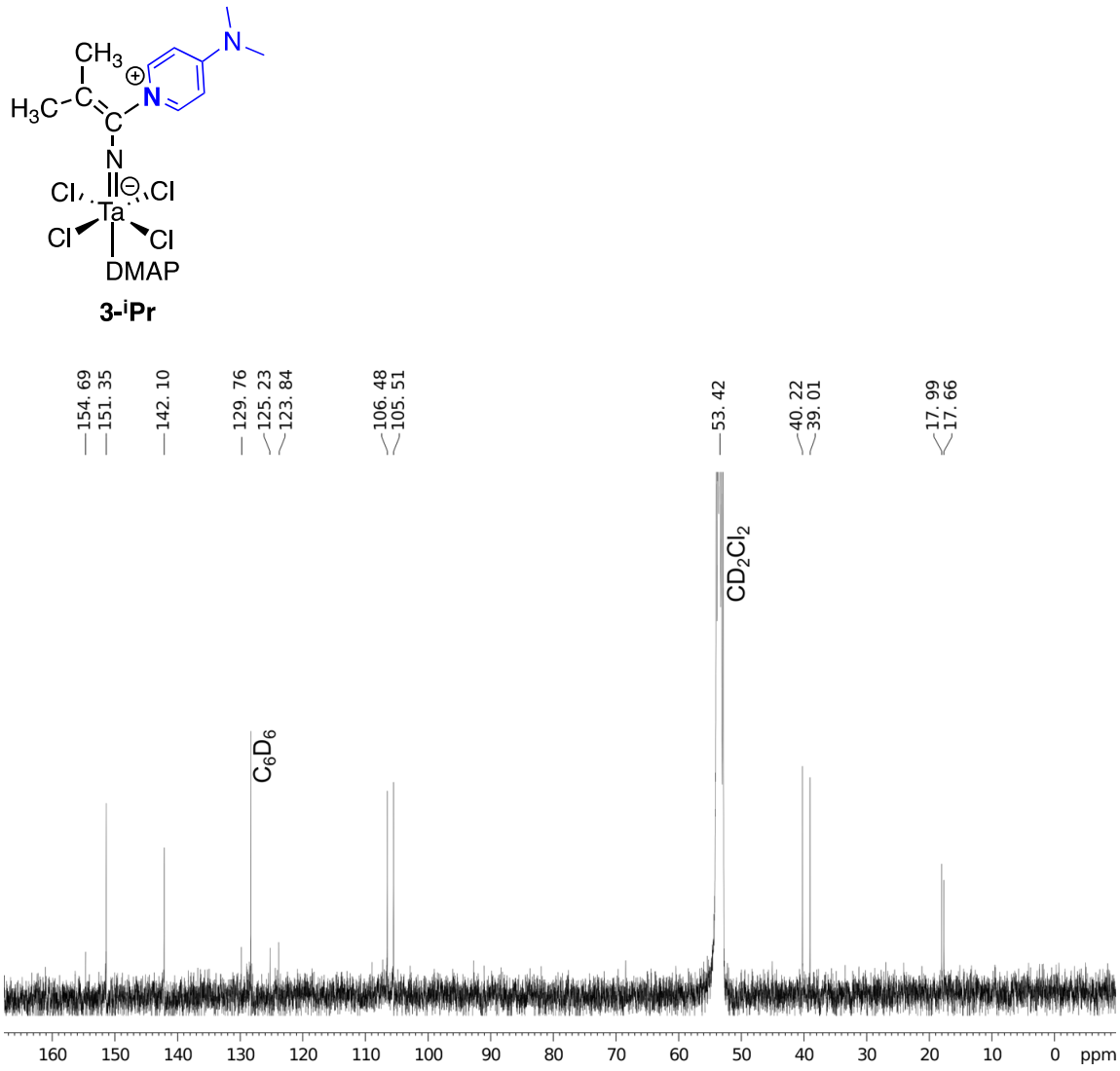

Figure 5.10 The ^{13}C NMR spectrum of **3-^{i}Pr** in CD_2Cl_2.

^{13}C (100 MHz, CD_2Cl_2): δ 154.7 (TaNC=*C*$(CH_3)_2$), 151.4 (N*C*$_5H_4N(CH_3)_2$), 142.1 (N*C*$_5H_4N(CH_3)_2$), 129.76 (TaN*C*=C$(CH_3)_2$), 125.2 (N*C*$_5H_4N(CH_3)_2$), 123.8 (N*C*$_5H_4N(CH_3)_2$), 106.5 (N*C*$_5H_4N(CH_3)_2$), 105.5 (N*C*$_5H_4N(CH_3)_2$), 40.2 (NC$_5H_4$N(*C*$H_3)_2$), 39.0 (NC$_5H_4$N(*C*$H_3)_2$), 18.0 (TaNC=C(*C*$H_3)_2$), 17.7 (TaNC=C(*C*$H_3)_2$).

Study of kinetics of imido interchange reactions

In a glovebox, **1-^{i}Pr** (0.009 – 0.027 mg) and naphthalene (5 mg) were weighted into a 20 mL vials. CD_2Cl_2 and weighed amount of propionitrile (3.5 – 24 equiv. relative to **1-^{i}Pr**) were then added to a total solution volume of 1.0 mL. Reaction mixtures were added to an NMR tube with the J. Young valve and heated at 40 ºC in an oil bath. Reaction progress was monitored by ^{1}H NMR spectroscopy with the use of naphthalene as an internal standard.

Experiment A: [**1-^{i}Pr**]$_0$ = 82.7 mM, [EtCN]$_0$ = 288 mM (3.5 equiv.)

Experiment B: [**1-^{i}Pr**]$_0$ = 82.8 mM, [EtCN]$_0$ = 618 mM (7.5 equiv.)

Experiment C: [**1-^{i}Pr**]$_0$ = 93.2 mM, [EtCN]$_0$ = 1410 mM (15.1 equiv.)

Experiment D: [**1-^{i}Pr**]$_0$ = 68.4 mM, [EtCN]$_0$ = 1628 mM (23.8 equiv.)

Experiment E: [**1-^{i}Pr**]$_0$ = 57.2 mM, [EtCN]$_0$ = 774 mM (13.5 equiv.), [NEt_3] = 713 mM (12.4 equiv.)

Experiment F: [**1-^{i}Pr**]$_0$ = 63.2 mM, [EtCN]$_0$ = 510 mM (8 equiv.), [^{t}BuCN] = 518 mM (8.2 equiv.)

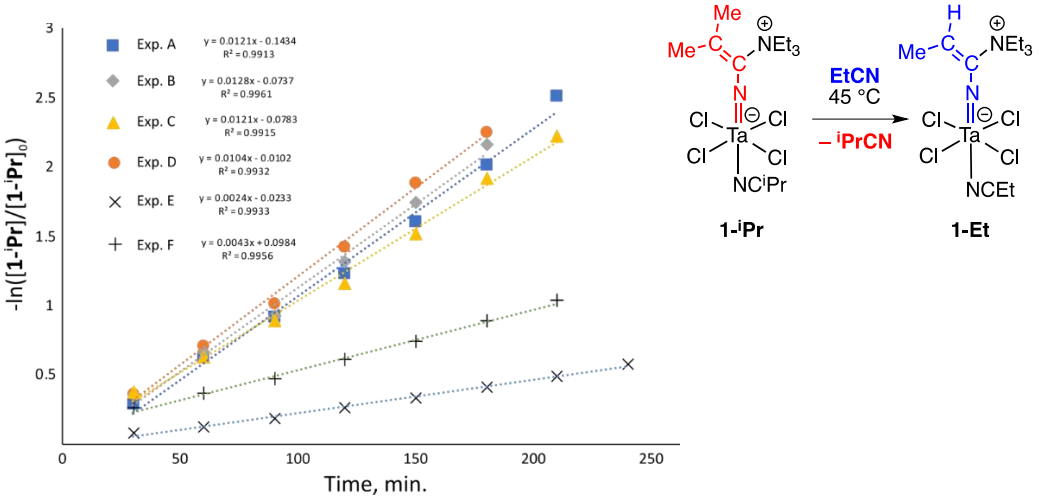

Figure 5.11 Kinetic data for the reaction of **1-^{i}Pr** with EtCN in CD_2Cl_2 at 40 ºC.

In a glovebox, **1-^{i}Pr** (0.009 – 0.027 mg) and naphthalene (5 mg) were weighted into a 5 mL vials. CD_2Cl_2 and weighed amount of acetonitrile (5 – 17 equiv. relative to **1-^{i}Pr**, experiments A – C). For the experiment D, 10 equiv. of CD_3CN were used. For the experiment E, 4 equiv. of CH_3CN and 5 equiv. of NEt_3 were used. were then added to a total solution volume of 1.0 mL. Reaction mixtures were added to an NMR tube with the J. Young valve and heated at 40 ºC in an oil bath. Reaction progress was monitored by ^{1}H NMR spectroscopy with the use of naphthalene as an internal standard.

Experiment A: [**1-^{i}Pr**]$_0$ = 63.3 mM, [CH_3CN]$_0$ = 317 mM (5 equiv.)

Experiment B: [**1-^{i}Pr**]$_0$ = 72.8 mM, [CH_3CN]$_0$ = 631 mM (8.7 equiv.)

Experiment C: [**1-^{i}Pr**]$_0$ = 79.2 mM, [CH_3CN]$_0$ = 1338 mM (16.8 equiv.)

Experiment D: [**1-^{i}Pr**]$_0$ = 44.1 mM, [CD_3CN]$_0$ = 452 mM (10.1 equiv.)

Experiment E: [**1-^{i}Pr**]$_0$ = 79.9 mM, [CH_3CN]$_0$ = 304 mM (3.8 equiv.), [NEt_3]$_0$ = 382 mM (4.8 equiv.)

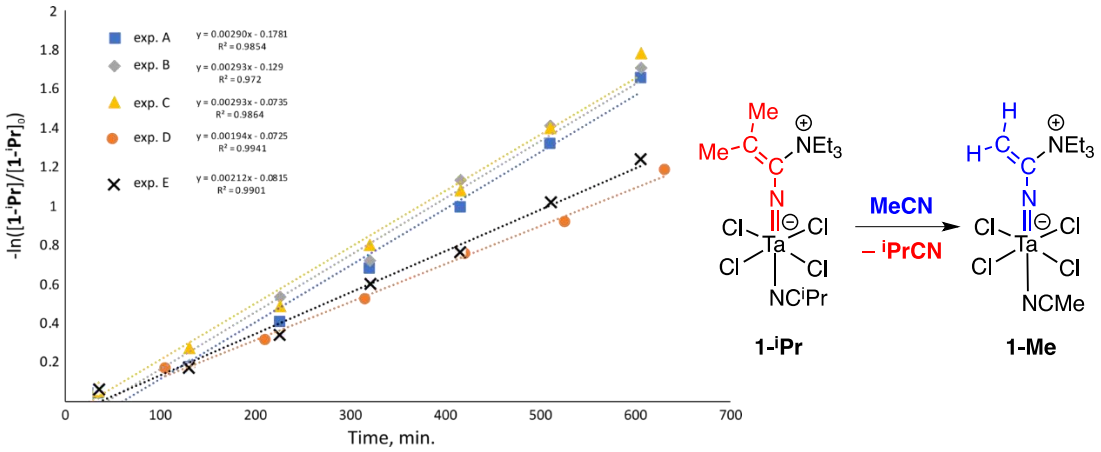

Figure 5.12 Kinetic data for the reaction of **1-^{i}Pr** with CH_3CN (or CD_3CN) in CD_2Cl_2 at 40 ºC.

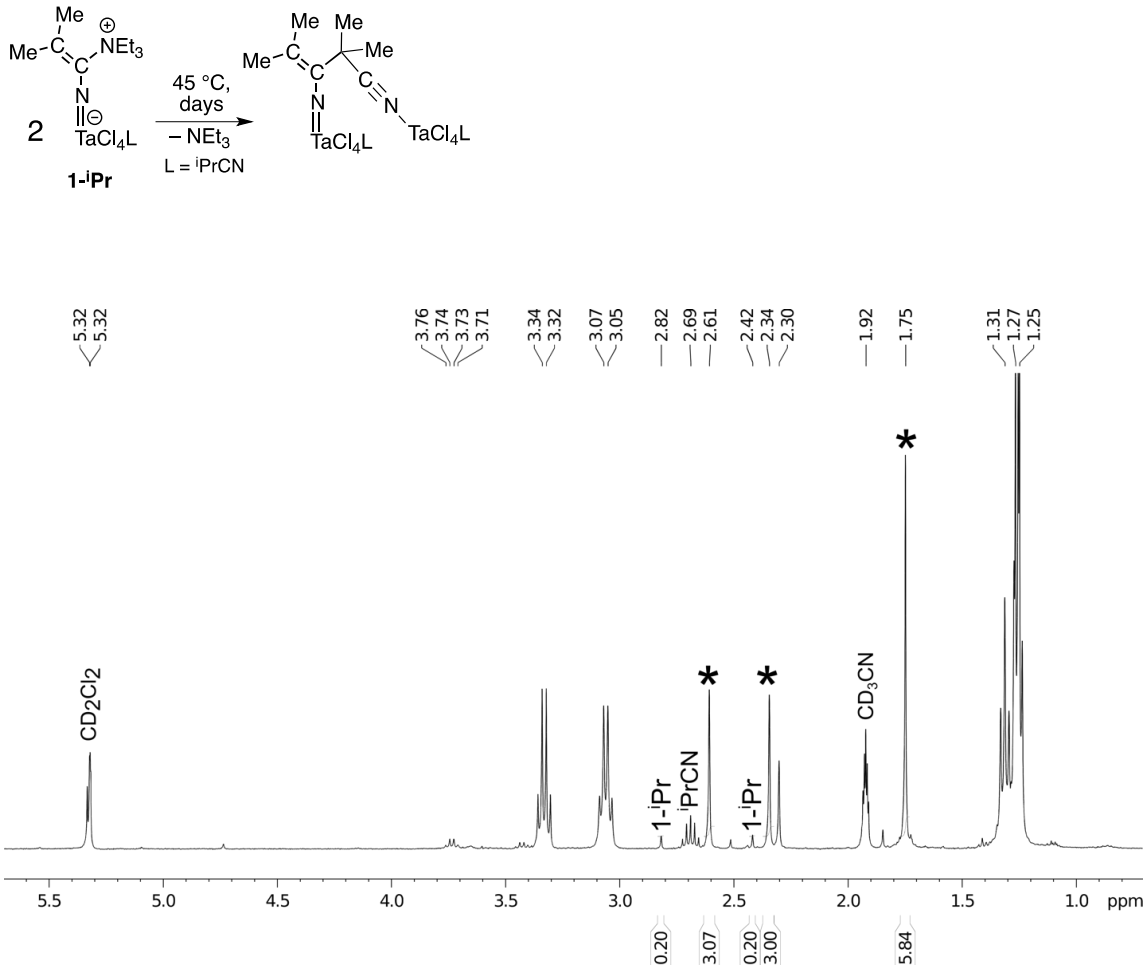

Figure 5.13 The ^{1}H NMR spectrum of a reaction mixture after heating **1-^{i}Pr** at 45 ºC in CD_2Cl_2 without an added nitrile (the spectrum has been recorded in the CD_2Cl_2/CD_3CN solvent mixture due to insolubility of products in CD_2Cl_2). Notice the disappearance of the signals from the starting imido complex and the emergence of the signals from the vinylimidocyanoalkyl group (labeled with asterisks) in 1:1:2 ratio. A similar complex has been synthesized in the reaction of $TaCl_5$ and ^{i}PrCN in the presence of Hunig's base.[1]

X-Ray Structure Determination, $TaCl_4(C_{11}H_{16}N_3)(C_7H_{10}N_2)\cdot CH_2Cl_2$ (3-^{i}Pr)

X-ray intensity data from a pale-yellow bladelike needle crystal were collected at 100(2) K using a Bruker D8 QUEST diffractometer equipped with a PHOTON 100 CMOS area detector and an Incoatec microfocus source (Mo Kα radiation, λ = 0.71073 Å).[13] The raw area detector data frames were reduced and corrected for absorption effects using the SAINT+ and SADABS programs.[13] Final unit cell parameters were determined by least-squares refinement of 9922 reflections taken from the data set. The structure was solved by direct methods with SHELXT.[14] Subsequent difference Fourier calculations and full-matrix least-squares refinement against F^2 were performed with SHELXL-2014[14] using OLEX2.[15]

The compound crystallizes in the triclinic system. The space group *P*-1 (No. 2) was confirmed by structure solution. The asymmetric unit consists of one $TaCl_4(C_{11}H_{16}N_3)(C_7H_{10}N_2)$ complex and one dichloromethane molecule. The dichloromethane disorder affects only one chlorine site and has a minor disorder population of 0.058(3). All non-hydrogen atoms were refined with anisotropic displacement parameters. Hydrogen atoms were located in Fourier difference maps before being placed in geometrically idealized positions included as riding atoms with *d*(C-H) = 0.95 Å and *U*iso(H) = 1.2*U*eq(C) for arene hydrogen atoms, *d*(C-H) = 0.99 Å and *U*iso(H) = 1.2*U*eq(C) for methylene hydrogens and *d*(C-H) = 0.98 Å and *U*iso(H) = 1.5*U*eq(C) for methyl hydrogens. The methyl hydrogens were allowed to rotate as a rigid group to the orientation of maximum observed electron density. All C-Cl distances were restrained to be similar. The largest residual electron density peak in the final difference map is 0.67 $e^-/Å^3$, located 0.94 Å from C1SB.

Table 5.1 Crystallographic table for single crystal X-ray data for compound **[Ta(NCCMe$_2${DMAP})Cl$_4$](DMAP) (3-^{i}Pr)**

	Isobutyronitrile imide (DMAP)
Empirical formula	$C_{19}H_{28}Cl_6N_5Ta$
Formula weight	720.11
Temperature/K	100(2)
Crystal system	triclinic
Space group	P-1
a/Å	8.5126(9)
b/Å	11.3367(11)
c/Å	15.0112(16)
α/°	70.324(3)
β/°	75.923(3)
γ/°	80.309(3)
Volume/Å^3	1317.2(2)
Z	2
ρ_{calc}g/cm^3	1.816
μ/mm^{-1}	4.798
	704.0
Crystal size/mm^3	0.42 × 0.08 × 0.04
Radiation	MoKα (λ = 0.71073)
2Θ range for data collection/°	4.956 to 52.748
	-10 ≤ h ≤ 10, -14 ≤ k ≤ 13, -18 ≤ l ≤ 18
Reflections collected	29266
Data/restraints/parameters	5326/3/291
Goodness-of-fit on F^2	1.041
Final R indexes [I>=2σ (I)]	R_1 = 0.0256, wR_2 = 0.0445
Final R indexes [all data]	R_1 = 0.0360, wR_2 = 0.0466
Largest diff. peak/hole / e Å^{-3}	0.67/-0.86

References

1. La Pierre, H. S.; Arnold, J.; Bergman, R. G.; Toste, F. D. *Inorg. Chem.* **2012**, *51* (24), 13334–13344.
2. Yuan, J.; Schrock, R. R.; Gerber, L. C. H.; Müller, P.; Smith, S. *Organometallics* **2013**, *32* (10), 2983–2992.
3. Basuli, F.; Bailey, B. C.; Watson, L. A.; Tomaszewski, J.; Huffman, J. C.; Mindiola, D. J. *Organometallics* **2005**, *24* (8), 1886–1906.
4. Townsend, E. M.; Kilyanek, S. M.; Schrock, R. R.; Müller, P.; Smith, S. J.; Hoveyda, A. H. *Organometallics* **2013**, *32* (16), 4612–4617.
5. Duhacek, J. C.; Siddiquee, T. A.; Bennett, D. W.; Duncan, D. C. *J. Chem. Crystallogr.* **2008**, *38* (6), 431–435.
6. Basuli, F.; Huffman, J. C.; Mindiola, D. J. *Inorg. Chem.* **2003**, *42* (24), 8003–8010.
7. Bolton, P. D.; Feliz, M.; Cowley, A. R.; Clot, E.; Mountford, P. Ti═NR vs Ti−R′ *Organometallics* **2008**, *27* (23), 6096–6110.
8. Lam, J. K.; Zhu, C.; Bukhryakov, K. V.; Müller, P.; Hoveyda, A.; Schrock, R. R. *J. Am. Chem. Soc.* **2016**, *138* (48), 15774–15783.
9. Pugh, S. M.; Trösch, D. J. M.; Wilson, D. J.; Bashall, A.; Cloke, F. G. N.; Gade, L. H.; Hitchcock, P. B.; McPartlin, M.; Nixon, J. F.; Mountford, P. *Organometallics* **2000**, *19* (16), 3205–3210.
10. Doxsee, K. M.; Farahi, J. B.; Hope, H. *J. Am. Chem. Soc.* **1991**, *113* (23), 8889–8898.
11. Rahman, M. M.; Smith, M. D.; Peryshkov, D. V. *Inorg. Chem.* **2016**, *55* (11), 5101–5103.

12. Rahman, M. M.; Smith, M. D.; Amaya, J. A.; Makris, T. M.; Peryshkov, D. V. *Inorg. Chem.* **2017**, *56* (19), 11798–11803.

13. APEX3 Version 2016.5-0 and SAINT+ Version 8.38A. Bruker AXS, Inc., Madison, Wisconsin, USA, 2016.

14. SADABS-2016/2: Krause, L., Herbst-Irmer, R., Sheldrick G.M. and Stalke D. *J. Appl. Cryst.* 2015, *48*, 3-10.

15. HELXT: Sheldrick, G.M. *Acta Cryst*. 2015, *A71*, 3-8.

16. Rahman, M. M.; Peryshkov, D.; *Abstr. Pap.—Am. Chem. Soc., Div. Inorg. Chem.* **2016**, *251*, INORG 2593815.

Chapter 6

Synthesis of Early Transition Metal Nitride Clusters

6.1 Introduction

In the first part of this chapter a novel star shaped tantalum nitride cluster compound with the formula of $Ta_6N_5Cl_{15}(CH_3CN)_7$ (**1**) is being reported. According to structural similarity there is one recent report on a triple-decked pentagonal prismatic structure of titanium oxides ($Ti_{18}O_{27}$).[1] This titanium compound has 6 Ti metal nuclei, one at the center and 5 at the terminal points all of them are connected by a μ_3-O ligand in each of the 3 layers. If all the nitrile and chloride ligands are omitted, this has a core structural similarity to our novel tantalum nitride structure (Ti_6N_5), as 5 terminal tantalum atoms are connected to the central tantalum atom with μ_3-N ligands. Also, from the top view the cluster has a star shaped molecular representation that resembles to our tantalum nitride cluster. Bradley and co-workers have studied a number of tantalum complexes those can be synthesized by reaction between $TaCl_5$ and lithiated HMDS or other amines and their thermolysis can yield to tantalum imides.[2]

Among many other early transition metal nitrides Yélamos and co-workers have been studying titanium cubanes for over more than couple of decades. For example, by ammonolysis of a simple titanium complex $[Cp^*Ti(NMe_2)_3]_4$ they have prepared simple cubic titanium nitride and trinuclear pre-cubane to incorporate other metals (Zr, Hf, Ga, Pb, etc.) that would form hetero nuclear cubanes.[3-7] Carmalt and co-workers on the other hand used simple amines to prepare mono- and dinuclear titanium amides that was used as precursor for titanium nitrides.[8,9] Also, there is a low cost method for titanium nitride synthesis from titanium imide with the use simple precursor $(Me_3)SiNTiCl_3$.[10] Moran and co-workers have reported a titanium oxides cluster ($Ti_4(\mu_3\text{-}O)_2(\mu_2\text{-}O^iPr)_2$) that has a ladder like core structure,[11] with a structural similarity to the work by Wolczanski *et al.*[12] In the

later part of this chapter the titanium nitride ladder like structure, Ti_4 cluster (**2**) and a Ti_9 Cluster (**3**) have been discussed.

6.2 Results and Discussions

In a straightforward synthetic route, the reaction between $TaCl_5$ and hexamethyldisilazane (HMDS) in a solvent of toluene at a moderate temperature (65 °C) can give the precursor for the tantalum nitride cluster as a yellow powder. The yellow powder was dissolved in minimum amount of acetonitrile solvent and the abundant colorless crystals were grown in four separate vials within several days to couple of weeks period of time that varies with different batches of reactions. The star-shaped $Ta_6N_5Cl_{15}(CH_3CN)_7$ cluster was characterized by X-ray crystallography. NMR characterization shows that the precursor contains NH_4Cl as residual salt even though the precipitates were repeatedly washed with excess of solvents. This hexanuclear tantalum cluster incorporates five μ_3-N groups. There is a central pentagonal bipyramidal Ta nucleus, with two axial chloride ligands and five equatorial bridging nitrido ligands, surrounded by five octahedrally coordinated tantalum atoms. These additional ligands are provided by remaining anionic chloride atoms and neutral acetonitrile ligands. The overall cluster molecule is planer in geometry. (**Figure 6.1**) The Ta1−N distances are in the range from 2.193(6) Å to 2.250(6) Å. The N−Ta1−N angles with the plane are in the range from 69.9(2)º to 73.5(2)º. Five octahedrally coordinated tantalum atoms compose the perimeter of the star cluster. For each of these tantalum centers, Ta−N distances vary slightly from 1.883(6) Å to 1.966(6) Å. Pairs of Ta−N−Ta1 angles are in the range from 99.4(2)º to 101.1(3)º and obtuse Ta−N−Ta angles at the periphery of the cluster in the range from 155.3(3)º to 159.2(3)º. Therefore, μ_3-N nitrido ligands can be considered to form distorted T-shaped NTa_3 fragments. The similar

T-shaped arrangement of triple-bridging nitrido groups has been observed in the alkyl nitrido complex [{Ta(CH_2*t*-Bu)$_2$}$_5$(μ_2-N)$_2$(μ_3-N)$_3$] reported by Wolczanski and co-workers.[13]

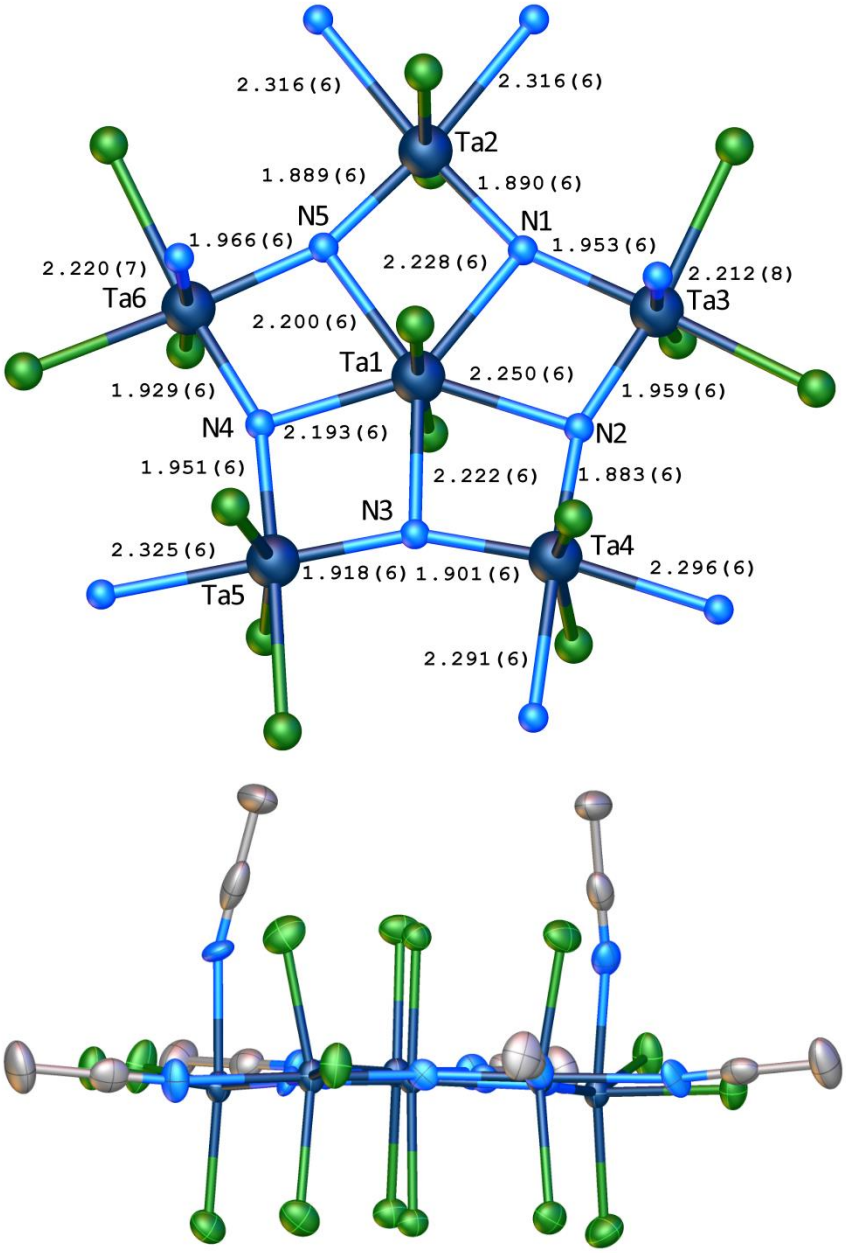

Figure 6.1 The X-ray crystallographic structure of $Ta_6N_5Cl_{15}(CH_3CN)_7$ (**1**)The top view showing pentagonal star shaped cluster and the side view at the bottom showing a planer geometry of the structure. The structure is simplified for clarity by removing methyl groups for the top view and only protons were omitted for the side view structure.

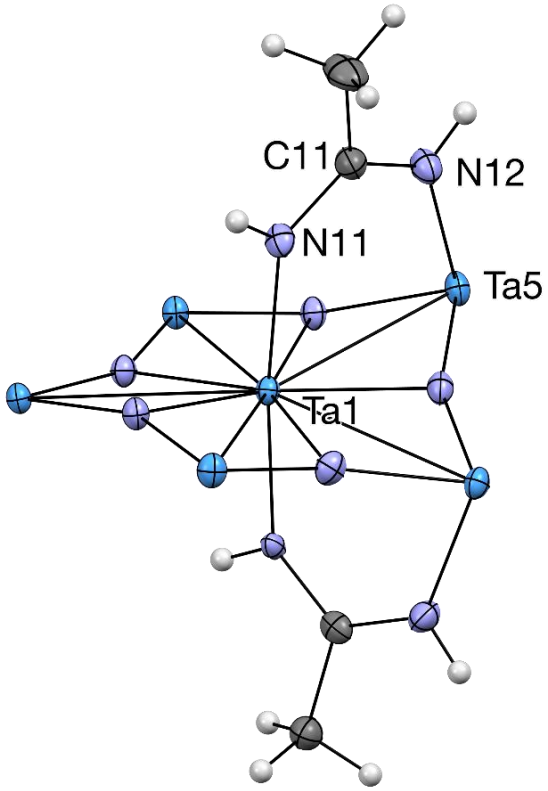

Figure 6.2 The X-ray crystallographic structure of **{$Ta_6(N)_5Cl_{13}(C_2H_5N_2)_2(CH_3CN)_5$ (1a)** The structure is simplified for clarity by removing all the chlorides and acetonitrile ligands.

A partially modified cluster was isolated in the case when the precursor precipitates were not washed with additional toluene after the reaction. The residual ammonium chloride and any remaining HMDS base potentially can activate two of the coordinated acetonitrile molecules by partially hydrogenating the cyanide group nitrogen and forming the guanidine structure ligand. Only central Ta and two of the five terminal Ta atoms are connected via the guanidine structure (**Figure 6.2**). The overall structure has deformed from its planer geometry of the parent structure but the structural framework of Ta_6N_5 otherwise remained the same.

Cyclic Voltammetry of $Ta_6N_5Cl_{15}(CH_3CN)_7$ (1) cluster

All electrochemical measurements were performed using a Pine instrument potentiostat, using a glassy carbon electrode as the working electrode. A platinum wire was

used as the counter electrode and saturated calomel electrode as the reference electrode. The cyclic voltammogram of the Ta complex shows 4 irreversible reduction peaks at -0.82 V, -1.72 V, -2.101 V and -2.439 V. Since Ta atom at the center has the highest oxidation state, it's easily reducible and therefore should be represented by the wave at -0.82 V. The other peaks should be representative of the reduction of different unidentified species.

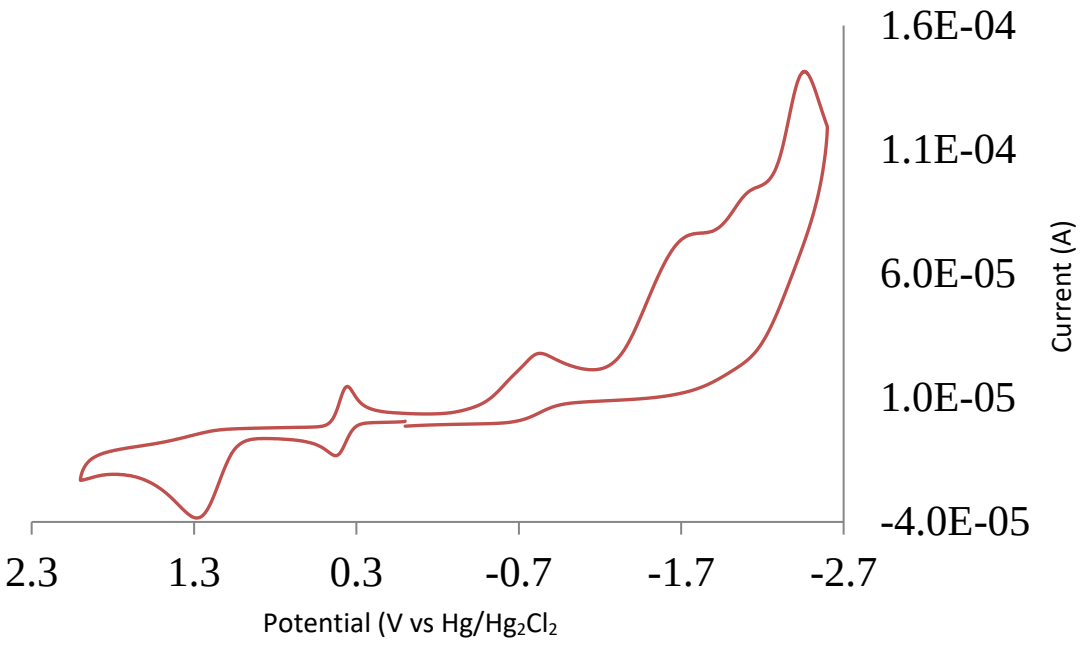

Figure 6.3 Cyclic voltammogram of $Ta_6N_5Cl_{15}(CH_3CN)_7$ (**1**) cluster.

Titanium nitride cluster

The reaction with a 5 to 6 molar equivalents of $TiCl_4$ and HMDS has in a solution of toluene resulted in an orange precipitate at room temperature. The isolated orange precipitate as the primary reaction product was dissolved in acetonitrile and yellow crystals formed overnight. The ladder-shaped $Ti_4(\mu_3\text{-}N)_2Cl_{10}(CH_3CN)_6{\cdot}C_7H_8$ cluster was characterized by X-ray crystallography. The twinned yellow plate shaped crystals were co-crystallized with toluene. This ladder cluster incorporates two μ_3-N groups. Each of the

four Ti nucleus has at least one axial acetonitrile ligand, one chloride ligand in trans position to each other, and one axial chloride ligand. There are two μ_2-Cl ligands and two more axial acetonitrile ligands for the two terminal Ti nuclei. The overall molecule has an inversion center and centrosymmetric (**Figure 6.4**). The Ti1−N distances are in the range from 1.835(3) Å to 2.045(3) Å for the two μ_3-N ligands. The N−Ti2−N angles with the plane are 83.46(13)º and pairs of Ti1−N−Ta2 angles are 113.22(15)º. The similar T-shaped arrangement of triple-bridging nitrido groups has been observed in the titanium oxides cluster ($Ti_4(\mu_3\text{-}O)_2(\mu_2\text{-}O^iPr)_2$) reported by Moran and co-workers.[11]

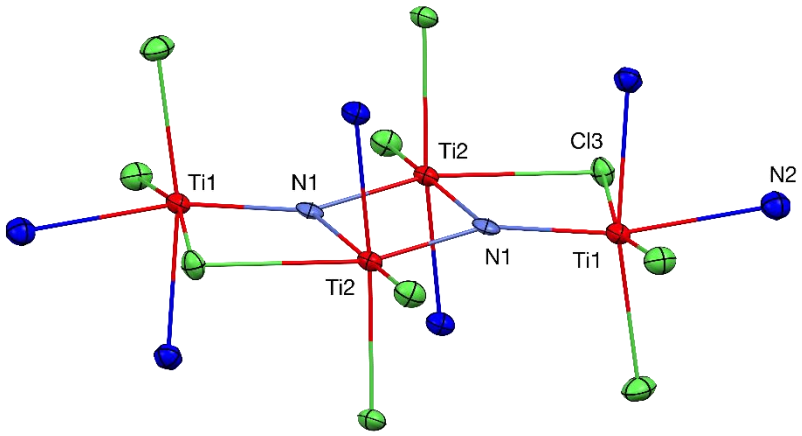

Figure 6.4 X-ray crystallographic structure of the $Ti_4(\mu_3\text{-}N)_2Cl_{10}(CH_3CN)_6\cdot C_7H_8$. (**2**) Displacement ellipsoids drawn at the 60% probability level. For clarity, the methyl groups from acetonitrile ligands were omitted.

A second set of crystals were grown from the leftover solution of the reaction mixture in toluene. These crystal of Ti_9N_6 cluster molecule was partially retaining their TMS group from the original HMDS amine and acting as a bridging trimethylsilyl imide in two neighboring Ti atoms. The entire molecule is co-crystallized with $[H_3NSi(CH_3)_3]^+$ cation. Thus, it explains the functional duality of the HMDS as both a base participating in

deprotonation and formation of an NH_4Cl salt and a source for the structural bridging nitride atom.

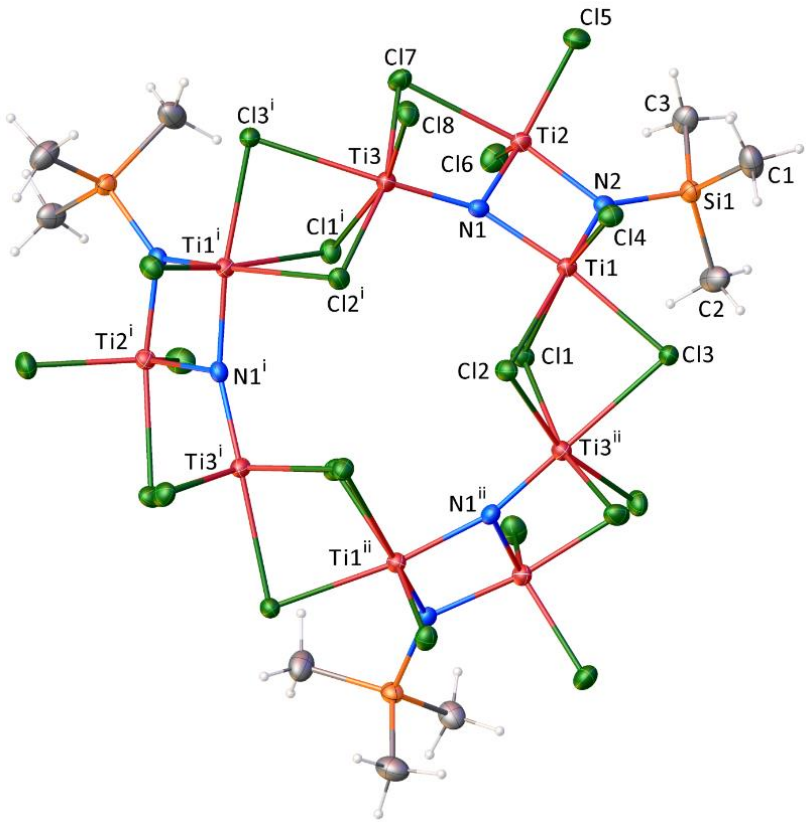

Figure 6.5 X-ray crystallographic structure of the $[H_3NSi(CH_3)_3]_3[Ti_9(\mu_3\text{-}N)_3Cl_{24}(NSi(CH_3)_3)_3]\cdot(C_7H_8)_3$ (**3**).

6.3 Synthesis

General procedure:

All synthetic manipulations were carried out either in a nitrogen-filled drybox or on an air free dual-manifold Schlenk line. Solvents (acetonitrile and toluene) were sparged with nitrogen, passed through activated alumina, and stored over activated 4 Å Linde-type molecular sieves. $TiCl_4$ (Sigma-Aldrich), $TaCl_5$ (Strem) was used as received. Hexamethylenedisilazane was purchased from commercial source, degassed by freeze-pump-thaw technique and stored over 4 Å Linde-type molecular sieves.

Tantalum Nitride 1 and 1a:

$TaCl_5$ (1g, 2.79mmol) was suspended in toluene (20ml) in a 500 ml closed glass reactor and hexamethyldisilazane (0.45g, 2.32mmol) was added into the suspension at room temperature. The suspension mixture was prepared inside nitrogen filled glove box and the reactor was taken outside to stir for 14 h at 65 ^oC. A yellow colored suspension was formed that was filtered over a glass frit and washed with additional toluene (20ml). The yellow powder (yield over 90%) was dried under vacuum and dissolved in acetonitrile (2ml) as an olive-green solution. Over a period of a week the solution gave colorless crystals (0.092g), achieving a final yield over 25%.

Synthesis of titanium nitride clusters

$TiCl_4$ (0.1g, .527 mmol) was dissolved in toluene (5 mL) in a 20 mL glass vial and hexamethyldisilazane (0.071g, 0.439 mmol) as a solution in toluene (5 mL) was added into the previous solution at room temperature. An orange suspension was formed that was filtered and dissolved in acetonitrile. Within two days period the solution gave pale yellow crystals (**2**) of **Ti_4N_2,** which was characterized by X-ray crystallography.

In order to grow the Ti_9N_6 cluster compounds (**3**), the residual solution in toluene from the reaction mixture was filtered and left undisturbed. A second type of titanium nitride crystals were collected from the glass vial and subjected for crystallographic characterizations.

X-Ray Structure Determination, $Ta_6N_5Cl_{15}(CH_3CN)_7 \cdot 2CH_3CN$ (1)

X-ray intensity data from a colorless oval plate were collected at 100(2) K using a Bruker SMART APEX diffractometer (Mo Kα radiation, λ = 0.71073 Å).[14] The raw area detector data frames were reduced and corrected for absorption effects using the SAINT+

and SADABS programs.[14] Final unit cell parameters were determined by least-squares refinement of 8544 reflections from the data set. The structure was solved by direct methods with SHELXT.[15] Subsequent difference Fourier calculations and full-matrix least-squares refinement against F^2 were performed with SHELXL-2014[2] using OLEX2.[15,16]

The compound crystallizes in the monoclinic space group $P2_1/n$ as determined by the pattern of systematic absences in the intensity data. The asymmetric unit consists of one $Ta_6N_5Cl_{15}(CH_3CN)_7$ cluster and two non-coordinated acetonitrile molecules. One of the non-coordinated acetonitrile molecules is disordered over two closely separated positions. These atoms were refined with the aid of six distance restraints and were assigned a common isotropic displacement parameter. All non-hydrogen atoms were refined with anisotropic displacement parameters except where noted. Hydrogen atoms were placed in geometrically idealized positions and included as riding atoms. The largest residual electron density peak in the final difference map is 1.96 $e^-/Å^3$, located 0.98 Å from Ta_3.

X-Ray Structure determination of $Ta_6(N)_5Cl_{13}(C_2H_5N_2)_2(CH_3CN)_5$ (1a)

X-ray intensity data from a colorless plate were collected at 100(2) K using a Bruker D8 QUEST diffractometer equipped with a PHOTON-100 CMOS area detector and an Incoatec microfocus source (Mo Kα radiation, λ = 0.71073 Å). The raw area detector data frames were reduced and corrected for absorption effects using the Bruker APEX3, SAINT+ and SADABS programs.[14,15] Final unit cell parameters were determined by least-squares refinement of 9659 reflections taken from the data set. The structure was solved with SHELXT.[16,17] Subsequent difference Fourier calculations and full-matrix

least-squares refinement against F^2 were performed with SHELXL-2018[3] using OLEX2.[18]

The compound crystallizes in the triclinic system. The space group *P*-1 (No. 2) was confirmed by structure solution. The asymmetric unit consists of one Ta_6 complex (see below) and three independent acetonitrile molecules. During normal refinement, one perimeter Ta site (Ta6) was found to be disordered over two positions. The observed electron density around the disordered Ta6 site was not consistent with two identical molecules in slightly different orientations, but rather two complexes having different compositions. They are disordered together such that most atomic positions are coincident, the exception primarily being atoms surrounding the split site Ta6A/B. Ta1-Ta5, the five bridging nitrido atoms, all atoms bonded to Ta2-Ta5 and the bridging anion N11/N12/C11/C12 are common to both complexes. In addition to bridging nitrido atoms N4 and N5, Ta6A is bonded to two Cl atoms, one acetonitrile and a $C_2H_5N_2^-$ NH donor (N14); Ta6B is bonded to three Cl atoms, and one acetonitrile. In the Ta6B complex, the Ta1 axial ligands are one $C_2H_5N_2^-$ anion (N11) and an acetonitrile molecule (N13B); in the Ta6A complex, the axial ligands of Ta1 are two $C_2H_5N_2^-$ anions (N11 and N13). The minor components atoms were generally given atom label suffixes “B” except for the Cl atoms (Cl22-Cl24, SHELX four-character limit). Disorder component occupancies refined to 0.929(1) and 0.071(1), which were constrained to sum to one. All non-hydrogen atoms were refined with anisotropic displacement parameters except for minor component atoms (isotropic). Those of nearly superimposed disordered atoms were held equal. Hydrogen atoms were located in difference Fourier maps before being placed in geometrically idealized positions and included as riding atoms with *d*(C-H) = 0.98 Å and *U*iso(H) =

1.5*U*eq(C) for methyl hydrogens. The methyl hydrogens were allowed to rotate as a rigid group to the orientation of maximum observed electron density. Hydrogen atoms bonded to nitrogen were located in difference Fourier maps and refined isotropically with their N-H distances restrained to 0.85(2) Å. The largest residual electron density peak in the final difference map is 2.04 $e^-/Å^3$, located 0.72 Å from Ta4.

X-Ray Structure Determination, $Ti_4(\mu_3\text{-}N)_2Cl_{10}(CH_3CN)_6 \cdot C_7H_8$ (2)

Crystals of the compound formed as clusters of yellow plates visibly exhibiting lamellar twinning. A single domain plate could not be cleaved apart. Several crystals examined persistently gave split diffraction peak profiles, along with difficulty in indexing the diffraction pattern to a single reasonable unit cell. Eventually it was determined that crystals of the material are twinned by non-merohedry. Using the Bruker Cell_Now program,[1] a set of 237 reflections from the data crystal were indexed entirely to two domains with the reported triclinic unit cell parameters. The derived twin law, relating indices of one domain to those of the other, is (-1 0 0 / 0 -1 0 / 0.934 0.677 1). The twin law corresponds to a 180° rotation about the reciprocal space [001] axis. X-ray intensity data were collected at 100(2) K using a Bruker D8 QUEST diffractometer equipped with a PHOTON 100 CMOS area detector and an Incoatec microfocus source (Mo Kα radiation, λ = 0.71073 Å).[(14)] The raw area detector data frames were processed and corrected for absorption effects using the SAINT+ and TWINABS programs.[(14)] TWINABS also constructed a SHELX HKLF-5 format reflection file for refinement. Final unit cell parameters were determined by least-squares refinement of 7318 reflections in the range 4.71° < 2θ < 52.78° taken from both twin domains of the crystal. An initial structure solution was obtained using the data taken by the major twin domain only with the dual-

space intrinsic phasing method with SHELXT.[14] Subsequent difference Fourier calculations and full-matrix least-squares refinement against F^2 of the full twinned dataset were performed with SHELXL-2016 using OLEX2.[15] The major twin domain volume fraction refined to 0.621(1).

The compound crystallizes in the space group *P*-1 (No. 2) of the triclinic system. The asymmetric unit consists of half of one $Ti_4(\mu_3\text{-}N)_2Cl_{10}(CH_3CN)_6$ molecule and half of one toluene molecule. Both species are located on crystallographic inversion centers. The toluene molecule is disordered about the inversion center and was refined with half-occupancy. Its C6 ring was refined as a rigid hexagon with *d*(C-C) = 1.39 Å (AFIX 66), and *d*(C11-C17) = 1.54(2) Å and similar C17-C12/C16 distance (SADI) restraints were applied for the methyl carbon atom C17. All non-hydrogen atoms were refined with anisotropic displacement parameters except for the toluene atoms (isotropic). Hydrogen atoms bonded to carbon were placed in geometrically idealized positions and included as riding atoms with *d*(C-H) = 0.95 Å and *U*iso(H) = 1.2*U*eq(C) for aromatic hydrogen atoms and *d*(C-H) = 0.98 Å and *U*iso(H) = 1.5*U*eq(C) for methyl hydrogens. The methyl hydrogens were allowed to rotate as a rigid group to the orientation of maximum observed electron density. The largest residual electron density peak in the final difference map is 0.44 $e^-/Å^3$, located 0.99 Å from C4.

X-Ray Structure Determination, $[H_3NSi(CH_3)_3]_3[Ti_9(\mu_3\text{-}N)_3Cl_{24}(NSi(CH_3)_3)_3]\cdot(C_7H_8)_3$ (3)

X-ray intensity data from an orange block were collected at 100(2) K using a Bruker D8 QUEST diffractometer equipped with a PHOTON-100 CMOS area detector and an Incoatec microfocus source (Mo Kα radiation, λ = 0.71073 Å). The crystals were transferred rapidly to the diffractometer cold stream, as they decompose to a powder within

seconds in air or under oil. The raw area detector data frames were reduced and corrected for absorption effects using the Bruker APEX3, SAINT+ and SADABS programs.[14,15] Final unit cell parameters were determined by least-squares refinement of 9888 reflections taken from the data set. The structure was solved with SHELXT.[16] Subsequent difference Fourier calculations and full-matrix least-squares refinement against F^2 were performed with SHELXL-2016[16] using OLEX2.[17]

The compound crystallizes in the trigonal (rhombohedral) system. The pattern of systematic absences in the intensity data was consistent with the space groups *R*3 and *R*-3, the latter of which was confirmed by structure solution. The asymmetric unit in *R*-3 consists of 1/3 of one $[Ti_9(\mu_3\text{-}N)_3Cl_{24}(NSi(CH_3)_3)_3]^{3-}$ anion, one $H_3NSi(CH_3)_3^+$ cation and one toluene molecule. The anion is located on a crystallographic three-fold axis of rotation, with three unique Ti atoms, eight chloride ligands, one μ_3-nitrido ligand and one trimethylsilylnitrido ligand in the asymmetric unit. All non-hydrogen atoms were refined with anisotropic displacement parameters. Hydrogen atoms bonded to carbon were placed in geometrically idealized positions and included as riding atoms with *d*(C-H) = 0.95 Å and *U*iso(H) = 1.2*U*eq(C) for aromatic hydrogen atoms and *d*(C-H) = 0.98 Å and *U*iso(H) = 1.5*U*eq(C) for methyl hydrogens. The methyl hydrogens were allowed to rotate as a rigid group to the orientation of maximum observed electron density. The hydrogen atoms of trimethylsilylammonium cation are disordered, appearing in the difference map as an umbrella of electron density circling the N atom. These hydrogen atoms were modeled with six equally spaced half-occupied hydrogen atoms (SHELX AFIX 127). The ammonium group disorder likely arises because of hydrogen bonding frustration to five nearly

equidistant Cl acceptors (N – Cl = 3.21 - 3.46 Å). The largest residual electron density peak in the final difference map is 0.53 $e^-/Å^3$, located 0.76 Å from H3B.

Table:6.1 Crystallographic table for single crystal X-ray data for compound Ta Star (**1**), (**1a**), Ti_4 Ladder (**2**), and Ti_9 Cluster (**3**).

	Ta Star (1)	**Ta Star (1a)**	**Ti_4 Ladder (2)**	**Ti_9 Cluster (3)**
Empirical formula	$C_{18}H_{27}Cl_{15}N_{14}Ta_6$	$C_{19.86}H_{33.65}Cl_{13.07}N_{16.86}Ta_6$	$C_{19}H_{26}Cl_{10}N_8Ti_4$	$C_{39}H_{87}Cl_{24}N_9Si_6Ti_9$
Formula weight	2056.98	2057.67	912.58	2132.61
Temperature/K	100(2)	100(2)	100(2)	100(2)
Crystal system	monoclinic	triclinic	triclinic	trigonal
Space group	$P2_1/n$	P-1	P-1	R-3
a/Å	11.7569(7)	10.0913(4)	8.7813(5)	23.5430(10)
b/Å	22.6387(13)	12.7843(5)	9.9181(6)	23.5430(10)
c/Å	18.2259(11)	21.7370(10)	11.9810(6)	28.0390(12)
α/°	90	82.831(2)	97.6720(19)	90
β/°	93.313(2)	82.246(2)	102.7122(19)	90
γ/°	90	67.166(2)	115.4235(18)	120
Volume/$Å^3$	4842.9(5)	2552.83(19)	888.01(9)	13459.1(13)
Z	4	2	1	6
$\rho_{calc}g/cm^3$	2.821	2.677	1.706	1.579
μ/mm^{-1}	14.361	13.525	1.645	1.585
Crystal size/mm^3	0.14 × 0.1 × 0.05	0.09 × 0.06 × 0.04	0.16 × 0.06 × 0.04	0.14 × 0.12 × 0.08
Radiation	MoKα (λ = 0.71073)	MoKα (λ = 0.71073)	MoKα (λ = 0.71073)	MoKα (λ = 0.71073)
2Θ range for data collection/°	2.872 to 52.936	4.4 to 61.238	4.708 to 52.914	4.252 to 52.81
Reflections collected	53243	147034	3647	54985
Data/restraints/parameters	9834/6/479	15722/13/568	3647/2/175	6145/0/270

Goodness-of-fit on F^2	1.016	1.026	1.085	1.019
Final R indexes [I>=2σ (I)]	R_1 = 0.0349, wR_2 = 0.0683	R_1 = 0.0226, wR_2 = 0.0383	R_1 = 0.0428, wR_2 = 0.0699	R_1 = 0.0402, wR_2 = 0.0699
Final R indexes [all data]	R_1 = 0.0526, wR_2 = 0.0743	R_1 = 0.0328, wR_2 = 0.0407	R_1 = 0.0612, wR_2 = 0.0746	R_1 = 0.0802, wR_2 = 0.0812
Largest diff. peak/hole / e $Å^{-3}$	1.96/-0.88	2.04/-1.41	0.44/-0.48	0.53/-0.45

References

1. Zhang, G., Liu, C., Long, D., Cronin, L., Tung, C. and Wang, Y. *Journal of the American Chemical Society*, **2016,** *138(35)*, 11097-11100.
2. Bradley, D., Hursthouse, M., Howes, A., de M. Jelfs, A., Runnacles, J. and Thornton-Pett, M. *Dalton Trans*., **1991**, 841-847.
3. Gómez-Sal, P., Martín, A., Mena, M. and Yélamos, C. *J. Chem. Soc., Chem. Commun.*, **1995**, *(21)*, 2185-2186.
4. García-Castro, M., Martín, A., Mena, M. and Yélamos, C. *Chemistry - A European Journal*, **2009,** *15(29)*, 7180-7191.
5. Abarca, A., Galakhov, M., Gracia, J., Martín, A., Mena, M., Poblet, J., Sarasa, J. and Yélamos, C. *Chemistry - A European Journal*, **2003,** *9(10)*, 2337-2346.
6. Caballo, J., Greño, M., Mena, M., Pérez-Redondo, A. and Yélamos, C. *Dalton Transactions*, **2015,** *44(41)*, pp.18145-18157.
7. Abarca, A., Gómez-Sal, P., Martín, A., Mena, M., Poblet, J. and Yélamos, C. *Inorganic Chemistry*, **2000,** *39(4)*, pp.642-651.
8. Carmalt, C., Mileham, J., White, A. and Williams, D. *New Journal of Chemistry*, **2000,** *24(12)*, 929-930.
9. Carmalt, C., Newport, A., Parkin, I., White, A. and Williams, D. *Journal of the Chemical Society, Dalton Transactions*, **2002** *(21)*, 4055-4059.
10. Narula, C., Czubarow, P. and Seyferth, D. *Chemical Vapor Deposition*, **1995,** *1(2)*, 51-53.
11. Moran, P., Rickard, C., Bowmaker, G., Cooney, R., Bartlett, J. and Woolfrey, J. *Inorganic Chemistry*, **1998,** *37(6)*, 1417-1419.

12. Holl, M., Wolczanski, P. and Van Duyne, G. *Journal of the American Chemical Society,* **1990,** *112,* 7989-7994.
13. Banaszak Holl, M., Wolczanski, P., Proserpio, D., Bielecki, A. and Zax, D. *Chemistry of Materials*, **1996,** *8(10),* pp.2468-2480.
14. APEX3 Version 2016.5-0 and SAINT+ Version 8.38A. Bruker AXS, Inc., Madison, Wisconsin, USA, 2016.
15. SADABS-2016/2: Krause, L., Herbst-Irmer, R., Sheldrick G.M. and Stalke D. *J. Appl. Cryst.* 2015, *48*, 3-10.
16. HELXT: Sheldrick, G.M. *Acta Cryst*. 2015, *A71*, 3-8.
17. SHELXL: Sheldrick, G.M. *Acta Cryst*. 2015, *C71*, 3-8.
18. OLEX2: a complete structure solution, refinement and analysis program. Dolomanov, O. V., Bourhis, L. J., Gildea, R. J., Howard J. A. K. and Puschmann, H. *J. Appl. Cryst.* 2009, *42*, 339-341.

Appendix A

Permissions to Reprint

Title: Imido Group Interchange in Reactions of Zwitterionic Tantalum(V) Vinylimido Complexes and Nitriles

Author: Md. Mamdudur Rahman, Mark D. Smith, Dmitry V. Peryshkov

Publication: Organometallics

Publisher: American Chemical Society

Date: Sep 1, 2018

PERMISSION/LICENSE IS GRANTED FOR YOUR ORDER AT NO CHARGE

This type of permission/license, instead of the standard Terms & Conditions, is sent to you because no fee is being charged for your order. Please note the following:

- Permission is granted for your request in both print and electronic formats, and translations.
- If figures and/or tables were requested, they may be adapted or used in part.
- Please print this page for your records and send a copy of it to your publisher/graduate school.
- Appropriate credit for the requested material should be given as follows: "Reprinted (adapted) with permission from (COMPLETE REFERENCE CITATION). Copyright (YEAR) American Chemical Society." Insert appropriate information in place of the capitalized words.
- One-time permission is granted only for the use specified in your request. No additional uses are granted (such as derivative works or other editions). For any other uses, please submit a new request.

BACK CLOSE WINDOW